The Dissertation Committee for Taemin Heo
certifies that this is the approved version of the following dissertation:

Efficient Climate Data Analyses in Decision Making for the Design and Operation of Land-Based and Ocean Infrastructure Systems

Committee:

_____

Lance Manuel, Supervisor

_____

Spyros Kinnas

_____

Zoltan Nagy

_____

Paola Passalacqua

_____

Preston Wilson

Efficient Climate Data Analyses in Decision Making for the Design and Operation of Land-Based and Ocean Infrastructure Systems

by

Taemin Heo

DISSERTATION

Presented to the Faculty of the Graduate School of

The University of Texas at Austin

in Partial Fulfillment

of the Requirements

for the Degree of

DOCTOR OF PHILOSOPHY

THE UNIVERSITY OF TEXAS AT AUSTIN

December 2022

Dedicated to my wife Ji Min Kim.

Acknowledgments

302, SDS 320E, and CE 311S courses for which I worked as a teaching assistant. They were wonderful and thoughtful mentors and mentees. I will never forget the times when we taught each other.

I sincerely appreciate my wife, my parents, my sister, and my parents-in-law. I could never finish this work without their unconditional support.

Efficient Climate Data Analyses in Decision Making for the Design and Operation of Land-Based and Ocean Infrastructure Systems

Publication No. _____

Taemin Heo, Ph.D.
The University of Texas at Austin, 2022

Supervisor: Lance Manuel

Climate change presents significant challenges to the built environment. To deal with them, optimized adaptation and mitigation strategies are needed. Rational data-driven approaches are needed that consider non-stationary characteristics of the climate processes to assess the changing risks. The transition to sustainable clean sources is one component of mitigation. Investment in ocean-based renewable energy has received much attention in this endeavor. Still, associated costs of such energy need to be reduced significantly. Some innovative ideas are being considered—such as, for instance: (1) offshore floating multi-purpose platforms (MPPs) that offer benefits from shared use of infrastructure assets for multiple services including resource extraction activities (such as renewable energy generation), aquaculture, leisure, and transport

functions; and (2) sustainable reuse of decommissioned oil and gas offshore jacket platforms for wind energy generation. Such investments have the potential to reduce costs but they are still in their early stages with many missing validated rational solutions.

In this dissertation, three studies are undertaken to develop scientific frameworks that use climate and ocean data to aid in making optimized decisions for climate change adaptation and mitigation. The first study targets judicious near-future modeling of non-stationary climate processes while employing past observations optimally. A Greedy Copula Segmentation (GCS) algorithm is developed that employs best-fit multivariate probability distributions and copula functions after data-driven time series segmentation is undertaken. Predictions based on the GCS approach more closely describe the actual future than those made by a traditional model using all the available data. The second study aims to maximize the benefits of the sustainable reuse of oil and gas platform for wind energy generation by establishing an optimized plan that accounts for the remaining life of the repurposed platform, overall platform construction and retrofit costs, and an expectation of a period of clean energy generation and associated revenues after the wind turbine installation. A realistic case study and sustainable reuse scenario for a site near Porto (Leixões), Portugal, are employed to illustrate the feasibility and advantages of the model developed. The last study involves the formulation of a Markov decision process (MDP) to provide an optimized policy that guides the scheduling of operation and maintenance (O&M) activities for MPPs. By

following the provided policy, the overall loss of revenue and costs of O&M are inherently minimized. The robustness of the method is validated by demonstrating that the optimized policy leads to lower accumulated costs than is possible with conventional practice and the benefits are realized for a wide range of general meteorological and oceanographic (metocean) conditions— i.e., the combined wind, wave and associated climate conditions.

Table of Contents

List of Tables

List of Figures

Acronyms

$AVHRR$ Advanced Very High Resolution Radiometer

$CapEx$ Capital Expenditure

CCA Climate Change Adaptation

CDF Cumulative Distribution Function

CGS Calm General Seas

CoE Cost of Energy

CoV Coefficient of Variation

DP Dynamic Programming

DRR Disaster Risk Reduction

FAO Food and Agriculture Organization

$FOWT$ Floating Offshore Wind Turbine

GCS Greedy Copula Segmentation

GGS Greedy Gaussian Segmentation

HVS Highly Variable Seas

$IPMA$ Portuguese Institute of Sea and Atmosphere

$JONSWAP$ Joint North Sea Wave Project

VSS Very Sustained Seas

WEC Wave Energy Converter

Chapter 1

Introduction

Climate change presents significant challenges to the coastal and off-shore built environment. Seaports are located in regions vulnerable to the effects of climate change, such as coastal regions susceptible to sea-level rise and frequent and severe storms, or at the mouths of rivers susceptible to flooding [12]. The offshore oil and gas sector contributes a large portion of CO_2 emissions worldwide; at the same time, it is also vulnerable to climate change [23, 44]. One of the major impacts of climate change is damage to coastal and offshore infrastructure, which can lead to oil spills and the release of hazardous and dangerous chemicals, which then pose health and environmental issues [38]. At the same time, the offshore wind sector can also be influenced by climate change [36, 160]. The amount of wind energy that a wind turbine can generate varies with the cube of the wind speed; thus, small changes in wind patterns brought on by climate change can lead to significant variations in wind energy production [40, 167, 168]. In addition, changes in the seasonality of wind speeds brought on by climate change can have an impact on the year-round balance of power supply and demand [21]. Wilkie and Galasso (2020) also found that fatigue damage and the structural safety of offshore wind turbine are sensitive to changes in the site environmental

conditions [180]. Aquaculture systems depend on the offshore environment and on coastal habitats that can be impacted by climate change [24]. Related infrastructure, including salmon cages, is at risk of structural failure in the face of more frequent and severe storms [78, 88]. Habitat sites suitable for aquaculture will be reduced as a result of changes in shoreline morphology brought about by sea level rise [113, 145]. Additionally, the biodiversity of coral reefs, wetlands, rivers, lakes, and estuaries as well as fisheries and aquaculture will be greatly impacted by ocean acidification, glacier melting, changes in precipitation, groundwater, and river flows [32].

It is widely known that temporal patterns of extreme climate events are changing due to the non-stationary nature of underlying processes and human-induced climate change. As elegantly summarized in Figure 1.1, originally presented by Slater et al., the frequency, severity, or spatially distributed features of many extreme climate events are changing in complex manners [157]. Extreme daily precipitation frequency and magnitude are going up globally [132]. There is an increasing trend in the temperature anomaly of the highest temperature each year [131]. Flood timing across Europe in days per decade and the magnitude of 20-year river floods are spatially complex in form and even locally concentrated in some regions [22, 156]. Some wet places are getting wetter, and dry regions are getting drier. This can eventually lead us to suffer from severe drought and flood simultaneously in different places over the globe. The 90th percentile of the 10-meter wind speed, and 850 hPa wind speed are also changing non-homogeneously [169]. These changes can lead to errors and

uncertainties in the risk assessment for almost every civil infrastructure.
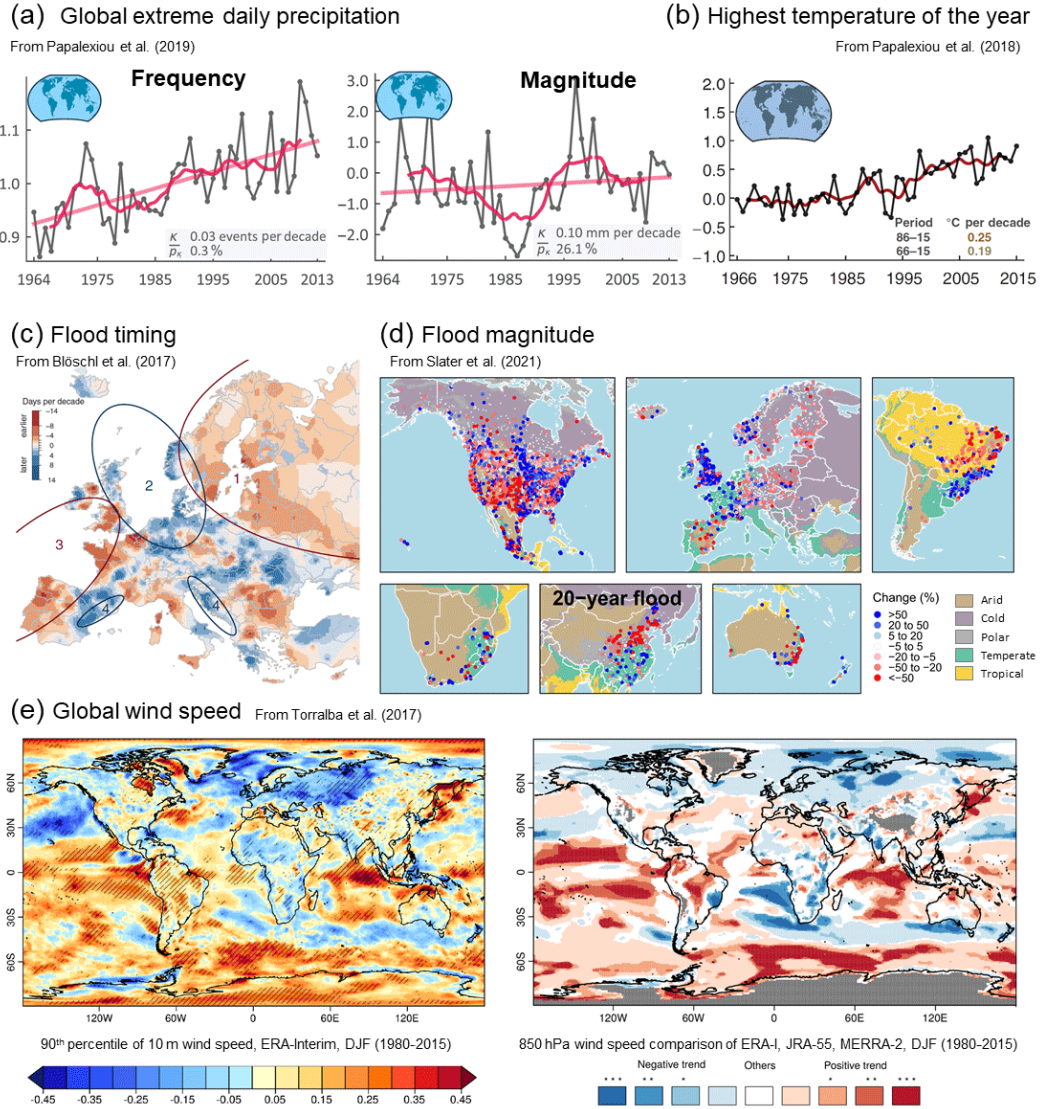
Figure 1.1: Examples of trends related to hydroclimatic extremes (reprinted from Reference [157] with permission).

To deal with these changing temporal patterns of extreme climate events, rational decision-making in climate change adaptation and mitigation strategies is necessary. As shown in Figure 1.2, adaptation consists of a set of actions to manage the risks of climate change impacts, such as retrofitting infrastructure and developing new approaches for design and management. Mitigation tackles the fundamental problem of global warming by reducing greenhouse gas emissions using, for instance, clean energy generation. We need to work on both sides—i.e., adaptation and mitigation—in order to achieve a sustainable future.
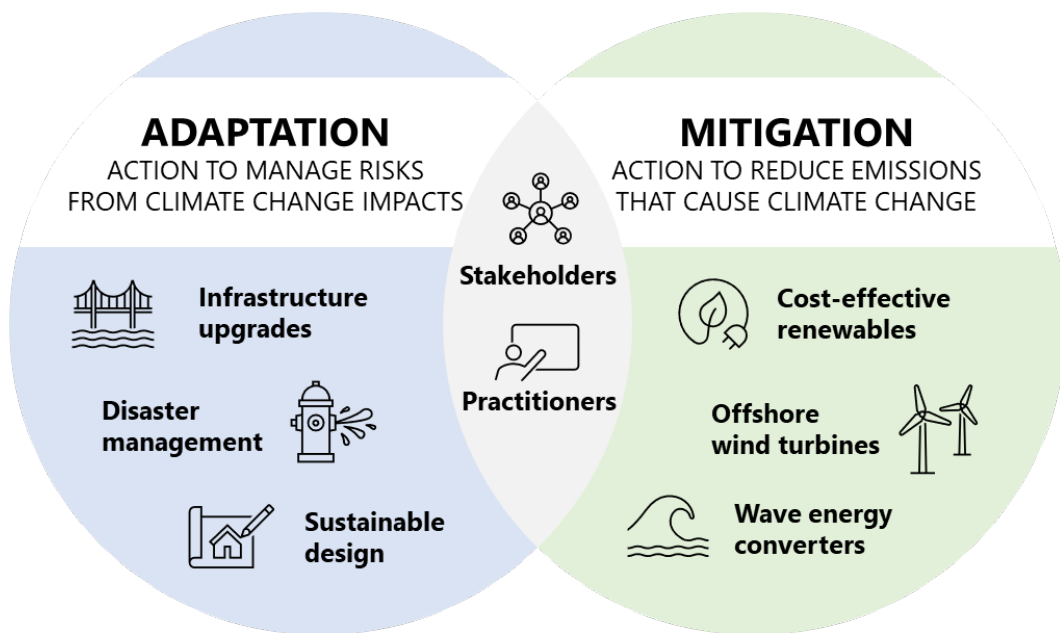
Figure 1.2: Climate change adaptation and mitigation.

Some challenges and barriers exist that hamper progress in adaptation

and mitigation. For adaptation, future risk assessment to deal with a changing climate can be challenging because most traditional approaches have been developed under stationary assumptions. Figure 1.3 shows a simple example comparing the distribution of past and future distributions of climate-related variables under stationary and non-stationary cases. As we can see, when the underlying process is non-stationary, it can be challenging to predict the future from the past (i.e., from historical data). Therefore, rational data-driven approaches are needed that consider non-stationary characteristics of climate processes to assess changing risks.

Traditional approach: stationary climate processes
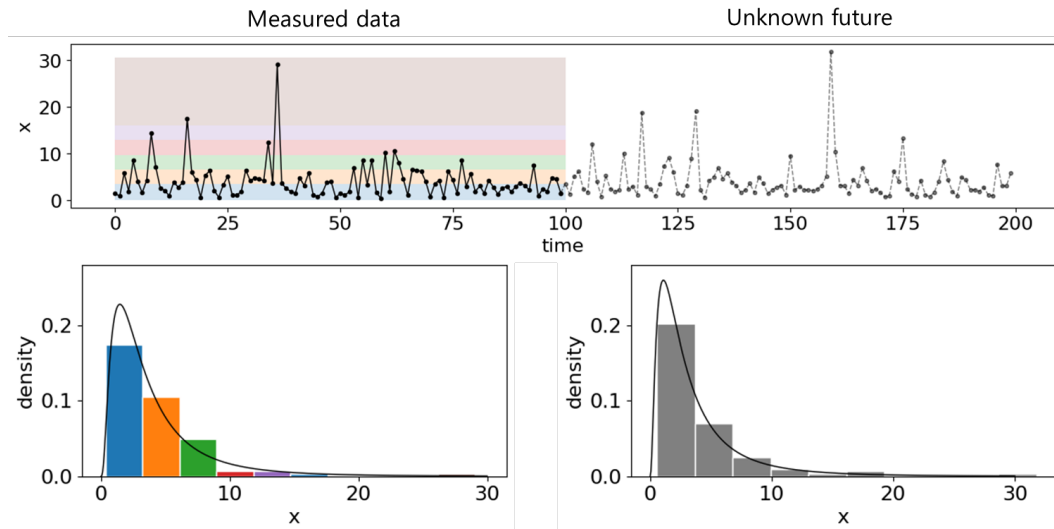
Climate change scenario: non-stationary climate processes
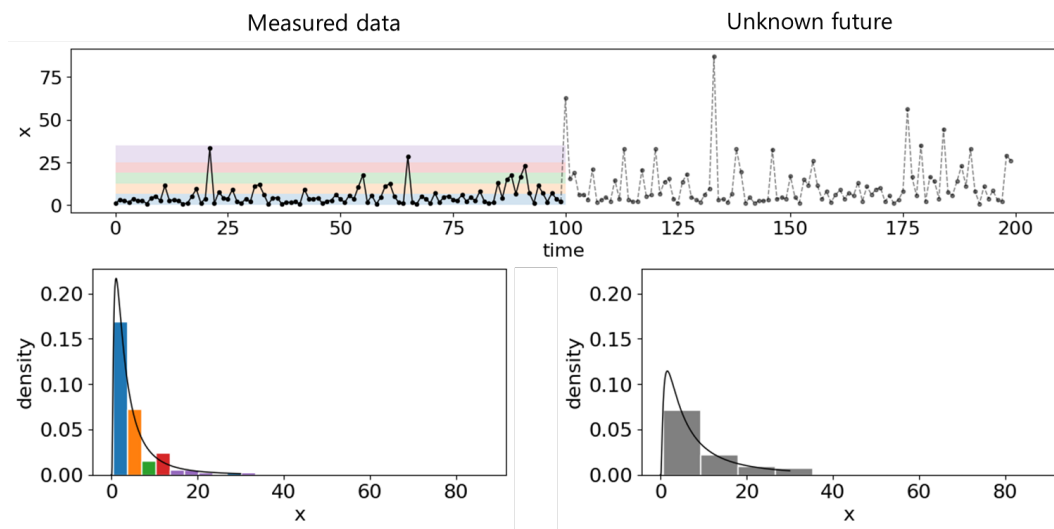
Figure 1.3: An example showing challenges associated with risk assessment when the underlying process of interest, $x(t)$, is non-stationary.

7

An energy transition toward more sustainable clean sources is one primary form of mitigation. As shown in Figure 1.4, clean energy provision and consumption need to be substantially amplified to achieve the goal of zero carbon emission in order to have sustainable development [146, 159].

Global direct primary energy consumption

Direct primary energy consumption does not take account of inefficiencies in fossil fuel production.

Source: Our World in Data based on Vaclav Smil (2017) and BP Statistical Review of World Energy   OurWorldInData.org/energy • CC BY
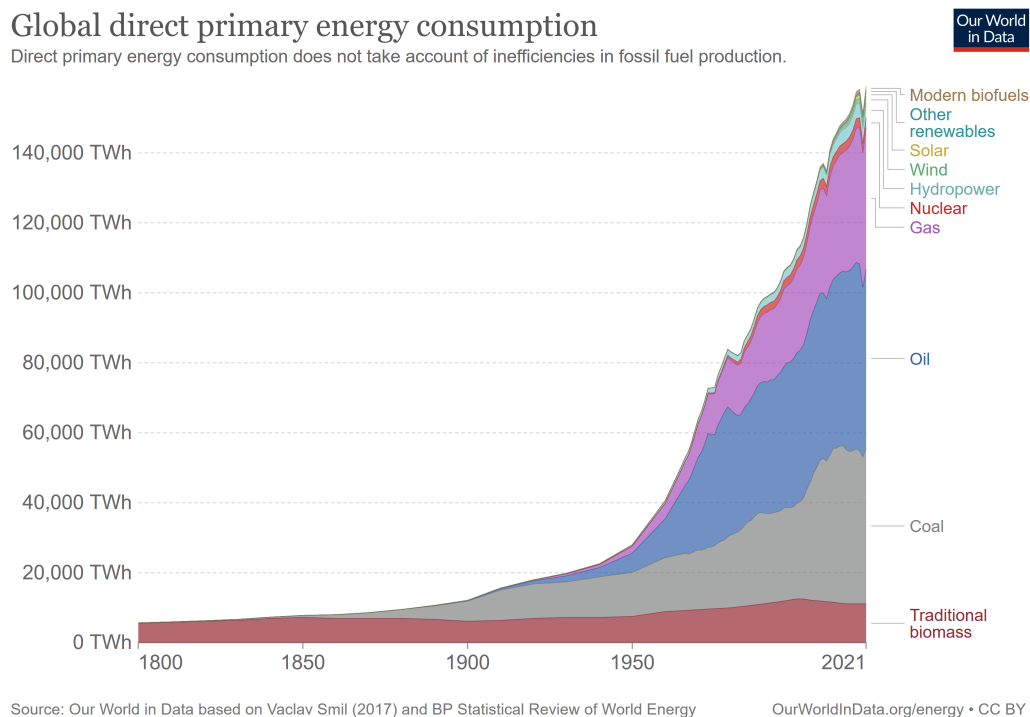
Figure 1.4: Global direct primary energy consumption (reprinted from Reference [146] with permission).

Ocean-based renewable energy has attracted much attention in this endeavor. Still, the associated costs of such energy need to be reduced significantly. Figure 1.5 shows that experts anticipate cost reductions for onshore, fixed-bottom offshore, and floating offshore wind power of 17%-35% in the

levelized cost of energy by 2035 and 37%-49% reductions by 2050 [30, 181]. Under this scenario, continued improvement and innovation in onshore and offshore wind technology is expected. Some innovative ideas are being considered—such as, for instance: (1) sustainable reuse of decommissioned oil and gas offshore jacket platforms for wind energy generation; (2) offshore floating multi-purpose platforms (MPPs) that offer benefits from shared use of infrastructure assets for multiple services including resource extraction activities such as renewable energy generation, aquaculture, leisure, and transport functions. These ideas have the potential to reduce costs but are still in their early stages with many missing validated rational solutions.
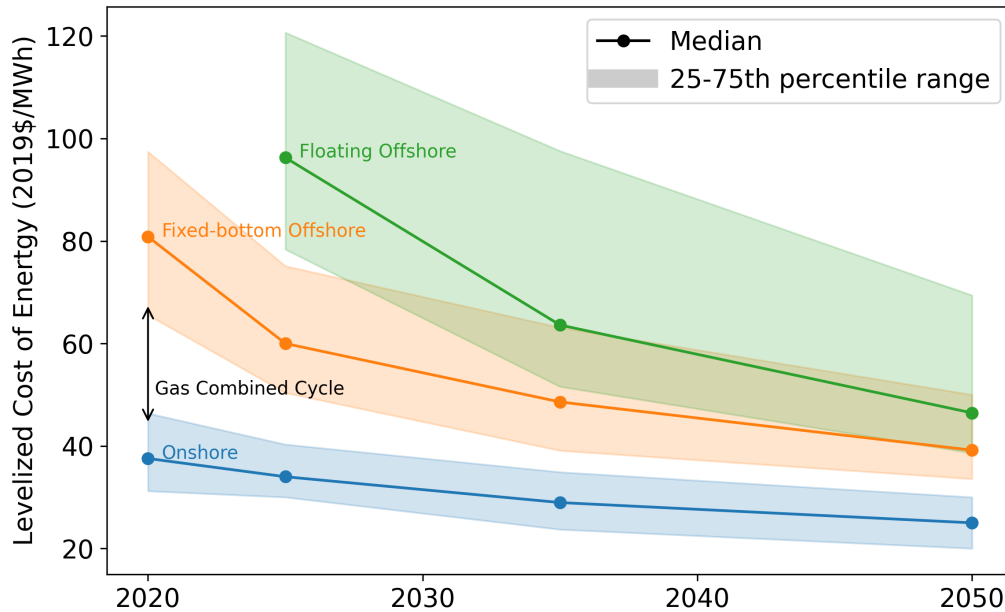
Figure 1.5: Experts anticipate substantial cost reductions for onshore, fixed-bottom offshore, and floating offshore wind power compared to gas combined cycle, but there is considerable uncertainty in such future cost estimates [30, 95, 181].

This dissertation aims at developing rational and scientific frameworks that make use of climate and ocean data to aid in making optimized decisions associated with climate change adaptation and mitigation. Three research questions listed below will be discussed in the next three chapters.

- How must one optimally use past data in near-future risk assessment of non-stationary extreme climate events for making better projections than a traditional approach that uses the entire historical observation under stationary assumptions?

- How does one identify and formulate an optimized plan for the sustainable reuse of decommissioned oil and gas jacket platforms for wind energy generation?

- How does one facilitate optimal decision-making in scheduling a wide-ranging set of operation and maintenance activities for multipurpose offshore platforms?

We will refer to three problems as "optimization," but they strictly all deal with rational decision-making using data-driven methods, while accounting for non-stationarity and uncertainty. These optimization exercises deal with different types of examples with varying time scales connected with and affected by climate change—both very long times (on the order of years) as in design and planning, as well as on the order of hours/days for operation.

The first study addressed in this dissertation targets judicious near-future modeling of non-stationary climate processes using past observations optimally. The methodology proposed seeks to divide up observed data into non-overlapping segments, each of which are separately treated as stationary but with underlying probability and dependence structure, while the long time series collectively yield multiple segments that are mutually independent; the segments are not known a priori but need to be statistically established for this analysis. A Greedy Copula Segmentation (GCS) algorithm is developed that employs best-fit multivariate probability distributions and copula functions after the data-driven time series segmentation is undertaken. Predictions based

on the GCS approach are closer to the actual future than those made by a traditional model that employs all the available data, i.e., the entire historical record.

The second study aims to maximize the benefits of sustainable reuse of an oil and gas platform for wind energy generation by establishing an optimized plan that accounts for the remaining life of the repurposed platform, the overall construction and platform retrofit costs, and an expectation of a period of clean energy generation and resulting revenues derived following the wind turbine installation. The proposed framework incorporates metocean data analysis, aero-hydro-servo-elastic simulations, fatigue damage assessment, reliability-based life cycle estimation, and economic revenue evaluation. For the choice of wind turbine, we consider various options with different associated power ratings and dimensions. An optimization problem is defined that considers large turbines with higher output ratings but possibly shorter expected service lives as well as contrasting alternatives. A realistic case study and sustainable reuse scenario for a site near Porto, Portugal, are employed to illustrate the advantages of the model developed.

The last study is the formulation of a Markov decision process (MDP) to derive an optimized policy that guides the scheduling of operation and maintenance (O&M) activities for MPPs. Satisfactory performance of multiple functions with MPPs requires dealing with a wide-ranging set of O&M activities that can take different amounts of time and require different levels of calmness in weather conditions. The right decision relating to the start or

delay/postponement of a needed O&M activity is key to resolving the O&M problem quickly, without interruption and accident, while carrying out work tasks in changeable weather. Historically, such decisions have been made by lead operators, based largely on experience. The formulated MDP involves a stochastic weather window analysis that operators can employ to decide upon the scheduling of work activities. By following the provided policy, the overall loss of revenue and costs related to O&M are inherently minimized. The robustness of the method is validated by demonstrating that the optimized policy leads to lower accumulated costs than is possible with conventional practice and the benefits are realized for a wide range of general meteorological and oceanographic (metocean) conditions—i.e., the combined wind, wave and associated climate conditions.

The remainder of this dissertation consists of four chapters introducing three journal article manuscripts followed by a summary and future work. The first chapter is a modification of a published article in Progress in Disaster Science, March 2022. The second and third chapters are manuscripts submitted to the ASME Journal of Offshore Mechanics and Arctic Engineering; note that the second chapter has been accepted for publication, while the third chapter is still under review. An overall summary of the research and planned future work, building from the three studies is provided in the last chapter.

Chapter 2

Greedy Copula Segmentation of Multivariate Non-Stationary Time Series for Climate Change Adaptation: Marine Heatwave Studies

The text and figures from this chapter are published in the Progress in Disaster Science (PDISAS)[1]

Taemin Heo and Lance Manuel. Greedy copula segmentation of multivariate non-stationary time series for climate change adaptation. *Progress in Disaster Science*, 14:100221, 2022

ABSTRACT

Non-stationary climate data are often encountered in dealing with natural hazards, climate change and disaster reduction. In studying marine heatwaves, for instance, it is common to encounter such non-stationary data sets (time series). The objectives of this work are to formulate a rational data-driven approach that can consider non-stationary and time series on multiple random variables that can have generalized underlying probability distribu-

---

[1]TH designed and conducted the research, developed the algorithm and analyzed the data, and wrote the manuscript.

tions and dependence structures. The methodology proposed seeks to divide up the data into non-overlapping segments, each of which is treated as stationary with some underlying probability and dependence structure, while the long time series available yield multiple such segments that are mutually independent. The Greedy Copula Segmentation (GCS) algorithm developed employs best-fit probability distributions and copula functions after data-driven time series segmentation. Validation of the proposed methodology is demonstrated using a benchmark problem as well as a single-site realistic marine heatwave example. The proposed GCS approach has potential use in climate change adaptation (CCA) and disaster risk reduction (DRR) for any climate-related hazards involving non-stationary time series data.

KEYWORDS

time series segmentation; greedy algorithm; non-stationary stochastic process; marine heatwaves

2.1 Introduction

Marine heatwaves (MHWs) - prolonged periods of anomalously high sea surface temperatures - are important events that can cause rapid changes in biodiversity patterns and in the structure and sustainability of marine communities and ecosystems [73, 124, 158]. MHWs have resulted in ecological and economic impacts, including the loss of kelp forests [53, 114], coral bleaching [45, 60], mass mortality of marine invertebrates, fish, seabirds, and marine

mammals [59, 82, 126, 134, 176, 179], loss of seagrass cover and its carbon stocks [6, 164]. Especially, the detrimental impacts of MHWs on the aquaculture and fishing industry have raised the need for urgent attention in management and adaptation [26, 28]. Closures and delays of the Dungeness crab fisheries from Washington to California in the 2015–2016 season due to unsafe and toxic algal blooms resulting from MHWs affected shellfish sales and industry job security, with losses through February of 2016 estimated at $48 million [29]. In the Pacific Northwest, recreational harvesting of the Pacific razor clam was prohibited, leading to economic losses of $22 million, and decreased tourism in coastal clamming areas [112, 177]. A recent study shows that 77% of exploited fishes and invertebrates will decrease in biomass while maximum catch potential will drop by 6% when an annual high temperature extreme occurs in an exclusive economic zone [31].

The frequency of MHWs and their duration and intensity have increased since the 1980s [77]. Oliver et al. found that from 1925 to 2016, the global average marine heatwave frequency and duration increased by 34% and 17%, respectively, resulting in a 54% increase in annual marine heatwave days globally [125]. Several studies identify that anthropogenic climate change is causing this trend and anticipate more accelerated increases under global warming conditions. Frolicher et al. [57] detected a doubling in the number of MHW days between 1982 and 2016, and this number was projected to further increase on average by a factor of 16 in a scenario with global warming of 1.5°C relative to pre-industrial levels and by a factor of 23 in a scenario with

global warming of 2.0°C. Laufkötter et al. [94] showed that the frequency of these events has already increased more than 20-fold because of anthropogenic global warming, making marine heatwaves, which typically occurred once in hundreds to thousands of years in pre-industrial times, now likely to occur on an annual to decadal basis if the global average air temperature rises by 3°C. Clearly, the pattern of MHWs is changing significantly and at a fast rate, and for sustainable development in many regions of the world, an advanced understanding and statistical/numerical modeling of the patterns is needed.

Traditionally, temporal patterns of extreme climate events such as MHWs are represented as a stationary stochastic process, which then implies that the risk assessment makes use of all the available historical data in prediction. As was already established, anthropogenic climate change is causing these patterns to change and become non-stationary. Such changing patterns highlight the possible incompatibility of traditional stationary assumptions, particularly when addressing climate change adaptation (CCA). Recently, Heo and Manuel proposed Greedy Copula Segmentation (GCS) which is a data-driven approach that can consider non-stationary time series on multiple random variables that can have generalized underlying probability distributions and dependence structures [70]. GCS is an extension of Greedy Gaussian Segmentation [62] and can be used with non-Gaussian climate data and any generalized copula model. GCS considers the non-stationary characteristics of the underlying climate process by defining sub-segments that are each stationary but mutually independent. Heo and Manuel showed that near-future

17

patterns could be reasonably assumed to be most similar to those in the most recent sub-segments, and a model derived from GCS-identified optimal data can lead to better predictions than what we get with the traditional approach that uses the entire historical sample. By using the GCS-identified optimal data, we rely on only informative recent data and discard outdated data to improve the prediction performance of risk assessment. The proposed method is flexible enough to be applied in climate change adaptation and disaster risk reduction for MHWs involving non-stationary time series data.

In this study, we investigate the changing patterns of duration and intensity of MHWs. An MHW and its features are defined by studying sea surface temperature (SST) with a seasonally varying site-specific threshold to take into account atmospheric forcing and oceanic conditions [73]. This definition presents an interesting distinction between land-based heat waves and MHWs. According to FEMA, a heat wave is a period of abnormally and *uncomfortably* hot and unusually humid weather, typically lasting two or more days with temperatures outside the historical averages for a given area [52]. This event definition focuses on the effect on human welfare. Such events typically occur in warmer months, and the temperature observed during the event is usually very high even above 37.8°C such as was seen during the 2006 California heat wave [89]. On the other hand, MHWs can occur on any day in the year even in the presence of low SSTs (cold temperatures). Because MHWs have impacts on biological appliations, their consideration in colder months can be important. For example, several seaweed species' reproduction

is pronounced in colder seasons, and the propagules and early post-settlement states are more susceptible to thermal stress than adults [5, 103, 149].

Accurate modeling of the duration and intensity of expected MHWs in a specific site of interest can result in proper preparation, management, and adaptation to changing risks of MHWs. We show GCS-identified optimal MHW events leading to better modeling of near-future patterns of MHWs. GCS discriminately detects and accounts for short-term climate abnormalities to discard dated data of the duration and intensity of MHWs and to select the optimal dataset for the near-future prediction without looking at the actual future. We use Advanced Very High Resolution Radiometer (AVHRR) satellite SSTs data which is $1/4°$ spatial resolution (global) and daily data from 1982 to 2020 (NOAA OISST) [10, 75, 142]. The predictive performance has been evaluated by a virtual end-of-2016 scenario and the development of a predictive model for the upcoming future period. Two models of the traditional approach, one using all available data and, the other, GCS-CCA using GCS-identified optimal data are considered, and GCS-CCA explains better the unseen future reality from 2017 to 2020. To demonstrate steps in the algorithms for GCS and GCS-CCA, an example analysis on a benchmark data set is first presented in Section 2.2. Details for an MHW risk assessment follow in Section 2.3. Discussions and conclusions follow at the end.

2.2 Methodology

2.2.1 Greedy Copula Segmentation

Assume we have bivariate climate data, available as time series data, as shown in Figure 2.1. Without loss of generality, assume that the time series are given at discrete data index values as shown.
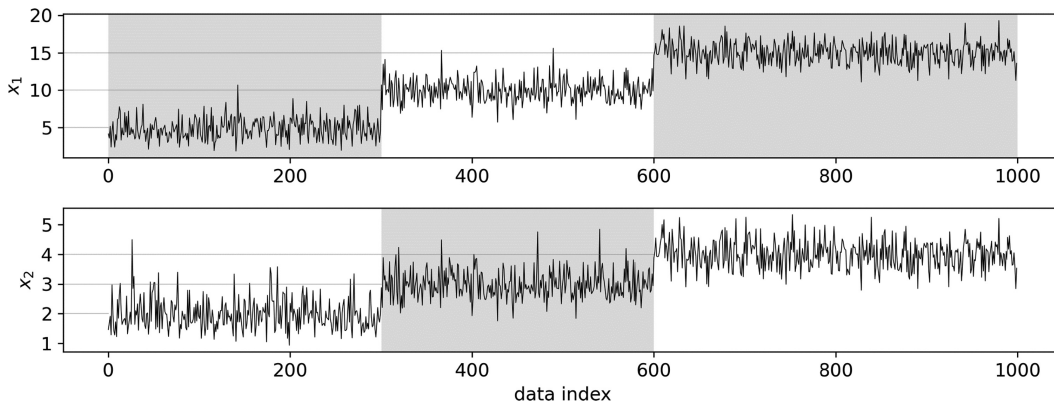
Figure 2.1: A realization of synthetic bivariate benchmark data time series: 3 separate data segments generated using 3 different parameter settings are highlighted.

In the synthetic data selected for this example, we have two climate-related variables that follow gamma and lognormal distributions, respectively. Their dependence structure is assumed to be represented by a Clayton copula. A total of 1,000 samples were generated with 3 different parameter settings to embed non-stationary character in the data. We have 5 parameters to define the two variables in each of the 3 subsets—they include a copula parameter, α; parameters describing the shape, a, and scale, b, for the gamma variable; and

the mean, μ, and standard deviation, σ, for the lognormal variable. Note that the mean and variance of the gamma variable are ab and ab^2, respectively.

For the data, the first 300 samples are synthetically generated using $\Theta_1 = (\alpha, a, b, \mu, \sigma) = (1, 10, 0.5, 2, 0.5)$, the next 300 samples use $\Theta_2 = (10, 40, 0.25, 3, 0.5)$, and the final 400 samples are from $\Theta_3 = (50, 100, 0.15, 4, 0.5)$. For the gamma-distributed variables, the different parameter settings are equivalent to setting different mean values of 5, 10, and 15, and variances of 2.5, 2.5, and 2.25. Figure 2.2 shows copulas according to the different parameter setting selections. As is clear from Figure 2.1, the generated time series are non-stationary; the values of both variables are seen to get higher with time (increasing data index value). As such, this synthetic bivariate climate benchmark data set could represent changing extreme climate events – such as storms, floods, droughts, etc. – that get more frequent and severe with time.
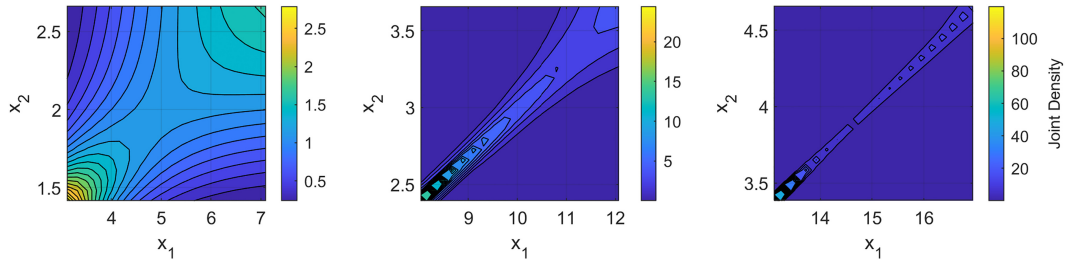
Figure 2.2: Copulas for the synthetic benchmark data generation using Θ_1, Θ_2, and Θ_3 (left to right).

From the above, one might expect that near-future patterns are most likely to be similar to the last 400 samples. The earlier 600 samples are likely

to be deemed outdated and would increase uncertainty in any near-future prediction. Our goal is to find and uncover the last stationary sub-segment from the data. To achieve this goal, we iterate the greedy segmentation approach until no further segmentation on the last segment offers any advantage.

2.2.1.1 Iteration 1

The GCS algorithm starts with the benchmark data that can be denoted as $X = [\mathbf{x}_1, \ldots, \mathbf{x}_{1,000}]^\top$, where $\mathbf{x}_i = (x_1(i), x_2(i))$. Also, $x_1(i)$ and $x_2(i)$ represent the ith index values of the first and the second variable, respectively. Note that $\mathbf{x}_i$ represents a 2-dimensional vector containing these ith index values of both variables and X represents the entire bivariate data set.

We consider the data as a segment and, thus, the number of current segments $K = 1$; by splitting the data into more segments, the value of K will be changed. In every GCS iteration, we will consider a new breakpoint that then divides one of the current segments into two sub-segments. In the first iteration, we have 999 possible new breakpoints denoted as $b_{1\backslash 2}, b_{2\backslash 3}, \ldots, b_{999\backslash 1,000}$, where the location of a breakpoint is indicated by the subscript. For instance, $b_{k\backslash k+1}$ is a breakpoint that divides the data into two sub-segments $X_1 = [\mathbf{x}_1, \ldots, \mathbf{x}_k]^\top$ and $X_2 = [\mathbf{x}_{k+1}, \ldots, \mathbf{x}_{1,000}]^\top$. Figure 2.3 shows an example with $b_{k\backslash k+1}$, where $k = 500$.
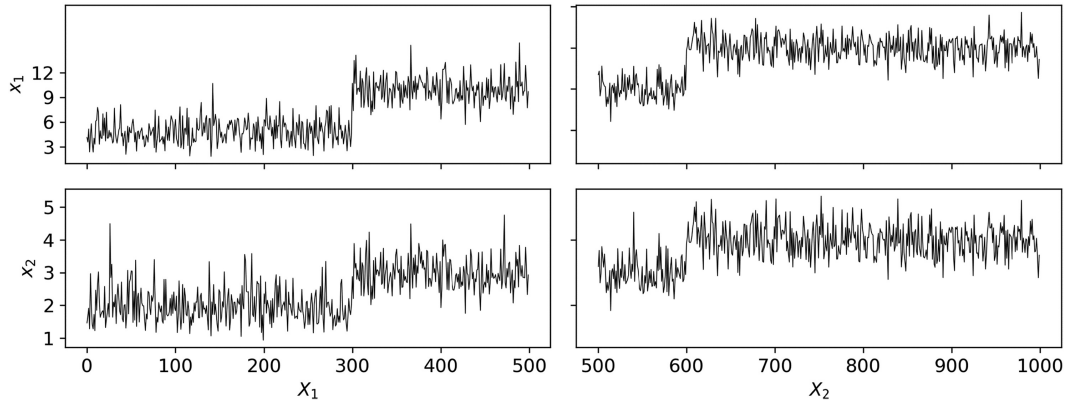
Figure 2.3: Example sub-segments generated by breakpoint, $b_{500\backslash 501}$.

Next, we compare two scenarios: 1) where X represents independent bivariate samples from a multivariate copula C_Θ based on all the data; and 2) where X_1 and X_2 represent separate bivariate samples from two different copulas, $C_{\Theta_{(1)}}$ and $C_{\Theta_{(2)}}$, respectively. For both scenarios, we assume that the same Clayton copula family and Gamma and lognormal marginal distributions, although different distribution and copula parameters apply in the two scenarios. Scenario 1 leads to fixed model parameters, while Scenario 2 considers that the model parameters change when one considers data before and after the breakpoint, $b_{k\backslash k+1}$. Using maximum likelihood, we will evaluate and maximize the following objective function:

$$\Psi_{k\backslash k+1} = \psi(X_1) + \psi(X_2) - \psi(X), \tag{2.1}$$

where $\psi(\cdot)$ is a function computed based on the regularized maximum log-likelihood of the available data with regard to the predefined copula family

23

and marginal distributions.

Note that $\psi(X)$, first, employs MLE model parameters, Θ, based on the assigned data, X. The MLE method allows estimation of the marginal distribution parameters and the copula family parameters; MATLAB provides functions named fitdist and copulafit that accomplish this task. The regularized maximum log-likelihood function is obtained as follows:

$$
\begin{aligned}
\psi\left(X\right) \ = \sum_{i=1}^{n} & \left[\log c_\alpha\left(F_1\left(x_1\left(i\right)|a,b\right),F_2\left(x_2\left(i\right)|\mu,\sigma\right)\right)\right. \\
& \left. + \log f_1\left(x_1\left(i\right)|a,b\right) + \log f_2\left(x_2\left(i\right)|\mu,\sigma\right)\right] - \frac{\lambda}{s_1^2 + s_2^2},
\end{aligned}
\tag{2.2}
$$

where n is the length of the input bivariate time series, X;

$$
c_\alpha = \frac{\partial^2 C_\alpha\left(u_1 = F_1\left(x_1|a,b\right), u_2 = F_2\left(x_2|\mu,\sigma\right)\right)}{\partial u_1 \partial u_2}
\tag{2.3}
$$

is the copula probability density function; $u_1 = F_1\left(x_1|a,b\right)$ and $u_2 = F_2\left(x_2|\mu,\sigma\right)$ are marginal cumulative distribution functions; $f_1\left(x_1|a,b\right)$ and $f_2\left(x_2|\mu,\sigma\right)$ are marginal probability density functions; s_1 and s_2 are marginal sample standard deviations. To avoid oversegmentation, marginal variance regularization is applied and $\lambda \geq 0$ is the regularization parameter. The order of magnitude of the marginal variances, together with λ, influences the role of regularization, which is discussed in Section 2.2.3.

Note that $\Psi_{k\backslash k+1}$, as defined, is the regularized maximum log-likelihood difference between the likelihood function based on data sub-segments divided at the breakpoint, $b_{k\backslash k+1}$, and the likelihood function based on the entire

24

unsegmented data set. We calculate $\Psi_{k\backslash k+1}$ for every possible breakpoint and then select an optimal breakpoint $b_{k^*\backslash k^*+1}$ as follows:

$$k_1^* = \operatorname*{argmax}_{k} \Psi_{k\backslash k+1}, \tag{2.4}$$

and we also ensure that $\Psi_{k_1^*\backslash k_1^*+1} > 0$. If every Ψ returns a negative value, it means that further segmentation has no advantage. In this case, the greedy algorithm stops the segmentation search and we go to the *Return* stage.

Figure 2.4 shows 999 Ψ values computed with $\lambda = 100$. The maximum Ψ value occurs for $k = 600$. Based on this result, we divide the data set into sub-segments at the breakpoint, $b_{600\backslash601}$. These resulting sub-segments are shown in Figure 2.5.
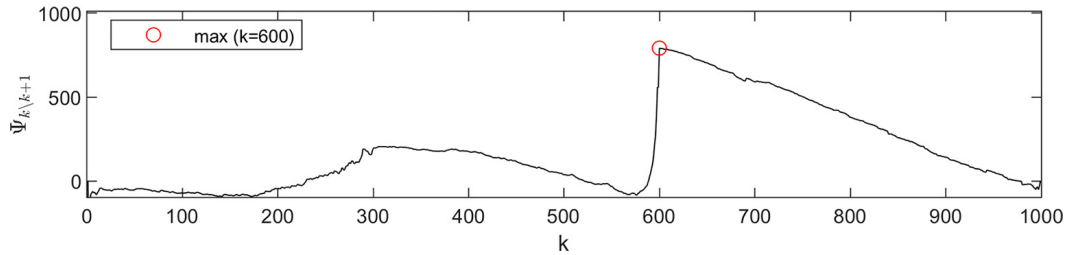
Figure 2.4: Calculated objective function Ψ for the benchmark data at the first iteration.
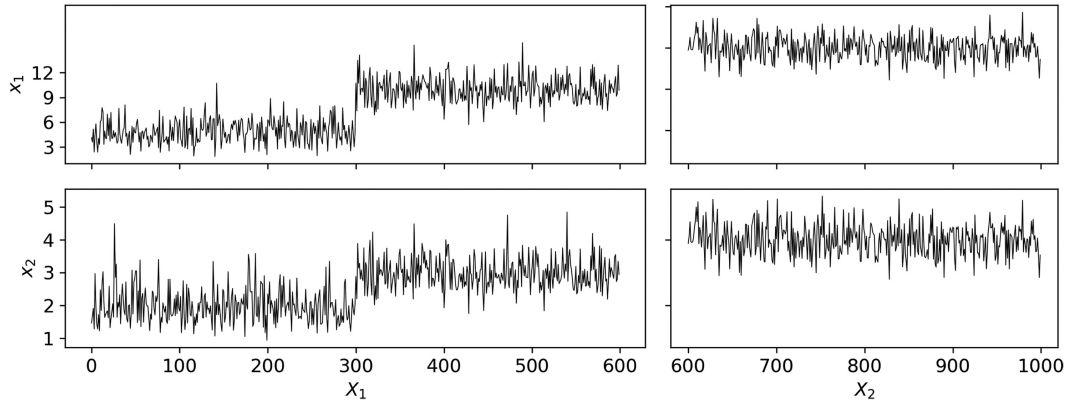
Figure 2.5: Sub-segments generated by the first identified breakpoint, $b_{k_1^* \setminus k_1^* + 1} = b_{600 \setminus 601}$.

2.2.1.2 Iteration 2

After the previous (first) iteration, what we have are new segmented data sets, $X_1 = [\mathbf{x}_1, \ldots, \mathbf{x}_{600}]^\top$ and $X_2 = [\mathbf{x}_{601}, \ldots, \mathbf{x}_{1,000}]^\top$. Thus, the number of current segments, $K = 2$, and the number of new breakpoints possible is now 998. Again, we compute Ψ for every possible breakpoint and ultimately select a new optimal breakpoint, $b_{k_2^* \setminus k_2^* + 1}$. We reject the new breakpoint and terminate the greedy algorithm if all Ψ values have a negative value. An additional termination condition is invoked in Iteration 2 and beyond, if the identified optimal breakpoint is not from the current last sub-segment. This is because our goal with the greedy search algorithm is to find and use only the last stationary sub-segment to be representative of the most likely series for the near future. Therefore, if further segmentation cannot be continued on the current last sub-segment, we terminate the search. On the other hand,

26

if there is a breakpoint, $b_{k_2^* \backslash k_2^*+1}$, within the last sub-segment (in Iteration 2, the last segment $=X_2$) and $\Psi_{k_2^* \backslash k_2^*+1} > 0$, we accept this new breakpoint and continue the iteration with the new segmented data sets, $X_1 = [\mathbf{x}_1, \ldots, \mathbf{x}_{600}]^\top$, $X_2 = [\mathbf{x}_{601}, \ldots, \mathbf{x}_{k_2^*}]^\top$, and $X_3 = [\mathbf{x}_{k_2^*+1}, \ldots, \mathbf{x}_{1,000}]^\top$. Otherwise, the algorithm moves to what we refer to as the *Return* stage.

2.2.1.3 Iteration 3+

We repeat the procedure above until any one of the termination conditions: 1) all $\Psi < 0$; 2) k^* does not match an index number in the last sub-segment. After we terminate this iterative greedy search, the algorithm moves to the final *Return* stage.

2.2.1.4 Return

As final output, the algorithm returns the current last segment as the identified optimal data sub-segment. We denote this data set as X_{opt}. Note that $X_{opt} \subseteq X$.

Figure 6 shows calculated 998 Ψ values for the benchmark data set at Iteration 2. The maximum value occurs at k=310 on the first segment. This means that we have reached the second termination condition. We stop the iterations and send the current last sub-segment $X_2 = [\mathbf{x}_{601}, \ldots, \mathbf{x}_{1,000}]^\top$ to the Return stage. As a result, the identified optimal data set, $X_{opt} = X_2 = [\mathbf{x}_{601}, \ldots, \mathbf{x}_{1,000}]^\top$.

27
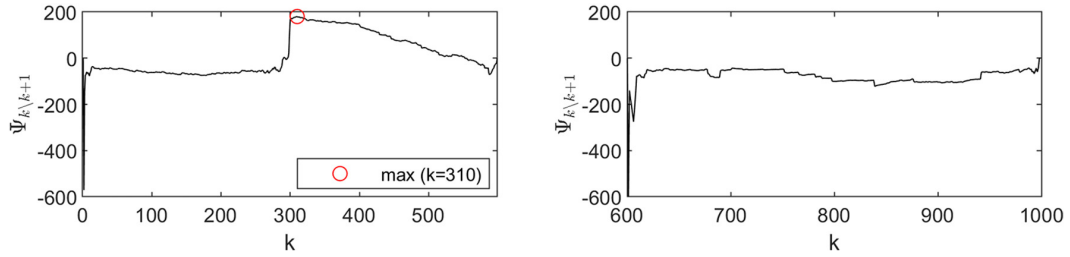
Figure 2.6: Calculated objective function Ψ for the benchmark data at the second iteration.

The GCS algorithm can be generalized to any d-dimensional multivariate data set, $X = [\mathbf{x}_1, \ldots, \mathbf{x}_N]^T \in \mathbb{R}^{N \times d}$, $\mathbf{x}_i = (x_1(i), \ldots, x_d(i))$. Let $f_i(x_i|\theta_i)$ be the probability density function and $u_i = F_i(x_i|\theta_i)$ be the cumulative distribution function for variable, x_i. Multivariate copulas can be denoted as $C_\Theta = C_\alpha(u_1, \ldots, u_d)$, where $\Theta = (\alpha, \theta_1, \ldots, \theta_d)$. The regularized maximum log-likelihood function for multivariate data, X, is given as:

$$\psi(X) = \sum_{i=1}^{N} \left(\log c_\alpha(u_1, \ldots, u_2) + \sum_{j=1}^{d} \log f_j(x_j|\theta_j) \right) - \frac{\lambda}{\sum_{j=1}^{d} s_j^2} \qquad (2.5)$$

Figure 2.7 shows the general GCS algorithm flowchart based on the preceding discussion.

28

Greedy Copula Segmentation
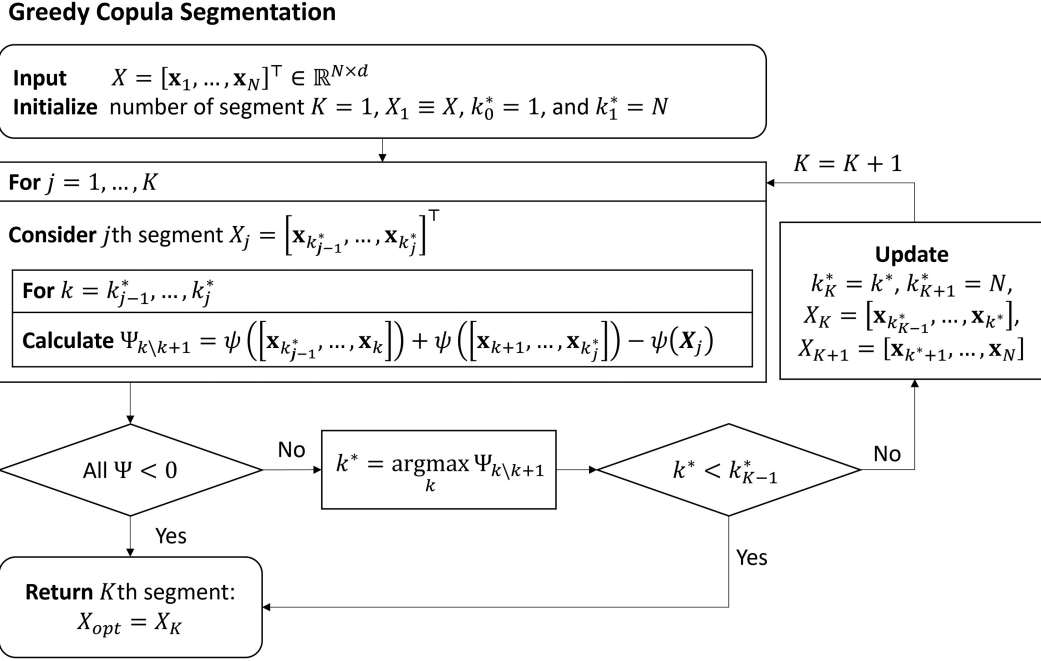
Figure 2.7: Greedy Copula Segmentation (GCS) algorithm flowchart.

2.2.2 Climate Change Adaptation with the Benchmark Data

We are interested in attempting a climate change adaptation strategy using GCS assuming that the bivariate data in Figure 2.1 describe climate parameters of interest. Suppose the benchmark data set, X, represents a 100 year-long set of observations with 10 records per year. Let us first consider a situation where only the first 40 year-long set (400 samples) represent the base data. The traditional approach would develop the base joint copula, $C_{\Theta_{(0)}}$ using all the base data, but our optimal approach will use the GCS-identified optimal data only for near-future projections. Then, such a derived

joint distribution will be used for any risk assessment until the new data are obtained, or the existing data set from 40 years is updated. Suppose this distribution is updated in increments corresponding to 10-year cycles. Again, the traditional approach would use all of the now 50 year-long set (500 samples) to obtain a new updated version of the joint copula, $C_{\Theta_{(1)}}$, but our optimal approach will again use the GCS-identified optimal data only. The procedure can be repeated every 10 years and two different joint copulas can be developed based on the two different approaches (traditional vs. GCS).

To highlight the comparative prediction performance of the two approaches, we compute log-likelihoods for m update cycles, each of 10-year length as follows:

$$LL_{trad}(m) = \log \prod_{i=1}^{n_m} C_{\Theta_{trad_m}}(\mathbf{x}_i), \quad LL_{opt}(m) = \log \prod_{i=1}^{n_m} C_{\Theta_{opt_m}}(\mathbf{x}_i) \qquad (2.6)$$

Two different joint copulas, $C_{\Theta_{trad_m}}$ and $C_{\Theta_{opt_m}}$, are derived using the base data and the same number of new 10-year data updates, $\mathbf{x}_i$, $i = 1, \ldots, n_m$, is applied to calculate the log-likelihood in Equation 2.6. As such, the calculated log-likelihoods are fair performance measures to allow comparisons between traditional and GCS approaches. The copula and corresponding approach that yields a higher likelihood when the new data are included is more accurate than the alternative. In other words, the traditional and GCS approaches offer models based on the base data that are then used to assess how well they perform against different lengths of update cycle data increments; relative comparison is possible using Equation 2.6.

A general formulation can be defined using t_{base} (the base period) and t_{cyc} (the period covered in each update cycle). At cycle m, the traditional approach uses all the data collected from the beginning until $t_{base} + m \cdot t_{cyc}$ to update the distribution, whereas GCS-CCA uses X_{opt_m} for the corresponding distribution. Note that each t_{cyc}-long data update can be used to evaluate predictive performance. Figure 2.8 shows a diagram summarizing the two different approaches with the formulation as presented.

Traditional Approach

$LL_{trad}(0) = \log \prod_{i=1}^{n_0} c_{\Theta_{trad\_0}}(\mathbf{x}_i)$

$LL_{trad}(1) = \log \prod_{i=1}^{n_1} c_{\Theta_{trad\_1}}(\mathbf{x}_i)$

$LL_{trad}(m) = \log \prod_{i=1}^{n_m} c_{\Theta_{trad\_m}}(\mathbf{x}_i)$

Optimal Approach

$LL_{opt}(0) = \log \prod_{i=1}^{n_0} c_{\Theta_{opt\_0}}(\mathbf{x}_i)$

$LL_{opt}(1) = \log \prod_{i=1}^{n_1} c_{\Theta_{opt\_1}}(\mathbf{x}_i)$

$LL_{opt}(m) = \log \prod_{i=1}^{n_m} c_{\Theta_{opt\_m}}(\mathbf{x}_i)$
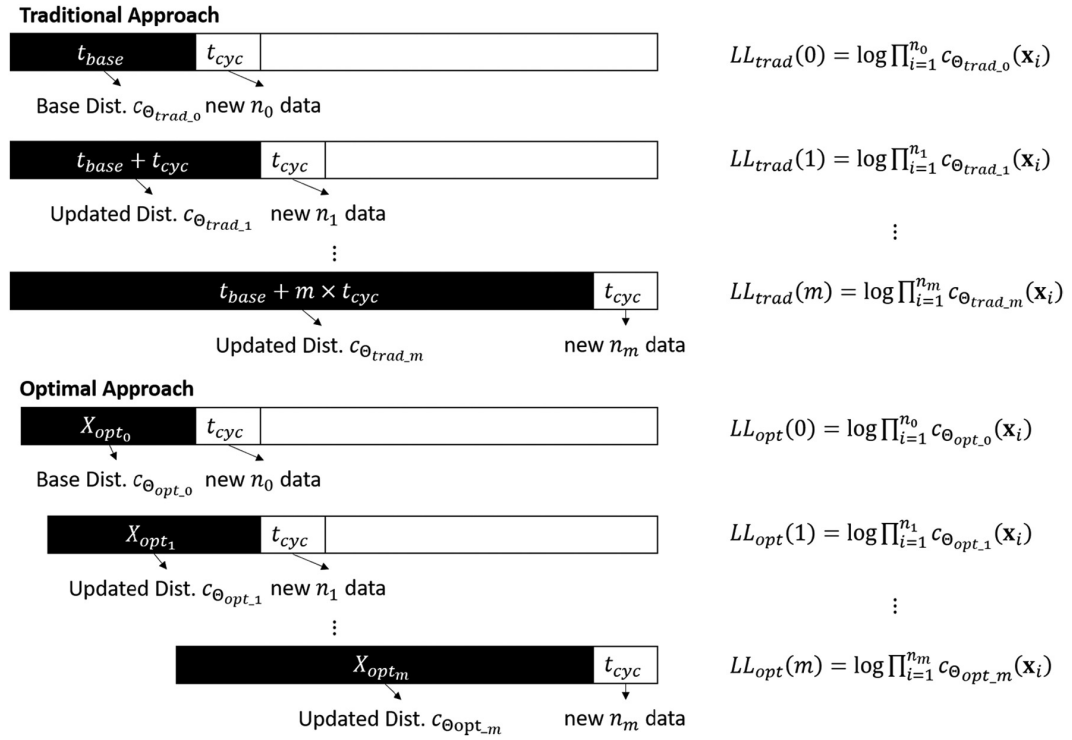
Figure 2.8: Traditional and optimal GCS approaches for climate change adaptation.

The predictive performance is evaluated 6 times since we choose, each

31

time, the first 400 samples as the base data and add 100 new samples in each update cycle. To allow overall predictive performance comparisons between the traditional CCA and GCS-CCA, we compute the mean predictive log-likelihood difference ratio, M, over all the update cycles:

$$M\left(\%\right) = \frac{1}{6} \sum_{i=0}^{5} \frac{LL_{opt}\left(i\right) - LL_{trad}\left(i\right)}{\left|LL_{trad}\left(i\right)\right|} \times 100. \tag{2.7}$$

We repeat this entire procedure 10 times by synthetically generating (using random sampling) a new benchmark data set each time. Figure 9 shows the mean and min-max error bars of $M\left(\%\right)$ with different regularization parameter choices, λ. We can easily confirm that GCS-CCA outperforms traditional CCA for sufficiently large parameters, λ, that range between 5 and 100. One can also directly evaluate the influence of λ; for lower values of λ, GCS-CCA performs better than traditional CCA. However, a lower-valued regularization parameter implies more oversegmentation and then its performance is not better than that with traditional CCA. Higher-valued regularization parameter levels restrict segmentation and then GCS-CCA is basically the same as traditional CCA. It is only for intermediate-valued λ values where GCS-CCA with associated segmentation is seen to be superior.
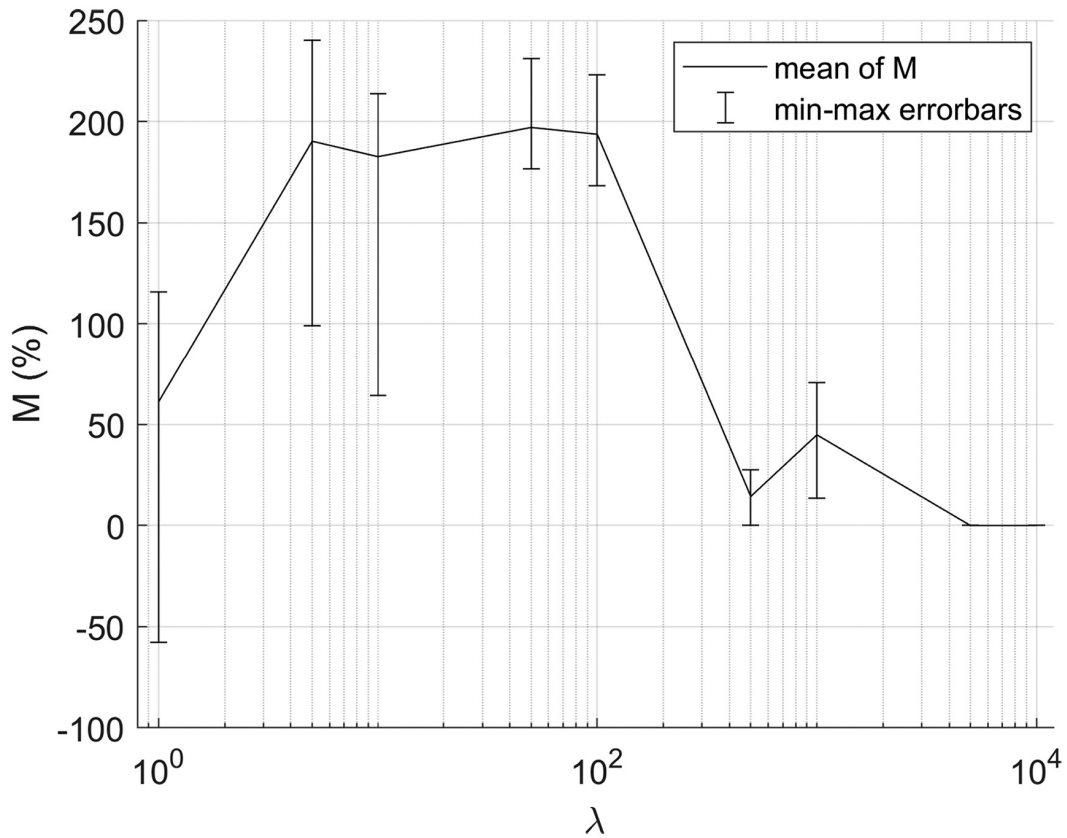
Figure 2.9: Calculated mean of predictive log-likelihood difference ratio, M, over all update cycles with different choices for regularization parameter, λ.

2.2.3 Regularization Parameter Selection

GCS-CCA leads to more accurate prediction than traditional CCA if we can select the proper regularization parameter, λ. Its value can be chosen by trial and error, using prior knowledge, or using a principled method, such as Bayesian or Akaike information criterion or cross validation (Hallac et al., 2019). In general, one needs a sufficiently high value for λ because this pa-

rameter directly influences the extent of segmentation that results. Too high a value for λ results in no segmentation, which is then equivalent to traditional CCA; on the other hand, a low value for λ leads to oversegmentation, which means that GCS will select a very short recent sub-segment as the optimal data. Then, the joint distribution of the underlying variables is overly fitted to this small amount of data. As we can see from Equation 2.5, the order of magnitude of the marginal variances, together with λ, influences the role of regularization. In Figure 2.9, we systematically evaluate the role of λ in assessing model quality. Results indicate that GCS-CCA's effectiveness is hurt by oversegmentation and inferior performance when λ values are low. Also, the results with traditional CCA are virtually the same as GCS-CCA when λ values are too high. Overall predictive performance of GCS-CCA is an improvement over traditional CCA over a considerably wide range of λ values from 5 to 100. This latter finding suggests too a lower sensitivity of λ on the benchmark data; if some moderate amount of regularization is imposed with GCS-CCA, superior performance over traditional CCA is assured. We recommend a practical way to select the sufficiently large λ based on the number of segments identified by GCS. We can monitor how the number of segmentation increases along with different regularizations without knowing the future. Among the λ that gives us the same segmentation result, a fairly large value would work best for the predictive performance.

2.3 Experiments with MHW Patterns in CCA

In the oceanography community, qualitative and quantitative definitions of marine heatwaves (MHWs) have been proposed [46, 58, 73, 133]. In those definitions, MHWs have been identified primarily using sea surface temperature (SST), although they may also extend below the surface [150]. Qualitatively, an MHW is a discrete prolonged anomalously warm water event at a particular location. Since it does not presuppose a particular heatwave driver, the qualitative definition can be tailored specifically to end-user application. On the other hand, this definition does not allow for empirical comparisons of the patterns of MHWs across different events in space and time. For this reason, Hobday et al. [73] proposed qualified definitions of 'anomalously warm,' 'prolonged,' and 'discrete'. The authors explained that an MHW must be defined relative to a baseline climatology and a high percentile threshold (e.g., 90%). A percentile threshold is recommended rather than an absolute value threshold or standard deviation definition due to its flexibility for spatiotemporal variability and the underlying distribution of anomalies. They also pointed out that the definition should be consistent globally, and this is possible when an MHW is required to persist for at least five days. For durations shorter than five days, there were significantly more events in tropical regions than elsewhere, yet for durations longer than five days, there were many regions with an average of less than one MHW per year.

In order to define MHWs as discrete with clear gaps between subsequent events, Hobday et al. [73] allowed temperature to be below the threshold for

two days or less for continuous events. They provided examples, where five anomalously warm days followed by two ordinary days and then seven anomalously warm days would be defined as a 14-day MHW event (5 hot, 2 ordinary, 7 hot = 12 MHW days). In contrast, five anomalously warm days, followed by one ordinary day, and then three more anomalously warm days would be defined as a 5-day event (5 hot, 1 ordinary, 3 hot = 5 MHW days). A sequence of five anomalously warm days followed by three ordinary days and then six anomalously warm days (5 hot, 3 ordinary, 6 hot) would be defined as two MHW events, one of five days duration and the other of six days duration.

For an experiment involving real data analysis and application of GCS-CCA, we use satellite data, NOAA OISST [10, 75, 142]. These remotely sensed global SST data are interpolated to have a $1/4°$ spatial resolution daily from 1982 to 2020 (a full 39 years). MHWs can be identified at any point in the grid based on the definition provided earlier. One grid cell near the northwest Atlantic ocean has been selected for a regional case study. The center of the selected $1/4°$ by $1/4°$ cell is at latitude 43.125 degrees north and longitude 66.875 degrees west. Figure 2.10 shows the coast and ocean near the selected grid cell. Figure 2.11 shows the collected daily SST time series from 1982/1/1 to 2020/12/31.
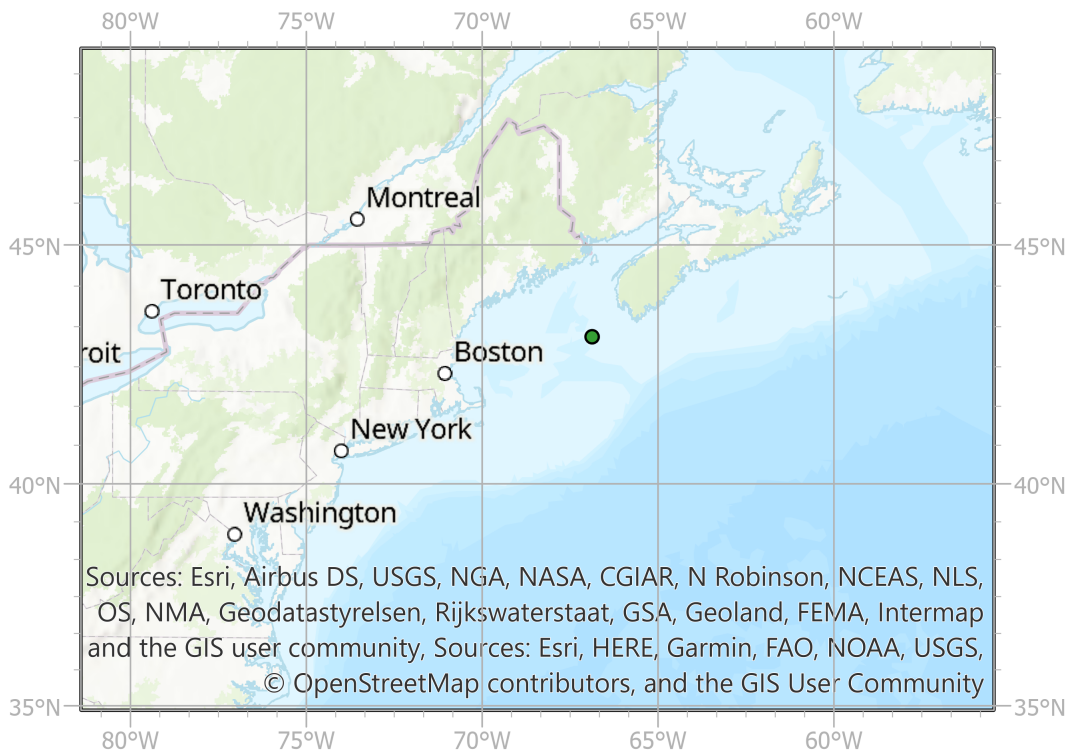
Figure 2.10: Selected site near the northwest Atlantic ocean. The green dot represents the center of the selected grid cell located at latitude 43.125 degrees north and longitude 66.875 degrees west.
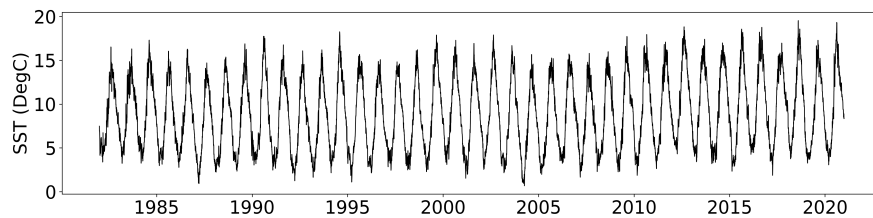
Figure 2.11: Collected daily SST time series from 1982/1/1 to 2020/12/31 near the northwest Atlantic grid cell of NOAA OISST centered at latitude 43.125 degrees north and longitude 66.875 degrees west.

This study describes the entire procedure that starts with preparing a bivariate MHW pattern time series and proceeds to a final predictive performance evaluation. We provide a step-by-step guide that can be used for extreme climate events and applications that have a similar problem setting and data structure.

2.3.1 Bivariate MHW Pattern Time Series

To apply GCS, first, we extract MHW events from the SST time series using a predefined definition originally introduced by Hobday et al. [73]. The overall concept of the MHW definition and its associated duration, D, and intensity, I are illustrated in Figure 2.12. In this study, MHW duration and intensity are selected for the analysis since they have been widely used to characterize changes in the patterns of MHWs. A similar concept can be applied to other climate data time series. We compute the climatological mean on day j ($j = 1, 2, \ldots, 365$), $T_m(j)$, as

$$
\begin{aligned}
T_m(j) &= \frac{1}{39} \sum_{y=1982}^{2020} T_{11d}(y, j) \\
\text{where} \quad T_{11d}(y, j) &= \frac{1}{11} \sum_{d=j-5}^{j+5} T(y, d),
\end{aligned}
\tag{2.8}
$$

$T(y, d)$ is the daily SST on day d of year y. $T_{11d}(y, j)$ is 11-day moving average of SST in year y. Then, $T_m(j)$ is calculated by taking the average over a reference period (for NOAA OISST, this period is from 1982 to 2020). The seasonally varying 90th percentile value that defines an MHW is denoted

$T_{90}(j)$ where j is again the day. Let us denote $P_{90}(X)$ as the 90th percentile of the dataset X. Then,

$$T_{90}(j) = P_{90}(\{T(y,d)|1982 \leq y \leq 2020, j - 5 \leq d \leq j + 5\}). \qquad (2.9)$$

The start of the MHW, t_s, is the time t, where $T(t) > T_{90}(j)$ and $T(t-1) < T_{90}(j)$. The end of the MHW, t_e, is the time t, where $T(t) < T_{90}(j)$ and $T(t-1) > T_{90}(j)$. Then, the duration of the MHW, D, is simply $t_e - t_s$ (days). Lastly, the intensity of the MHW, I, is the highest temperature anomaly value relative to the climatological mean during the MHW.
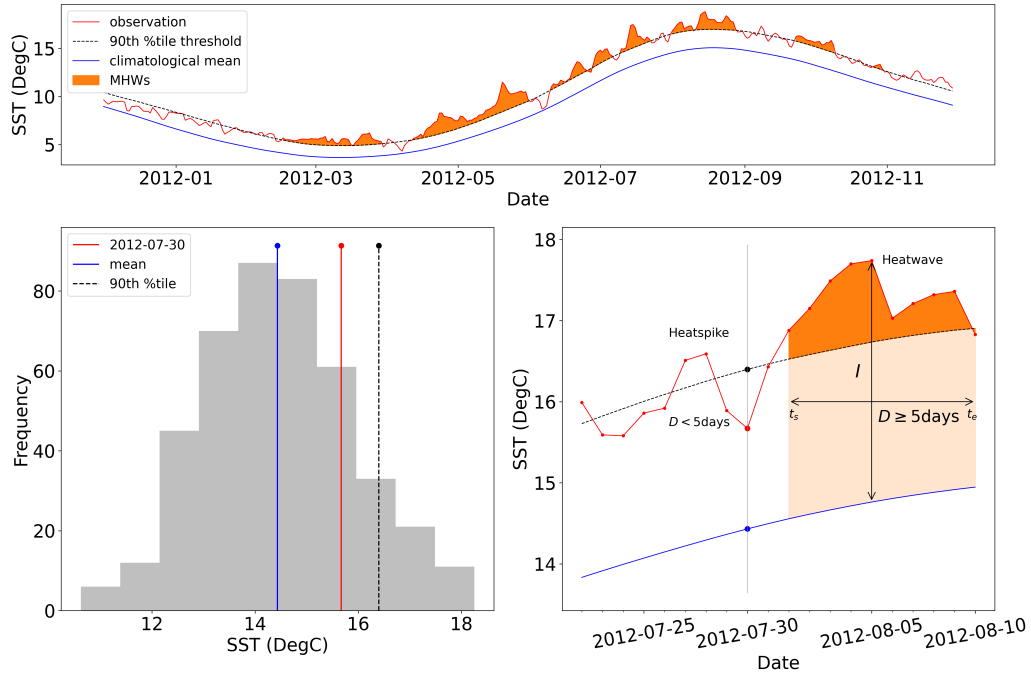
Figure 2.12: A concept diagram showing definitions of a marine heatwave (MHW) duration and intensity. (Top) MHWs are defined relative to the climatological mean (solid blue line) and the 90th percentile value (dashed line) that vary through the year. (Bottom left) Sea surface temperature (SST) in an 11-day window around each day for every year is averaged to compute the climatological mean, and the 90th percentile is used to define the threshold. (Bottom right) Short-duration heat spikes of duration shorter than five days are not MHWs. A temperature event that is at least five days or longer than this minimum duration is defined according to the duration (D) above the threshold value. The start and end days of the MHW are represented by t_s and t_e, respectively. Intensity is the maximum temperature above the climatological mean during the event.

Suppose we extract N MHW events from the given SST time series. Then, the input data, $X = [\mathbf{x}_1, \ldots, \mathbf{x}_N] \in \mathbb{R}^{N \times 2}$, where $\mathbf{x}_i = (D_i, I_i)$ and

40

(D_i, I_i) are the duration and intensity of MHW event i, respectively. Each data point can now be considered as data obtained when the temperature reaches the peak of the corresponding MHW event.

We can now apply GCS-CCA to the input MHW data. A total of 63 MHW events with associated duration and intensity are extracted from the selected SST time series. Figure 2.13 shows the duration and intensity values considering all the MHW events extracted over the period of measurements (1982-2020) in the selected northwest Atlantic region. The time series trend indicates non-stationary characteristics in the duration and intensity of the MHWs. In this case study, we focus on the changing pattern of duration and intensity of an MHW, although occurrence of MHWs is getting more frequent as well. To address this non-stationary process which has a changing occurrence rate of the extreme event of interest, we need to consider a non-homogeneous Poisson process and associated theory of waiting time. We will discuss this issue in Section 2.4.

Figure 2.14 shows two marginal histograms and a scatter plot showing the dependence structure of duration and intensity of MHWs. In Figures 2.13 and 2.14, 63 MHW events are divided into two groups: 1) those occurring before 2013-06-19 and 2) those occurring after 2013-06-19. By doing so, we seek to show the temporal connection between actual date and event numbers in Figure 2.13. Also, marginal histograms suggest they are shifting toward the right recently. This means that the duration and intensity of MHWs are getting more prolonged and more severe simultaneously. These also indicate

the non-stationarity of the pattern of MHWs.

Based on the physical meaning of duration and intensity and their histogram shapes, gamma and lognormal distributions are selected as marginal probability distributions for duration and intensity, respectively. The Clayton copula family is selected to model the pairwise dependence structure for these two variables.
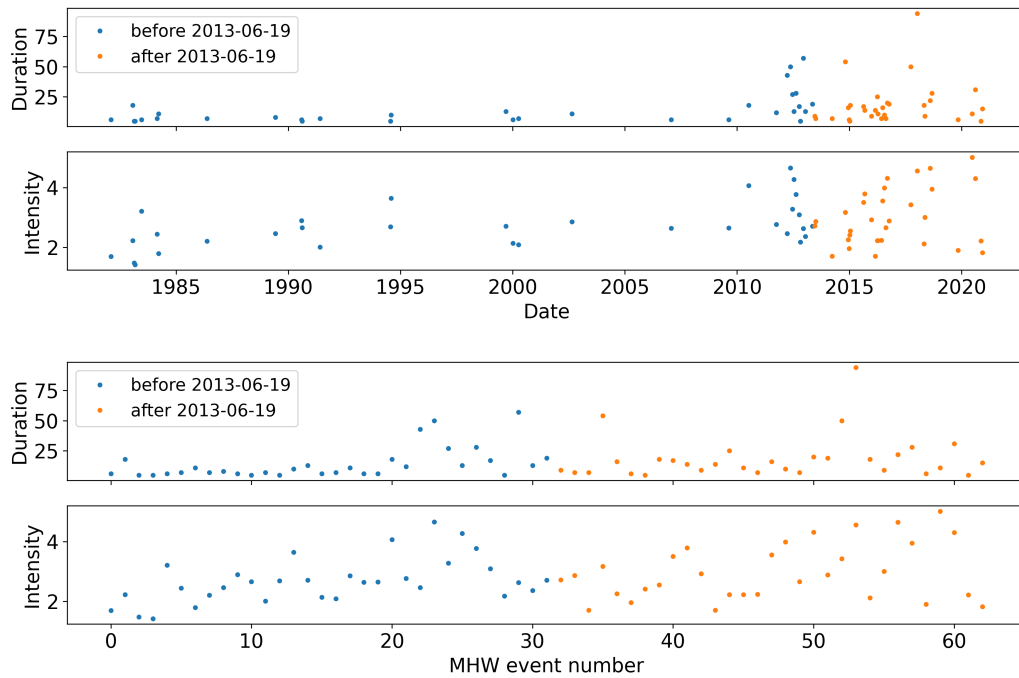
Figure 2.13: Duration and intensity values from 63 extracted MHW events. blue dots indicate data from before 2013-06-19 and orange dots indicate data from after 2013-06-19.

42
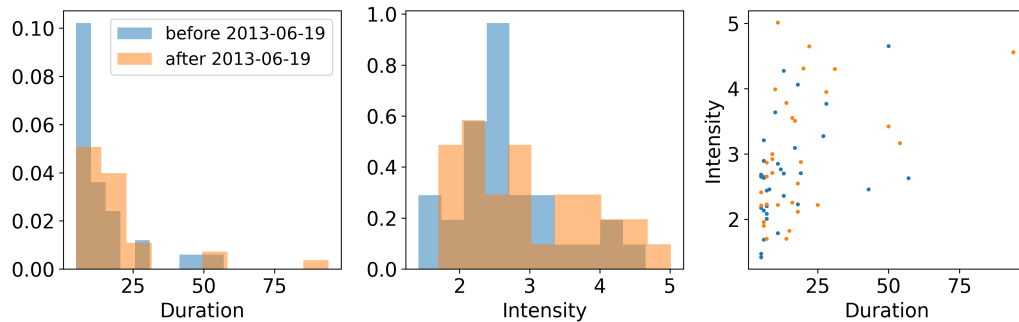
Figure 2.14: Marginal histograms and a scatter plot of the duration and intensity of MHWs. blue indicates MHWs that occurred before 2013-06-19, and orange indicates data from after 2013-06-19.

Due to the relatively short history of satellite remote sensing for sea surface temperature, the number of events and possible breakpoints that discriminate between two segments is less than for the benchmark problem in Section 2.2. Therefore, we consider one update cycle in projections to be used in possible climate change adaptation, where the GCS-CCA approach seeks to optimize justified use of only the most recent data. We design the virtual scenario in which we are at the end of 2016 and, thus, SST records from 1982-01-01 to 2016-12-31 containing 52 MHW events are available. A predictive performance evaluation of GCS-CCA versus a traditional one that ignores non-stationary trends has been carried out on the unseen test data from 2017-01-01 to 2020-12-31 containing 11 MHW events.

Figure 15 shows results summarized in terms of the mean predictive

log-likelihood difference ratio, M, which is defined as follows:

$$M\ (\%) = \frac{LL_{opt} - LL_{trad}}{|LL_{trad}|} \times 100. \qquad (2.10)$$

We can easily verify that GCS-CCA outperforms traditional CCA for sufficiently large λ values that range from 32 to 68. This finding suggests that GCS-identified optimal data sub-segments explain near-future MHW patterns better than when all of the historical observed data are used. Figure 2.15 shows that lower values of λ lead to oversegmentation while higher values makes GCS-CCA essentially equivalent to traditional CCA. Pre-processing of the data and application and selection of an appropriate regularization parameter is recommended for such analyses.
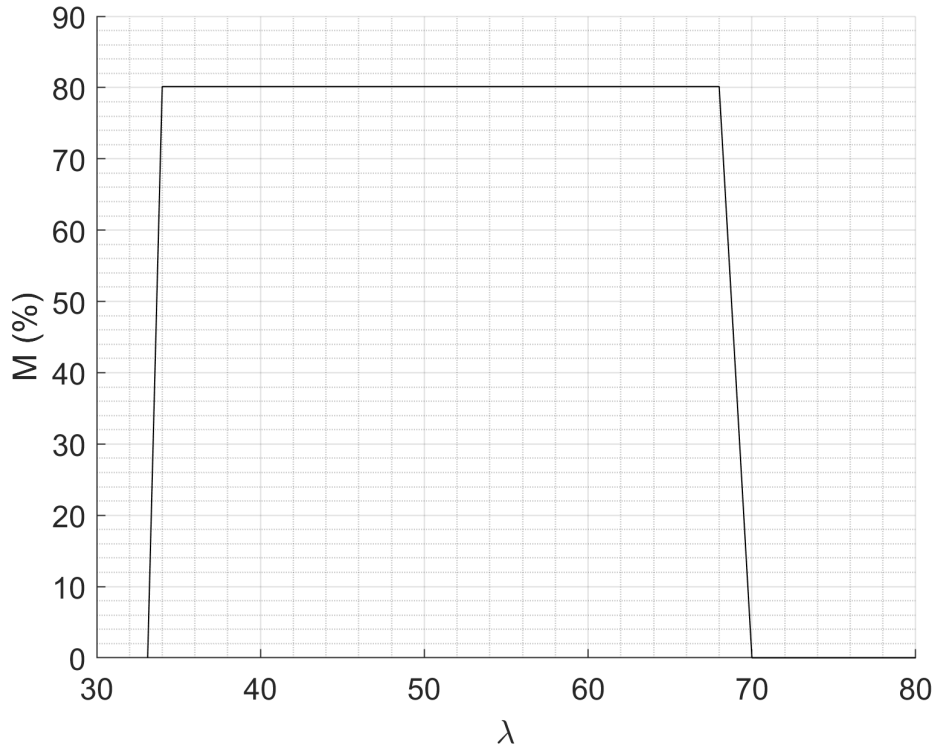
Figure 2.15: Calculated predictive log-likelihood difference ratio, M for the MHW data with different choices for regularization parameter, λ.

For all the λ values ranging from 32 to 68, GCS identifies the latest 45 MHW events as the optimal data for the near-future prediction. In other words, GCS suggests discarding the dated 7 MHW events without knowing the future. The model based on the pruned data explains the future better than the traditional one with all available data. Figure 2.16 compares the marginal distributions estimated using a Gaussian kernel with all data versus GCS-identified optimal data. A total of 11 MHW events in the test period are

shown together as green markers. It can be easily noted that discarding seven outdated events adequately shifts the marginal distributions to the right. The newly observed 11 MHW events are better explained by the GCS-identified optimal data based model.
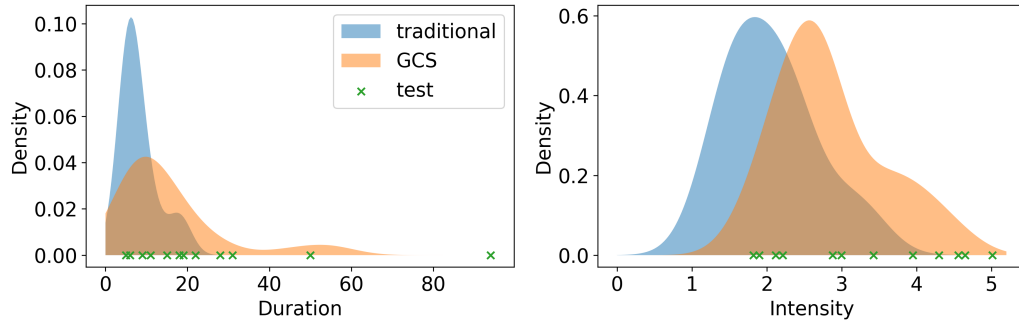
Figure 2.16: Marginal distributions estimated by Gaussian kernel with (blue) all available data and (orange) GCS-identified optimal data. Note that the 11 MHW events in the test period are shown as green markers.

All the computations were executed in MATLAB on a 64-bit Microsoft desktop computer with 6 Intel i7-9750H CPUs at 2.60 GHz and 32 GB of RAM. We compare CPU times for the predictive performance evaluations using the traditional CCA and the proposed GCS-CCA with $\lambda = 60$ (sufficiently large regularization). The computation was repeated 30 times to get the mean and standard deviation of CPU Time. Traditional CCA takes a mean of 0.07 seconds with a standard deviation of 0.12 seconds. GCS-CCA takes a mean of 3.5 seconds with a standard deviation of 0.7 seconds. Because GCS-CCA requires additional computation using the greedy segmentation algorithm, which

attempts to select the optimal segments out of a combinatorically large pool, GCS-CCA requires a greater amount of CPU time than traditional CCA. Nevertheless, GCS-CCA is still a fairly light computational exercise easily undertaken on a common laptop computer that was used in the experiments. While also considering the update cycle, it allows easy and efficient prediction of MHW patterns over a window covering the next 4 years.

2.4 Discussion

Patterns in extreme climate time series will continue to change due to inherent non-stationary characteristics as well as constantly changing anthropogenic influences. Figures 2.9 and 2.15 have clearly shown what can be learned by considering climate as a piecewise stationary process in decision-making for near-future prediction. Accurate data-driven prediction provides objective information to policymakers to aid in addressing disaster risk reduction (DRR) and climate change adaptation (CCA). A quantitative assessment of mitigation strategies based on GCS application can aid in CCA policy amendments; such strategies will depend on collaboration with domain experts from various disciplines including civil and environmental engineering, marine and geosciences, public affairs, management, and economics.

We have offered a validation of the proposed GCS-CCA methodology, highlighting its advantages in the context of single-site MHW events. GCS-CCA can easily be extended to apply to other types of disasters that are characterized by multiple climate variables. Since GCS-CCA is formulated

47

to work with multivariate data, analysis for multiple sites and/or for greater spatial coverage can readily be undertaken. By utilizing multivariate copulas, GCS offers the mathematical tractability to enable its use in general multivariate non-stationary time series. Human-induced variables that influence disaster risks can as well be incorporated along with climate-related variables for comprehensive near-future DRR and CCA.

One limitation of the proposed GCS-CCA methodology is the need for pre-processing of the data. The selection of regularization parameters in the assessment has been briefly discussed in Section 2.2.3. This selection choice will introduce more complexity when a high-dimensional space of variables must be considered. In addition, some basic domain knowledge is required to establish appropriate marginal distributions and copula families for the variables. If these are not available or otherwise known, model selection using criteria such as AIC, BIC, or cross-validation is unavoidable. To allow even more generalized formulation, non-parametric kernel density functions and non-parametric copula dependence structures may also be employed. Such options and decisions would then be model-free; however, interpretation of results should be done with care since nonparametric approaches can lead to greater error in extreme values when input data are insufficient.

2.5 Conclusions

In this work, we have utilized Greedy Copula Segmentation (GCS) extended from the Greedy Gaussian segmentation (GGS) algorithm developed

by Hallac (2019) by allowing multivariate Gaussian distributions in the copula definition [70]. This extension is well-suited for use with climate data since many climate-related variables are non-Gaussian and non-stationary. Based on the wide coverage of different dependence structures possible with the copula family choice, it is expected that GCS could be used in various applications that involve long sequences of multivariate time series data. We have explained GCS, iteration by iteration, so as to offer an accessible description of the greedy algorithm.

Using a synthetic data set as well as an observed marine heatwave (MHW) data set, we have shown that GCS can optimize future projections for possible use in climate change adaptation. Climate change adaptation needs to rationally consider periodic updates of the joint distribution of climate variables by focusing on patterns seen in extreme climate events. We introduce the notion of considering trends in any climate parameter as best understood by defining a piecewise process consisting of several stationary subsegments to represent the data. In such a piecewise stationary representation, the latest (most recent) stationary sub-segment (whose length must be iteratively established, using maximum likelihood with regularization) can predict most rationally and precisely any near-future patterns in the extreme climate that are to be expected. The proposed GCS approach identifies the most informative data sampled from the latest stationary sub-segment; it iteratively evaluates the benefit of further segmentation on the last segment. By doing so, the algorithm greedily searches for the optimal last segment of input data.

We show that the GCS-identified optimal data produce better predictive performance for possible climate change adaptation by illustrative examples using a benchmark synthetic data set as well as a real 39-year MHW data set from the northwest Atlantic ocean. GCS-CCA shows superior predictive performance for the non-stationary benchmark problem. For the real-world application, we collect sea surface temperature (SST) time series data and extract the bivariate MHW event (duration and intensity) data. The GCS-CCA results suggest that the proposed approach can rationally uncover changing climate patterns in the time series and can produce accurate near-future projection for adaptation plans compared to more traditional approaches that seek to use long or complete historical data sets. The outlined framework can be easily communicated to policymakers who are non-scientific experts. We expect that our model will reduce the gap between academia, researchers, and data scientists on the one hand and policymakers on the other. We also expect that the GCS-CCA framework can help towards achieving the Sendai framework goals by offering a rational approach to risk reduction in the face of non-stationary climate hazards.

Chapter 3

Assessing Fatigue Damage and Reuse of a Decommissioned Offshore Jacket Platform to Support a Wind Turbine: Time-Domain Studies

The text and figures from this chapter are presented in the ASME 2022 41st International Conference on Ocean, Offshore and Arctic Engineering (OMAE2022), June 5-10, 2022, Hamburg, Germany and submitted in associated journal, the Journal of Offshore Mechanics and Arctic Engineering (JOMAE)[1]

Taemin Heo, Ding Peng Liu, Lance Manuel, Jose AFO Correia, and Paulo Mendes. Sustainable reuse of decommissioned jacket platforms for offshore wind energy accounting for accumulated fatigue damage. In *International Conference on Offshore Mechanics and Arctic Engineering*, volume 85932, page V008T09A040. American Society of Mechanical Engineers, 2022

---

[1]TH designed and conducted the research, formulated the framework and analyzed the data, and wrote the manuscript.

ABSTRACT

An offshore energy transition, even if only a gradual one, from carbon-emitting fossil fuel extraction to cleaner sources is recommended, if we are to slow down the harmful impacts of climate change. The potential for sustainable reuse of decommissioned offshore jacket platforms to support wind turbines is being considered as an attractive proposition in such a transition. To maximize the benefits of such reuse of assets, what is needed is a rational optimization strategy that considers the remaining life of a repurposed platform, associated retrofit and construction costs, and a future period of gross renewable energy generation following installation of the wind turbine. We outline a study that employs a fatigue reliability-based framework, based on the global fatigue approach and Palmgren-Miner's rule, to aid in such sustainable reuse planning and optimization. The framework proposed identifies an optimized reuse plan that incorporates metocean data analysis, structural analysis, life-cycle evaluation, and revenue optimization. We employ a case study and sustainable reuse scenario for a site in the vicinity of Porto (Leixões), Portugal.

KEYWORDS

3.1 Introduction

Renewable energy generation devices such as offshore wind turbines (OWTs) and wave energy converters (WECs) have been deployed in offshore areas in aims toward achieving carbon neutrality. However, available sites for development are limited due to unfavorable environmental conditions or other uses of the marine space including for fishing activities and oil & gas production. Currently, there are over 4,000 offshore oil & gas production installations located in the Gulf of Mexico, accounting for 60% of such installations worldwide. Competition for marine space has motivated the need for research that examines the potential for reusing oil & gas platforms for renewable energy while, at the same time, offering a possibly economical and sustainable transition from fossil fuel to renewable energy [96]. Over the period from 2007 to 2017, between 100 and 290 structures were decommissioned annually [86]. Reuse of these structures, instead of dismantling them, is seen as a possible way to reduce the cost of decommissioning and provide additional benefits for renewable energy developers. Even though the cost of grid connection and maintenance for a single OWT might seem unprofitable, oil & gas platforms still have the possibility of being reused as support structures while seeking to develop wind farms in the same offshore space and environment where oil & gas platforms are now located. Given the large share of costs needed for each OWT support structure, towards the overall costs, the economic benefit of reusing oil & gas platforms is evident. Accordingly, allowing for some simplifying assumptions, we study revenues and costs associated with reuse of

53

a decommissioned platform during the design and operation phase of offshore wind projects.

Conventional decommissioning plans for offshore oil & gas facilities include the removal of all the components as part, sometimes, of efforts such as the Rigs-to-Reefs program [170]. In 2018, a study projected that the estimated cost of all platform decommissioning worldwide from 2018 to 2022 would exceed $38 billion [99]; very recent studies confirm this trend of increasing decommissioning. There have been various ideas proposed for reusing offshore facilities, including platforms, pipelines, reservoirs, and wells, with different new end uses/purposes. For example, reservoirs and pipelines with appropriate specifications are ideal for restoring pure CO_2. Offshore platforms can be repurposed for tourism or fishing activities, and even for renewable energy such as to support OWTs, WECs, or for wind-powered hydrogen generation [9]. Without the need for dismantlement, the decommissioning plan can be more cost-effective and can increase the financial value of these facilities. However, an assessment should be conducted to prove the feasibility and safety of any reuse plan. In 2017, Barros et al. [11] proposed a framework to evaluate the feasibility of a reuse plan, from choosing a target platform to estimating the cost of energy. Moreover, Quissanga et al. [138] conducted an in-place analysis for a wellhead platform with different types of wind turbines in a structural model. Nevertheless, more detailed environmental data studies and revenue optimization must be conducted to ensure the reliability and retrofit of any reuse plan.

In general, for such reuse projects, site-specific measurements may not be available, particularly during the early planning phase. A characterization of metocean states or environmental conditions is required in order to describe the wind and wave conditions as well as atmospheric and other relevant physical conditions of the ocean environment, which are part of the basis for the design of an offshore wind facility [43]. Metocean states for the planned application can best be described using a joint distribution of variables such as the wind speed, wave height and wave period [17, 19, 81, 100]. Several approaches have been proposed for joint metocean modeling [18, 20, 64, 66, 80, 111, 148, 172]. It is critical to evaluate site-specific environmental conditions in the design of offshore wind support structures. Therefore, at different stages in the life cycle of offshore wind structures, account must be taken of metocean conditions to ensure the appropriate level of safety and reliability. Site-specific conditions representative of the offshore wind site installation should, therefore, be taken into account in the project. Research studies are needed that allow a structural designer to evaluate the environmental loads, the dynamic characteristics of the structure, and the effect of changing the structural behavior and intended use of the original oil & gas platform. All these analyses should be available in the early design phase when data about the site's environment and seabed conditions are limited. Alessi et al. [3] proposed using the MATLAB or Strand7 software to simulate the effects of the wave kinematics; needed parameters were defined based on Stokes 5th order wave theory. Together with these parameters, Morison's equation can then be used to calculate

the hydrodynamic forces on the structure, as was also presented by Lesiuk et al. [97]. Mendes et al. [115, 116] offered a structural analysis methodology and retrofitting strategies for offshore jacket platforms supporting horizontal- and vertical-axis wind turbines.

Instead of using wind and wave spectra for specific wind speeds and significant wave heights as is done in conventional analyses, it is important to evaluate the long-term performance in all likely sea states as part of the metocean data analysis. Then, an analysis of a specific offshore wind structure and foundation can be done using available metocean data. Additionally, an assessment for the fatigue performance, in the time or frequency domain, considering variability in the sea conditions concerned should also be proposed. The calculation of local stresses at critical structural details should be evaluated while considering local fatigue damage parameters [33, 140]. Fatigue design codes have proposed the use of nominal, hot-spot and notch strain approaches to define the most appropriate S-N design curve of a considered structural detail. Recently, Correia et al. [34] presented an evaluation of fatigue design curves based on statistical analysis for a double-side welded connection used in offshore applications and a comparison with current codes was made. In this way, it is possible to evaluate the remaining life of a jacket-type platform for its new intended use to support the wind turbine, while taking into account the loading history of the structural elements in their previous use.

This study focuses on the reuse of an oil & gas platform to support an OWT. We separate the overall life cycle of the asset into two phases: OG

(Oil & Gas) and OWT (Offshore Wind Turbine). The design load cases for the two phases are different due to the characteristics of the operational situations. Therefore, the proposed framework for reuse assessment based on the metocean data analysis for long-term wind and wave conditions at a candidate site considers all the possible design load cases during both phases in the structural model for fatigue analysis, using the global fatigue approach and Miner's rule. The framework also involves a revenue optimization analysis according to different possible energy generation options. Using this framework, we demonstrate, with needed simplifying assumptions, how one can evaluate a platform's endurance over the life cycle and also assess the financial benefits and economic benefits of such a reuse plan. The paper is organized as follows. Section 3.2 introduces the proposed framework with details. Section 3.3 outlines a case study and sustainable reuse scenario for a hypothetical site near Porto, Portugal. Section 3.4 discusses assumptions made in the framework. Finally, Section 3.5 presents conclusions drawn and discusses possible directions for future investigation.

3.2 Methodology

The proposed framework is comprised of four steps: 1) metocean data analysis; 2) structural analysis; 3) life cycle evaluation; and 4) revenue optimization. In principle, one might consider different choices for the wind turbine rated power output for the planned sustainable reuse. For simplicity, in this work, we assume there are two candidate wind turbines—of 1.5-MW

and 5-MW rated power. Steps 1 to 3 are conducted separately for each candidate wind turbine, and an optimal plan is identified in Step 4 after comparing the options. In Steps 1 to 3, the life cycle evaluation of the jacket platform considers two phases: OG (Oil & Gas) and OWT (Offshore Wind Turbine). Using the National Renewable Energy Laboratory (NREL) software suite, OpenFAST, stochastic response simulations are conducted for the OG and OWT phases and fatigue damage is assessed at a single location on the jacket platform, selected to demonstrate the methodology.

3.2.1   Metocean Data Analysis

First, metocean statistics considering wind and wave conditions at the candidate site are analyzed using available data. Significant wave height, H_s, and wave period, T_p, characterize the wave conditions, while only the wind speed at 10 meters above the mean sea level, V_{10}, is used to describe the wind conditions. In the OWT phase, the wind speed, V_{hub}, at the hub height, z_{hub}, is usually preferred for assessing loads and power output. Thus, V_{10} is extrapolated to V_{hub} using an assumed wind profile power law relationship:

$$V_{hub} = V_{10} \left(\frac{z_{hub}}{10} \right)^{\alpha}, \tag{3.1}$$

where the power-law exponent, α, in general, depends upon the stability of the atmosphere as well as underlying surface characteristics. Hsu et al. [74] found that near-neutral stability conditions prevail at sea; thus, $\alpha = 0.11$ is considered in this work.

58

The expected fatigue damage over the entire life cycle accounts for the accumulated damage over all the possible metocean states, each defined by the triad, (H_s, T_p, V_{hub}) during the OWT phase and by (H_s, T_p) during the earlier OG phase. It is computationally expensive to account exhaustively for all the metocean states. Because this study is conducted largely to outline the framework for an OG-OWT reuse plan, we select a subset of representative states in our assessment. For the selected wind turbine, we consider different V_{hub} values corresponding to its operating range of wind speeds. Figure 3.1 shows how, for a typical wind turbine with variable speed and pitch control, power is generated at wind speeds below and above the rated wind speed, V_{rated}. Operation is not assumed for extreme winds greater than $V_{cut-out}$; these are, of course, rare conditions when addressed in a fatigue reliability analysis. In this study, wind loads where $V_{hub} \geq V_{rated}$ are all represented by those for $V_{hub} = V_{rated}$; this is admittedly a simplifying assumption made only to limit computation. Note that for wind speeds below V_{cut-in}, no power is generated but loads can result and such low winds occur often; loads at all such low wind-speed conditions are represented by loads computed at one-half of the cut-in speed. Along with these very high and very low winds, we divide the operating wind speed range into two bins:

$$V_{cut-in} \leq V_{hub} < V_{50\%},$$

$$V_{50\%} \leq V_{hub} < V_{rated}, \tag{3.2}$$

where $V_{50\%} = \frac{V_{cut-in} + V_{rated}}{2}$. We also select two other wind speed levels,
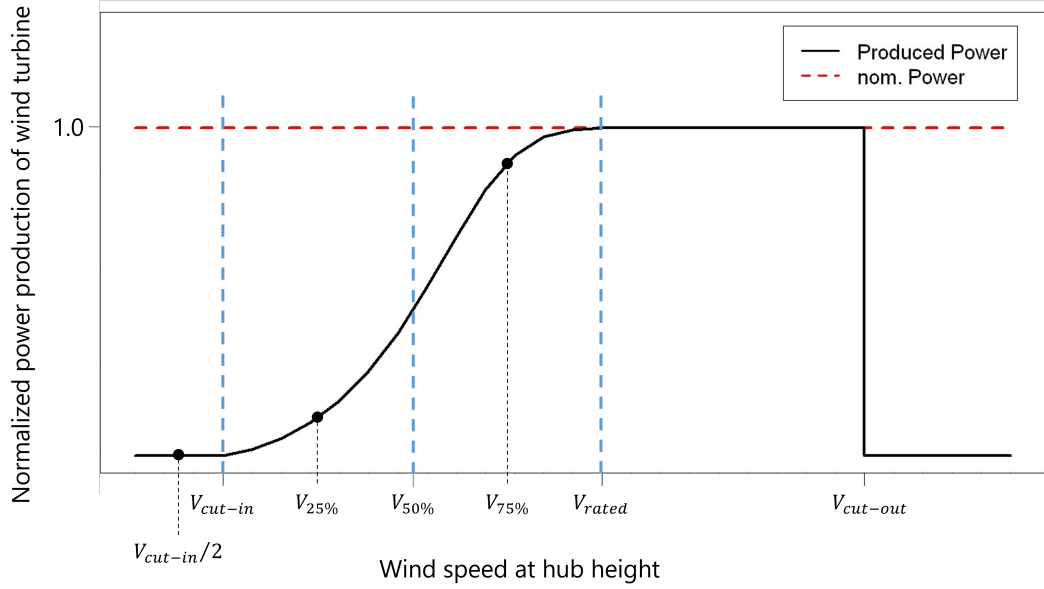
Figure 3.1: A power curve for a typical wind turbine with four wind speed bins defined over the operating range of wind speeds

$V_{25\%}$ and $V_{75\%}$, such that:

$$V_{25\%} = \frac{V_{cut-in} + V_{50\%}}{2},$$
$$V_{75\%} = \frac{V_{50\%} + V_{rated}}{2}. \tag{3.3}$$

Based on the wind speed binning described, we consider four subsets of conditions for analysis:

$$X_1 \equiv \{(H_s, T_p, V_{hub}) : V_{hub} < V_{cut-in}\},$$
$$X_2 \equiv \{(H_s, T_p, V_{hub}) : V_{cut-in} \leq V_{hub} < V_{50\%}\},$$
$$X_3 \equiv \{(H_s, T_p, V_{hub}) : V_{50\%} \leq V_{hub} < V_{rated}\},$$
$$X_4 \equiv \{(H_s, T_p, V_{hub}) : V_{hub} \geq V_{rated}\}, \tag{3.4}$$

60

where the metocean data for the site are assumed to be drawn from unknown joint distributions for the wind and wave variables. We estimate four subset joint distributions by utilizing multiplicative kernel density functions. For bin X_k, the joint probability density function is:

$$\hat{f}_k(H_s, T_p) = \frac{1}{n_k h_{k1} h_{k2}} \sum_{i=1}^{n_k} \left(K\left(\frac{H_s - H_{s,i}}{h_{k1}}\right) \cdot K\left(\frac{T_p - T_{p,i}}{h_{k2}}\right) \right), \qquad (3.5)$$

where n_k represents the number of elements in X_k; $(H_{s,i}, T_{p,i})$ are metocean (wave) parameters for elements in X_k; K is the selected non-negative kernel density function; and $h_{k1}, h_{k2} > 0$ are smoothing parameters that define the kernel bandwidth. We select the Gaussian kernel in this work; bandwidth size is estimated using Scott's rule, so that $h_{k1} = \sigma_{H_s} \cdot n_k^{-1/6}$ and $h_{k2} = \sigma_{T_p} \cdot n_k^{-1/6}$, where σ_{H_s} and σ_{T_p} are the marginal sample standard deviations based on the data in X_k [152]. For the OG phase, we do not consider wind data. Thus, we analyze all of the collected data, $X = X_1 \cup X_2 \cup X_3 \cup X_4$, to obtain the joint density function, $\hat{f}(H_s, T_p)$, using Eq. 3.5.

From the established joint distribution for the OG phase, $\hat{f}(H_s, T_p)$, we select 24 representative sea states, (H_s, T_p), to adequately cover the entire domain of sea states. To do this, two principal components of the bivariate data are identified. The first component with larger variance is divided into eight intervals, each with an equal (i.e., one-eighth) probability when considered in the marginal component distribution. Similarly, the second component is divided into three intervals. Together, this division yields a total of 24 non-overlapping metocean condition subsets. Representative (H_s, T_p) pairs are then selected

from these 24 regions based on computed joint density-weighted centers. Figure 3.2 presents a schematic illustration showing how the representative sea states are selected. The effectiveness of using principal components instead of the original variables, (H_s, T_p), can be visually assessed upon comparing Fig. 3.2(a) and 3.2(b). Division using the original coordinates would yield less meaningful grid cells, such as at the right bottom corner of Fig. 3.2(a) (i.e., a high H_s and low T_p region). Whereas Fig. 3.2(b) shows that the grid based on principal components efficiently covers the body and tail. As a result of this binning exercise, we have a total of 24 representative metocean states for the OG phase and $24 \times 4 = 96$ representative metocean states for the subsequent OWT phase (the same 24 sea states, with 4 different representative V_{hub} values in each case). To facilitate future discussion, we define indices, $i = 1, \ldots, 24$ and $j = 1, \ldots, 96$, to indicate the metocean states selected for the two phases in our assessment.

3.2.2 Structural Response

Next, we discuss the structural response assessment for the jacket structure with the oil & gas platform on its own as well as with a supported wind turbine atop. Representative hot spots—critical locations at the weld toes (or weld ends) on a jacket platform members where fatigue cracks can initiate [121]—are of interest. Without loss of generality, we assume there is a hot spot of interest located at the same point of the jacket structure that governs fatigue failure for both the OG- and OWT-phase structural systems. Recall
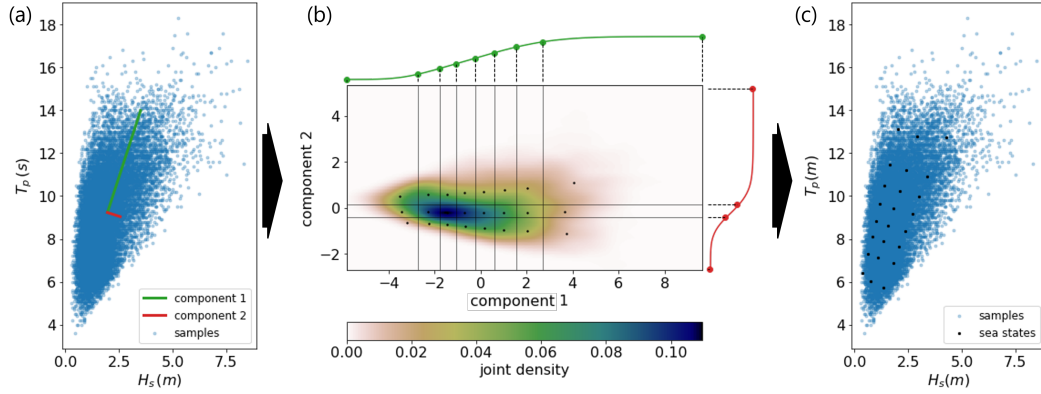
Figure 3.2: Procedure for selection of representative metocean states: (a) identification of principal components; (b) divided transformed domain onto 8-by-3 iso-probabilistic (marginal) grid; (c) inverse transformation identifying the selected representative states

that we are only considering the possible use of two candidate wind turbines— of 1.5-MW and 5-MW ratings—in the OWT phase. For the stochastic loading, we use the Kaimal wind spectrum [85, 173] and the Joint North Sea Wave Project (JONSWAP) wave spectrum [41]. Then, time-domain dynamic response simulations for three different structural configurations (OG, 1.5-MW OWT, 5-MW OWT) are conducted using OpenFAST. We run one-hour simulations of the OG jacket structure for all the 24 representative sea states to obtain the stress time series at the hot spot of interest. For the same duration, aero-hydro-servo-elastic simulations are next carried out for the OWT phase (with 1.5-MW and 5-MW turbines) where 96 representative metocean states are analyzed.

3.2.3 Life Cycle Evaluation

We assume that a peak and following trough together define a half cycle when we assess damage and fatigue life using Palmgren-Miner's rule [117]. Estimates of the stress range, S, are used to compute damage. The total fatigue damage represents an aggregation of damage from all the representative metocean states. For the OG phase, the expected damage is computed as:

$$E[D] = \sum_i E[D_i] = \sum_i \frac{\nu_{0,i}^+ p_i T}{c} SCF^b E[S_i^b] \qquad (3.6)$$

where $\nu_{0,i}^+$ is the zero upcrossing rate (in s^{-1}) of the underlying stress process and p_i is the fraction of time accounted for by the ith metocean state. These are both used to account for the number of half cycles in duration, T, as $N_i = 2\nu_{0,i}^+ p_i T$. Note that c and b are Basquin or equation constants, respectively, the intercept of the mean S-N curve with the $\log N$ axis and the negative inverse slope of the S-N curve, describing the applicable S-N curve for the structural detail of interest. Also, $N_f = cS^{-b}$, relates the amplitude of the stress range, S, with the number of cycles to failure, N_f [25, 49]. Also, SCF is the stress concentration factor for the selected hot spot.

The expected total fatigue damage in the OWT phase can be similarly calculated as:

$$E[D] = \sum_j E[D_j] = \sum_j \frac{\nu_{0,j}^+ q_j T}{c} SCF^b E[S_j^b]. \qquad (3.7)$$

In Eqs. 3.6 and 3.7, we empirically estimate $\nu_{0,i \text{ or } j}^+$ and $E[S_{i \text{ or } j}^b]$ directly from the simulated stress time series at the hot spot. Additionally,

$\nu_{0,i \text{ or } j}^+$ estimates are obtained by counting the number of zero upcrossings of each stress time series in the simulated hour or 3,600 seconds. To compute $E[S_{i \text{ or } j}^b]$, we make use of the rainflow cycle-counting algorithm applied to the stress ranges [147].

Note that p_i can be computed as follows:

$$p_i = \iint_{\Omega_i} \hat{f}(H_s, T_P) dH_s dT_p \tag{3.8}$$

where Ω_i is the domain represented by the ith metocean state. A similar approach applies for the OWT phase, so that $N_j = 2\nu_{0,j}^+ q_j T$ where

$$q_j = \int_{\Psi_j} \hat{f}(V_{hub}) dV_{hub} \iint_{\Omega_j} \hat{f}_k(H_s, T_P) dH_s dT_p, \tag{3.9}$$

Ψ_j is the domain represented by $V_{hub,j}$, while Ω_j is the domain represented by $(H_{s,j}, T_{p,j})$; also, $\hat{f}(V_{hub})$ is an estimated marginal distribution for V_{hub} using the Gaussian kernel with the wind data.

The fatigue damage, D can be considered approximately Gaussian due to the short half-cycle length compared with the exposure time, T, and assuming that the central limit theorem applies [37]. Assuming that the wave spectra are narrow-banded and that wave loads have a dominant influence on the jacket platform response, relative to the more broad-banded wind spectra, the coefficient of variation (CoV) of D, C_D, is derived as [16]:

$$C_D = \sqrt{\frac{N + 2\chi}{N^2} \left(\frac{\Gamma(1 + b)}{\Gamma^2(1 + b/2)} - 1 \right)},$$
$$\chi = \sum_{k=1}^{N-1} (N - k) \rho_{d_0 d_k}, \tag{3.10}$$

where N is the total number of half cycles and $\rho_{d_0 d_k}$ is the auto-correlation function of the stress process at lag k. As discussed in another study dealing with fatigue damage and associated uncertainty [104], for large N, χ is roughly proportional to N because the number of effective terms in the summation is largely defined by the fast decay rate of $\rho_{d_0 d_k}$. Effectively, then, C_D is inversely proportional to $\sqrt{N}$. We assume in this study that C_D is small due to the relatively large value, $N = 2\nu_0^+ pT$, resulting from the high-frequency zero upcrossing rate and the long exposure time implied by the long life cycle considered. As a consequence of these assumptions, the total fatigue damage is represented using the expected value alone, without uncertainty. It is possible to account for uncertainty in damage estimation in a more comprehensive analysis as described in other studies [104], but this is not done here, because the main objective is to offer a framework for assessing reuse of OG facilities for an OWT.

The limit state function to evaluate fatigue failure in the OG phase may be defined as follows:

$$g(\Delta, c, SCF) = \Delta - E[D] = \Delta - \sum_i E[D_i] \tag{3.11}$$

where Δ is the level or threshold of accumulated damage at which failure occurs. Note that $\Delta = 1$ corresponds to failure but variability in Δ is introduced to account for uncertainty in Palmgren-Miner's rule—e.g., due to load sequence effects [174]. Note that $E[D_i]$ is stochastically related to the S-N curve parameters, b and c, as well as to SCF. In this study, we only

account for variability in one S-N curve parameter, c; variability in b can, in general, also be considered in a more comprehensive analysis. The effect of uncertainty in SCF is inherent in the computation of σ_{Y_i}. Finally, Eq. 3.11 can be rewritten to account for time in service, T, in any phase. A time- or exposure-dependent limit state function is introduced in terms of random variables, $\boldsymbol{\theta} = (\Delta, c, SCF)$, as follows:

$$g(T; \boldsymbol{\theta}) = \Delta - \frac{T}{c} SCF^b \sum_i \nu_{0,i}^+ p_i E[S_i^b] \tag{3.12}$$

where $T = \{1, 2, \ldots, t_{reuse}\} \times 365 \times 24 \times 3600$ (in seconds) and t_{reuse} is the age in years of the jacket platform when it is repurposed. The time-dependent limit state function for the subsequent OWT phase is then:

$$g(T; \boldsymbol{\theta}) = \Delta + \Delta_{\text{retrofit}} - \frac{t_{reuse}}{c} SCF^b \sum_i \nu_{0,i}^+ p_i E[S_i^b] - \frac{T}{c} SCF^b \sum_j \nu_{0,j}^+ p_j E[S_j^b] \tag{3.13}$$

where $T = t_{reuse} + \{0, 1, 2, \ldots\} \times 365 \times 24 \times 3600$ (in seconds). Here, Δ_{retrofit} is the increase in fatigue capacity resulting from any retrofit or structural improvement before the wind turbine is installed. In evaluations such as the one undertaken here for repurposing a jacket platform, a fracture mechanics-based fatigue reliability analysis is arguably more appropriate since it deals with crack growth, which can be measured any time and especially between the OG and OWT phases. This allows one to estimate the remaining life based on crack size and geometry following an inspection. Relating retrofit action to $\Delta_{retrofit}$ is also more straightforward. Future studies are planned to

67

formulate the presented framework based on a fracture mechanics approach. Note that there are other retrofit options that must be considered that are not all related to the accumulated fatigue damage but depend rather on the economics and life cycle evaluation. Alessi et al. [3] introduced two examples of structural retrofit options: 1) a crown pile configuration that places additional piles at the mid span of each side of the base of the platform; and 2) a mooring line system that links the midspan horizontal plane point of the jacket to the seabed. Such retrofit options would, of course, change the structural configurations and reduce the dynamic response from wind and wave loading.

Finally, the time-dependent fatigue failure probability, $P_f(T)$, and related reliability indices, $\beta(T)$, are computed using Monte Carlo Simulation (MCS) with random samples drawn for $\boldsymbol{\theta} = (\Delta, c, SCF)$. Based on N_{MCS} simulations, $P_f(T) = n(g(T; \boldsymbol{\theta}) < 0)/N_{MCS}$ and $\beta(T) = \Phi^{-1}(1 - P_f(T))$ where $n(A)$ is the number of elements in set A and $\Phi^{-1}(.)$ is the inverse cumulative distribution function (CDF) of a standard normal variable. Figure 3.3 shows a conceptual illustration of a life cycle evaluation using time-dependent reliability indices. The expected period of wind energy production t_{energy} is the longest time interval, following the OG-to-OWT transition, for which $\beta(t_{energy}) > \beta_{allow}$. We denote the expected wind energy production period for the two candidate wind turbines as $t_{energy,1.5-MW}$ and $t_{energy,5-MW}$.
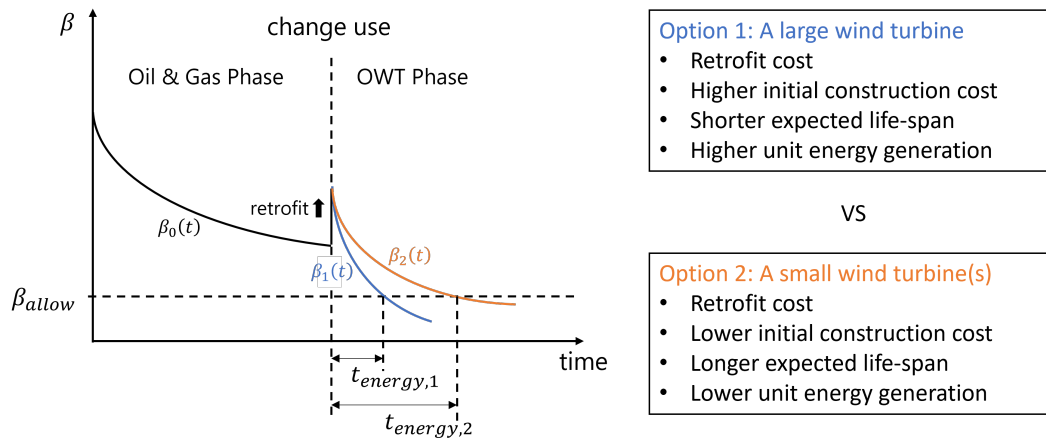
Figure 3.3: A conceptual summary of life cycle evaluation of a jacket platform for changed use from OG to OWT

3.2.4 Life Cycle Evaluation and Optimization

Based on the planned use and time of service in the two phases, capital expenditure (CapEx), operational expenditure (OpEx), and net annual energy production (AEP_{net}), an optimal design choice that maximizes overall revenue is identified in this last step. The general idea in such a revenue optimization is summarized in Fig. 3.3. For the two candidate wind turbines, expected life cycles for an acceptable reliability are different. It is reasonable to assume that a larger wind turbine will involve a higher a CapEx and OpEx than a smaller wind turbine. However, the gross energy production cannot be easily compared because this higher AEP_{net} is also associated with a shorter life cycle. Therefore, gross energy generation should be projected by multiplying AEP_{net} with the expected life cycle.

69

In this study, we assume that no new grid connection system is needed in the OWT phase. We assume too that the sustainable reuse plan can save some portion of general CapEx associated with wind turbine installation by reusing the decommissioned platform, compared to that for a normal OWT installation. On the other hand, there is additional expenditure needed for the retrofit. Let us denote the saved expenditure as SavEx and the retrofit cost as RetEx. In addition to the retrofit cost, we need to consider expected failure costs that will be incurred if fatigue failure results before the intended service life has passed. Any failure of the structure will lead to loss of residual value of the structure, StrVal. Finally, the cost of energy (CoE) associated with sustainable reuse can be written as:

$$\text{CoE} = \frac{\text{CapEx} - \text{SavEx} + \text{RetEx} + \text{OpEx} + \text{StrVal} \cdot P_{f,early}}{\text{AEP}_{\text{net}} \cdot t_{energy}} \tag{3.14}$$

where AEP_{net}, t_{energy}, CapEx, SavEx, RetEx, OpEx and StrVal are wind turbine candidate-specific quantities, each defined earlier, and $P_{f,early}$ is the number of simulations that failed earlier than t_{energy}, divided by N_{MCS} (i.e., $P_{f,early} = n(g(t_{energy}; \boldsymbol{\theta}) < 0)/N_{MCS}$). A higher CoE indicates that we need greater investment to generate the same amount of energy. Therefore, a candidate with the lowest CoE is the best option that maximizes the overall revenue associated with the sustainable reuse.

For a more comprehensive optimization, the economic and structural details that will relate cost to an associated increase in reliability must be considered as one assesses retrofit options. Retrofit options can also affect

70

the life cycle evaluation since they directly impact the stress response transfer functions (and resulting fatigue damage) considered in the OWT phase. In addition, various other considerations such as interest rates, corporation taxes, and depreciation play a role in influencing the overall revenue and selected plan. Due to complexity in project-specific details, retrofit and financing options are not considered in this study.

3.3 Case Study

An offshore site near Leixões—one of Portugal's major seaports, located north of Porto, Portugal—is selected as the hypothetical site where the study jacket platform is located. For the jacket structure, we use the OC4 jacket support structure [83, 137]. To demonstrate the reuse evaluation methodology, the WindPACT 1.5-MW baseline wind turbine [109] and the NREL offshore 5-MW baseline wind turbine [83] are selected to represent two candidate wind turbines for this site. Both wind turbines are assumed to have the same hub height = 90 m, with V_{cut-in}= 3 m/s, V_{rated} = 11.4 m/s, and $V_{cut-out}$ = 25 m/s, similar to 5-MW reference [83]. Metocean data from 2008 to 2019 are collected from the Portuguese Institute of Sea and Atmosphere (IPMA) and the V_{10} data are extrapolated to V_{90} and presented in Fig. 3.4 along with the metocean wave data. The estimated marginal probability density function (PDF) for V_{90} is presented in Fig. 3.5, along with the four selected bins and associated wind speeds defined earlier. A total of 24 representative sea states with 4 hub height wind speeds and associated p_i and q_j values are estimated
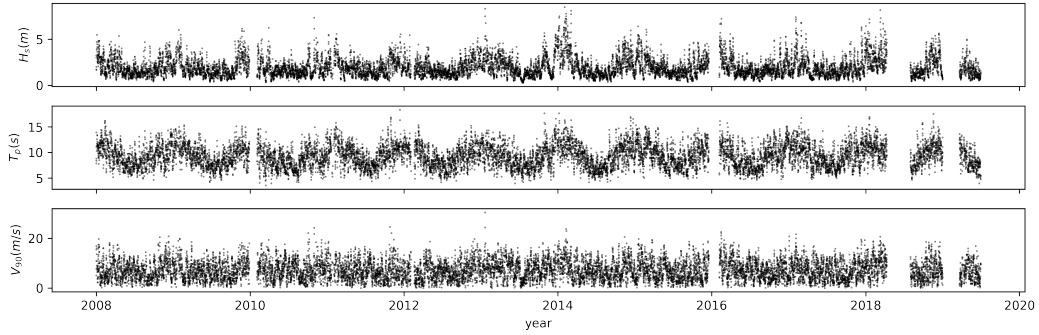
Figure 3.4: Collected metocean data for the hypothetical site in Porto, Portugal

as discussed before. We select the axial stress in a leg at the mudbrace level as the hot spot of interest only for the sake of demonstration of the framework and methodology.

For the life cycle economic evaluation, we assume that the 3 random variables, (Δ, c, SCF), are independent. Note that Δ is assumed to follow a triangular distribution with a lower limit of 0.5, an upper limit of 2.0 and a mode of 1.0 [174]. Also, c is assumed to be normally distributed random variable with mean of $10^{11.764}$ and a coefficient of variation (CoV) of 0.6 [41]. Lastly, SCF is assumed to follow a lognormal distribution with a mean of 3.5 and CoV of 0.1 [174]. In this study, $b = 3$ is selected. We assume that Δ_{retrofit}, which represents an enhancement in fatigue capacity following retrofit, is equivalent to 30% of the accumulated damage during the OG phase. Figure 3.6 shows time-dependent fatigue reliability indices for $t_{reuse} = 30$ years. Assuming a minimum permissible reliability index of 2.0 to define the end of
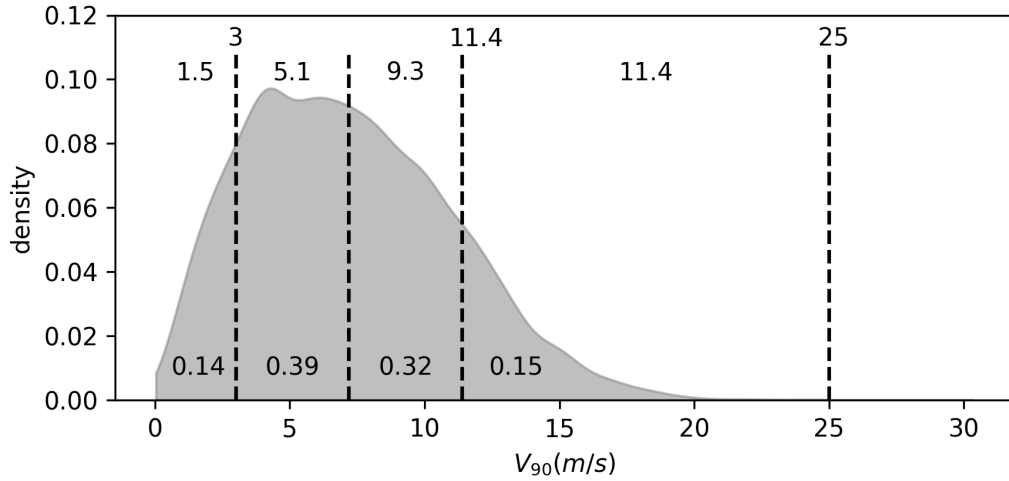
Figure 3.5: Estimated PDF for V_{90}, shown with 4 selected wind speed bins and representative wind speeds (top) and probabilities (bottom)

safe life cycle in reuse state, the two candidate wind turbines' acceptable life cycle values are $t_{energy,1.5-MW} = 17$ years and $t_{energy,5-MW} = 1.4$ years. The early failure probability, $P_{f,early}$, is also calculated; it has a low value of 0.024 for all the cases with the two OWT candidates.

Note that, based on trade-off considerations that developers might explore, a lower reliability index may be justified that would allow a longer service life because it might be argued that OWT platforms are considered as unmanned platforms with a lower exposure category L-2 according to API RP 2A-WSD [76]. As well, the proposed framework is general enough to be applied even for projects requiring a more conservative design and/or ineffective retrofit enhancements in fatigue capacity.
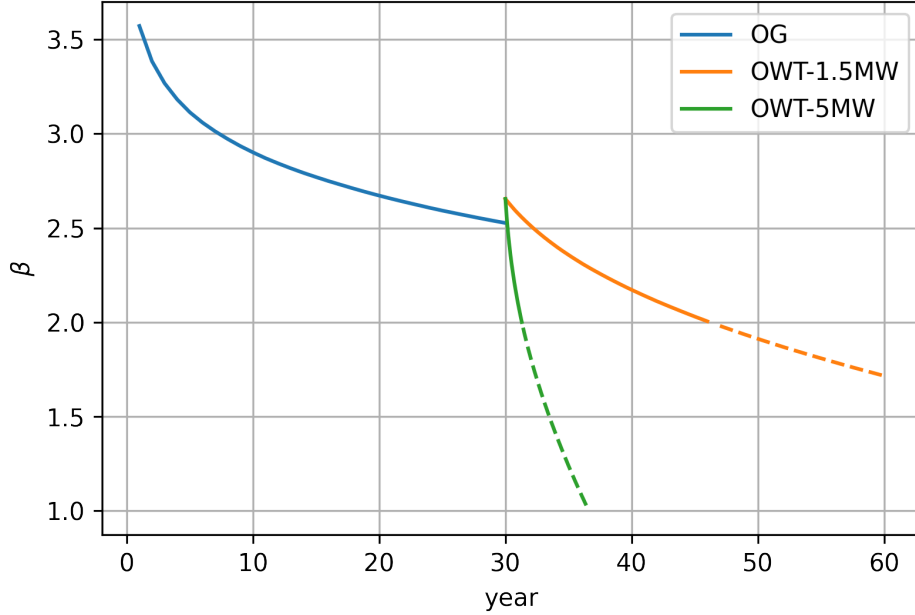
Figure 3.6: Life cycle evaluation for two candidate turbines: 1) the WindPACT 1.5-MW baseline wind turbine and 2) the NREL offshore 5-MW baseline wind turbine.

Finally, an optimal plan is identified using NREL's 2019 cost of wind energy review [163]. We assume that reported cost data from the summary of that work, for a fixed-bottom reference project using 6.1-MW wind turbines with a monopile substructure, can be used here, for reference. In general, however, better matching site-specific and project-specific information will help. All the data reported are in 2019 US dollars. With the assumed data, figures for this study are summarized in Table 3.1. Inserting these into Eq. 3.14 yields CoE estimates for both OWT candidates for all of the five cases. These results

Table 3.1: Reference data for revenue optimization and evaluated Cost of Energy (CoE).

	1.5-MW	5-MW
CapEx	$6M	$20M
SavEx	$1.2M	$4M
RetEx	$0.6M	$2M
OpEx	$0.18M	$0.6M
StrVal	$1.8M	$6M
$P_{f,early}$	0.024	0.024
AEP_{net}	6,400 MWh/yr	21,350 MWh/yr
t_{energy}	17 yr	1.4 yr
CoE	$ 51.6 /MWh	$ 627 /MWh

are summarized in Table 3.1. From these results, we conclude that, overall, the 1.5-MW OWT option is a preferred choice over the 5-MW OWT.

3.4 Discussion

The proposed framework has some acknowledged limitations in accuracy mainly due to the assumptions made to facilitate all the computations. Under our assumptions, 1-hour time-domain simulation took approximately 10 hours by OpenFAST. In this study, we analyzed 24 sea states in the OG phase and 96 metocean states in the OWT phase for each wind turbine candidate. Running these 216 (24 + 96 + 96) simulations serially will take 2160 hours = 90 days. We utilized a high performance computing machine that allowed us to run 24 simulations concurrently. As a result, all simulations can be done in 108 hours = 4.5 days. We summarize all assumptions and their

75

justification/limitations. While doing so, we also suggest exercising caution in using the proposed framework in similar studies.

First, we used only a limited number of metocean states to represent a continuous and complex domain defining various combinations of environmental conditions involving wind and waves. Accuracy in such evaluations increases as more sea states cover the space, but computational costs will increase as well. It would be useful to assess what would be the optimal number of states one should use in such studies. In addition to the number of representative metocean states, how to select them can also affect the findings. This study utilized an iso-probabilistic grid in a principal component space; other approaches such as the use of importance sampling and low-discrepancy sampling could be considered as well in evaluating accuracy and computational efficiency.

Second, we assumed that the hot-spot stress of interest may be described as a stationary random process. These assumptions can be relaxed by the use of evolutionary power spectral density functions and other time series analysis techniques such as with a hidden Markov model or a Markov switching autoregressive model, but these effects are not expected to be significant for the duration (1 hour) of the time-domain simulations. Other considerations such as that of climate change and aging could, on the other hand, influence non-stationary characteristics; these are not considered in the present study. It is possible to take these into account in the metocean data analysis. Active research efforts are underway that can help in selecting metocean states

that consider climate change and temporal correlation patterns in climate processes [65, 107]. For offshore structures, corrosion can lead to aging and changes in structural properties. The DNVGL-RP-C203 standard addresses this issue by proposing two stages for S-N curves in seawater with cathodic protection [42]. The proposed S-N curves adopt different c and b values when the number of cycles exceeds 10^6 considering the corrosion effect in seawater. Such modifications are also not introduced in the present work.

This study used standard Kaimal and JONSWAP spectrum for generating input wind and wave time series. Other models can also be justified and would introduce model uncertainties in the input load spectrum [110, 135, 173]. As suggested by Solari [161], model uncertainties can be included by considering spectral parameters as random variables. In addition to model uncertainties, system reliability evaluations that consider multiple hot spots in the structure can be additionally included in a fatigue reliability-based life cycle evaluation [184]. Several theoretical and computational assumptions are imposed in OpenFAST for the time-domain simulation. The assumptions are briefly listed following, and a detailed explanation can be found in reference [84]. Irregular and long-crested (unidirectional) wave is assumed, and the effect of current is ignored. Wave kinematics are only computed in the domain between the flat seabed and still-water level without wave stretching. First-order (linear Airy) wave theory and strip-theory (Morison's) solution for calculating the hydrodynamic loads on a structure are used. For the inflow wind, Taylor's frozen turbulence hypothesis is assumed to translate wind de-

fined in two-dimensional planes into three spatial dimensions, using the mean wind speed as the advection speed. Three-dimensional flow around a structural body is approximated by local two-dimensional flow at cross sections, and distributed pressure and shear stress are approximated by lift forces, drag forces, and pitching moments lumped at a node in a two-dimensional cross section. Analysis nodes are distributed along the length of each blade and tower. Forces and moment at each node are computed as distributed loads per unit length, and the total three-dimensional aerodynamic loads are found by integrating the two-dimensional distributed loads along the length.

Finally, the revenue optimization study presented was simplified. A more comprehensive optimization problem can be formulated with additional detailed retrofit and financing options. This would require site- and project-specific economic and structural information. Useful details and databases that are publicly available in reports and models [13, 47, 119, 163] can be employed in such evaluations.

3.5 Conclusions

In this work, we have formulated a fatigue reliability-based framework, based on the global fatigue approach and Palmgren-Miner's rule, for assessing the expected life cycle of a repurposed jacket platform that takes into consideration the overall revenue associated with sustainable reuse of the platform to support an OWT. Based on the estimated life cycle of the candidate wind turbines, each option's gross wind energy generation is calculated and com-

pared with expenditures to evaluate the cost of wind energy. The candidate OWT leading to lower costs in generating energy is chosen to define an optimal plan for the reuse. A case study for a site in Porto (Leixões), Portugal, was used to demonstrate the entire procedure that extended from metocean data analysis to revenue optimization. Our proposed framework can be employed in actual sustainable reuse projects. With site- and project-specific information, the framework can be readily advanced to consider more detailed and complex issues that one must deal with in sustainable reuse of offshore platforms.

Chapter 4

Weather Window Analysis in Operations and Maintenance Policies for Offshore Floating Multi-Purpose Platforms

The text and figures from this chapter are presented in the ASME 2022 41st International Conference on Ocean, Offshore and Arctic Engineering (OMAE2022), June 5-10, 2022, Hamburg, Germany and accepted in associated journal, the Journal of Offshore Mechanics and Arctic Engineering (JOMAE)[1]

Taemin Heo, Ding Peng Liu, and Lance Manuel. Stochastic weather window analysis in operations and maintenance planning policies for offshore floating multi-purpose platforms. In *International Conference on Offshore Mechanics and Arctic Engineering*, volume 85888, page V004T05A019. American Society of Mechanical Engineers, 2022

---

[1]TH designed and conducted the research, formulated the framework and analyzed the data, and wrote the manuscript.

ABSTRACT

In an emerging "blue economy," the use of large multipurpose floating platforms in the open ocean is being considered. Such platforms could possibly support a diversified range of commercial activities including energy generation, aquaculture, seabed mining, transport, tourism, and sea-based laboratories. A Markov Decision Process (MDP) framework is proposed to deal with operations and maintenance issues that are inevitable; challenges arise from the complex stochastic weather conditions that need to be accounted for. Using data as well as contrasting synthetic simulations of relevant weather variables, we demonstrate the robustness/versatility of the MDP model. Two case studies—one involving constant and another involving time-dependent downtime costs—are conducted to demonstrate how the proposed MDP framework incorporates weather patterns from available data and can offer optimal policies for distinct metocean conditions (i.e., temporal variations in the weather). A realistic example that illustrates the implementation of the proposed framework for multiple O&M issues involving salmon net pens and wave energy converters demonstrates how our optimal policies can minimize O&M costs and maximize crew safety almost as if the true future were known for scheduling.

KEYWORDS

Markov decision process; offshore floating multipurpose platform; operation and maintenance; optimized scheduling

4.1 Introduction

The sustainable use of a various forms of renewable energy in the marine environment – e.g., wind, wave, tides and currents – can be important in any plans to slow down the harmful impacts of climate change [1]. Bottom-supported offshore wind turbines are commercially mature, but the demand for floating offshore wind turbines (FOWTs) has increased because many resource-rich sites are in deeper waters, where they are also accompanied by stronger high-quality offshore winds and limited visual or social impacts farther out from the shore [1, 143]. To achieve installed offshore wind capacity and deployment targets, it is necessary to lower the overall energy generation cost of FOWTs.

In parallel with an ongoing energy transition in our oceans, the United Nation's Food and Agriculture Organization (FAO) estimates that, globally, over the last 60 years, fish consumption has increased at a very significant rate to keep up with population growth[54]. The FAO also reports that contributions of aquaculture to worldwide fish production have constantly increased, reaching 46 percent over the period 2016–18, up from about 26 percent in 2000. It is evident that open-ocean aquaculture has emerged as a viable alternative to overcoming problems of limited supply from inland and near-shore fisheries [48, 55, 79].

These noted trends toward energy and other needs, especially from deeper waters, and goals to reduce costs have led to serious consideration for the development of offshore floating multipurpose platforms (MPPs), see

Fig. 4.1. They could prove especially advantageous in an emerging "blue economy," with their significant benefits derived from shared use of infrastructure, resources, and services. They can combine, for instance, energy generation such as from wind and waves, aquaculture, leisure, and transport functions. Satisfactory performance of these multiple functions requires that we must deal with a wide-ranging set of operations and maintenance (O&M) activities that can take different amounts of time and might require different levels of calmness in weather conditions. In 2015, Zanuttigh et al. [185] examined 12 multipurpose platforms schemes for aquaculture, wind and wave energy to identify their benefits, costs, impacts on environment and risks. In 2019, as part of the European Commission-awarded Maribe H2020 project, Dalton et al. [39] reviewed the background and context of Blue growth and MPPs by examining policy and business cases and examined the techno-economic feasibility of a few case studies. Special issues such as the frequent feeding for aquaculture systems and fouling problems of wave energy converters (WECs) can lead to greater transportation costs while, in contrast, the frequency of O&M tasks for offshore wind turbines is much lower. A rational strategy for O&M planning can lead to significant cost reduction so as to make planned activities comparable to those at single-purpose platforms [56].

Although there have been other schedule-planning O&M strategies proposed for offshore wind farms [153] and wave energy converter arrays [4], relatively few studies have considered multipurpose platforms. For example, a risk-based O&M planning approach was proposed for offshore wind farms that

83
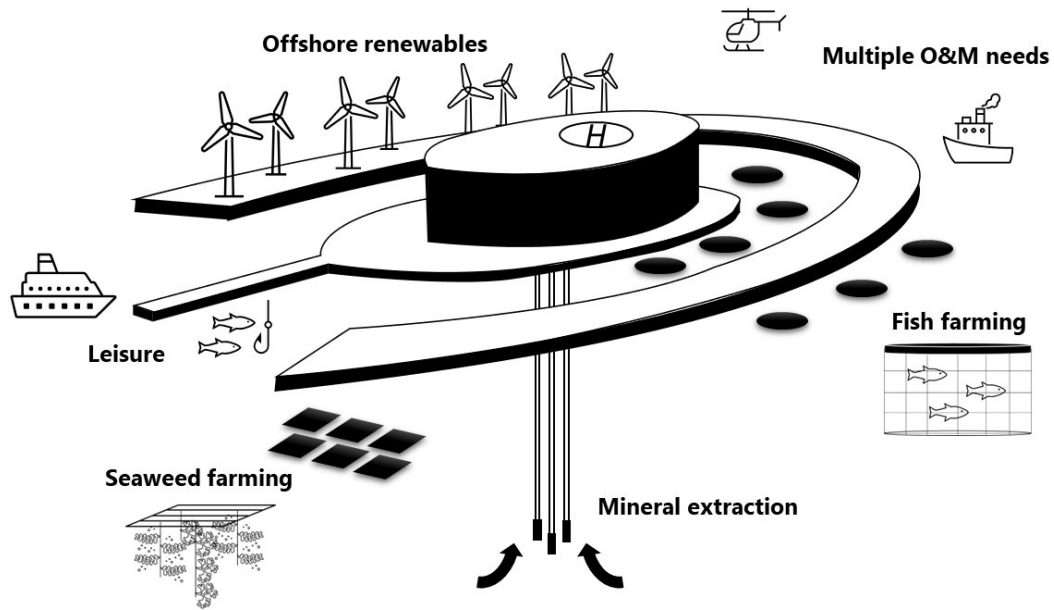
Figure 4.1: Multipurpose Platform Concept [155].

accounts for findings from inspection and monitoring that deal with deterioration [162]. To establish a more robust policy, a Markov Decision Process (MDP) approach has also been applied in optimization of wind turbine components that directly addresses reduction in maintenance costs [151, 154]. These past studies, however, have focused on monthly or yearly maintenance tasks and offered solutions for related schedule planning. Since O&M tasks at multipurpose platform systems are often required over shorter time windows and even on a daily or weekly rate, their management takes on greater importance [144]. In a derived O&M schedule with such frequent activities and service operations, there are elevated hazards and risks to personnel and a need for better short-term accessibility targets. Decision processes that em-

phasize accessibility and crew safety are needed in addition to routine task scheduling.

Recently, a MDP approach was introduced for MPP O&M optimization [71]. The method involves a stochastic weather window analysis that operators can employ to decide upon scheduling of work activities. Note that, in the ocean, wind, waves, and other weather-related variables influence the so-called Beaufort scale navigability, the selection of service vessels, crew personnel, etc. The MDP approach addresses balancing of loss of revenue and unsuccessfully completed O&M activities in overall cost minimization. The method was illustrated using observed metocean data at a planned site but was not assessed for robustness in performance for general metocean conditions. The present study aims to fill that gap using synthetic weather time series. Distinct weather patterns are simulated so as to represent: (1) highly variable seas (HVS); (2) very sustained seas (VSS); and (3) calm general seas (CGS). The proposed approach seeks optimal policies in each of these distinct weather patterns to assess robustness. We compare the optimized policy for the observed metocean data set with policies for the synthetic data sets; robustness of the method is thus assessed. In addition to assessing the robustness of our model, we conduct a 10-year-long simulation of the operation of a hypothetical MPP consisting of collocated salmon net pens and wave energy converters. For weather conditions, our simulations consider significant wave height data obtained every 6 hours from 2008 to 2017 at the offshore MPP assumed to be located at the Scotland (SCT) site. The optimal policies derived using the

proposed MDP framework and incorporating uncertain forecast-based O&M scheduling are compared by considering accumulated losses in revenue and failure costs in the simulation. Results show that our optimal policy offers an efficient approach for dealing with O&M activities at offshore MPP sites.

This work is organized as follows. Section 4.2 introduces the theoretical background of modeling sequential decision-making problems, the formulation and solution of the MDP framework for O&M optimization, and how the Markov Chain has generated synthetic weather conditions. Section 4.3 shows the optimal policy calculated for different cases with performance comparison. Section 4.4 discusses how the proposed framework can be implemented and extended in the field. Section 4.5 draws conclusions and discusses possible directions for future investigation.

4.2   Methods

4.2.1   Theoretical Background

Figure 4.2 shows the agent-environment interaction that describes the general framework for the sequential decision-making problem. Distinct interface elements can define reinforcement learning including MDP, Multi-Armed Bandit (MAB), or Partially Observable Markov Decision Process (POMDP). The decision maker, also called the agent, seeks to maximize rewards by taking optimized actions.

For MDPs, actions influence immediate rewards and subsequent states through future rewards [165]. They involve state transitions and state-dependent
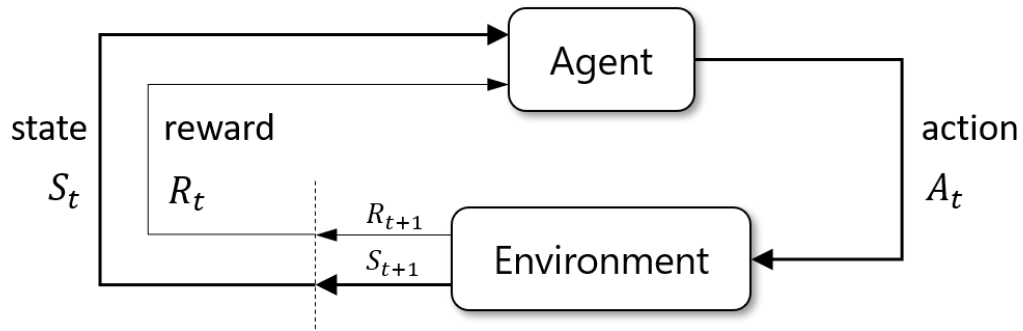
Figure 4.2: The agent-environment interaction.

delayed rewards, whereas bandits only explore best actions, regardless of state. POMDP further generalizes MDP by assuming noisy or hidden observations of the environment. We use MDP since we assume that O&M needs at the MPPs and weather conditions are fully observable in our problem.

There are three classes of methods for solving MDPs (i.e., finding the optimal policy that maximizes the expected accumulated rewards): dynamic programming (DP), Monte Carlo (MC) methods, and temporal-difference (TD) learning. MC methods are simple but not well suited for step-by-step incremental computation. TD methods are a hybrid of MC and DP; they are model-free and fully incremental but complex to analyze. This study approximates a complete model of the environment from metocean data. DP methods are well established and best for a complete MDP. For these reasons, we use one type of DP—value iteration—to determine the optimized policy (see [130]). Value iteration is described in the following.
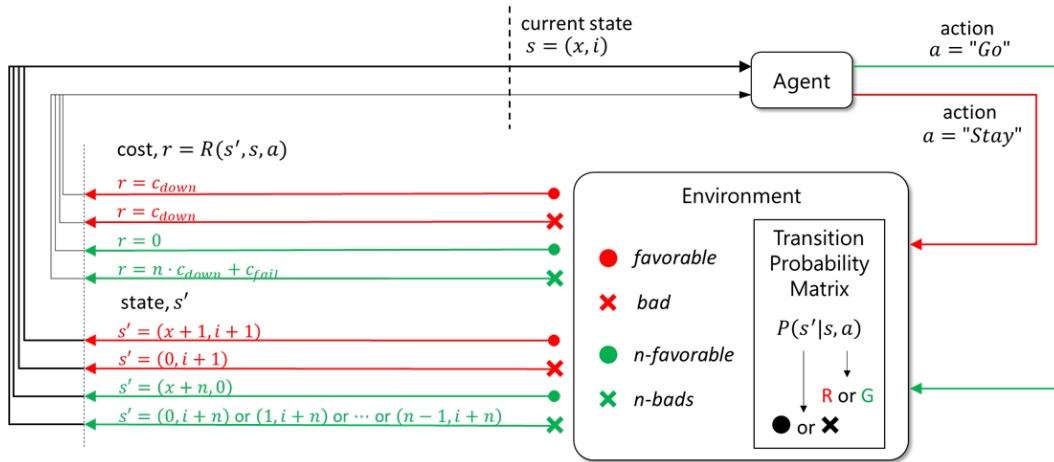
Figure 4.3: Markov decision process framework for offshore multi-purpose platform operation and maintenance optimization.

4.2.2 MDP Framework for O&M optimization

An MDP is a discrete-time stochastic control process defined by a 4-tuple comprising state (S), action (A), transition probability (P), and cost or reward (R) (see Figs. 4.2 and 4.3). To define one for this study, we partition the weather conditions into two groups: *favorable* and *bad*. Favorable conditions represent a calm sea state providing an operable environment. Figure 4.4 shows an illustrative situation; an operable environment is defined as those times when the Beaufort scale is below 5. Weather conditions are converted into a sequence of binary F *(favorable)* or B *(bad)* states for this work.

In such a binary sequence, the state space, S, is represented by a 2-tuple (x, i), where x represents the sustained duration of favorable conditions,
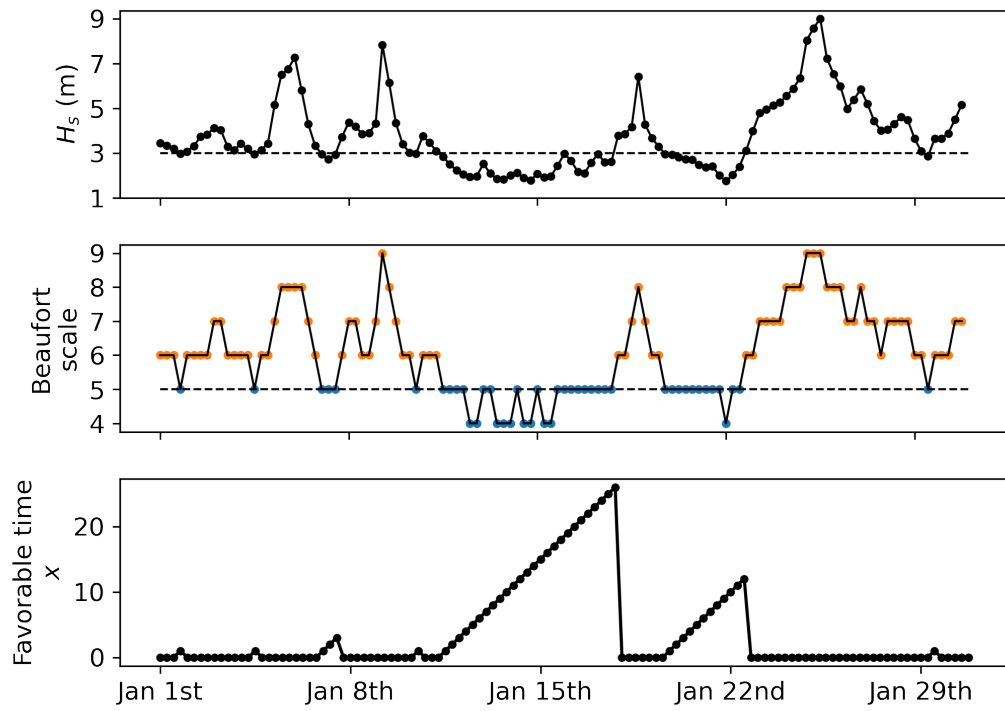
Figure 4.4: Example time series of significant wave height, H_s, along with corresponding Beaufort scale values color-coded as favorable (blue) and bad (orange). Sustained intervals of favorable conditions are also indicated.

indicating how long favorable weather has been continuing, while i represents downtime or how much time has passed since an O&M issue or need emerged.

The operator can take one of two actions: "Stay" or "Go". A "Stay" action means that the operator (or work crew) will stay at the port and wait for weather conditions to improve, while a "Go" action means the operator will set out for the needed work activity. Regardless of which action is taken by the operator, the weather stochastically changes its condition. Following a "Stay" action, the state (x, i) will transition to $(x+1, i+1)$ or $(0, i+1)$, where the former occurs when favorable conditions continue, while the latter occurs when weather conditions turn bad. Following a "Go" action, the state (x, i) will transition to $(x+1, 0)$ or $(0, i+1)$, where the former occurs when favorable conditions continue and the operator can complete the needed O&M activity, while the latter occurs when the operator fails to complete the O&M activity due to an inoperable environment in the middle of the work. To clarify these definitions, we provide an example.

Example. Assume that *BFFF* is a binary sequence that has been observed when an O&M need has emerged. At this point, $x = 3$ and $i = 4$. If the next update of the weather condition is favorable, the sequence becomes *BFFFF* but if the next weather condition is bad, the sequence becomes *BFFFB*. We must choose an action without knowing what the next weather condition will be. Thus, we have four possible outcomes from the action. For action "Stay", $(3, 4)$ can transition to $(4, 5)$ if the next condition turns out to be *F* or $(0, 5)$

if it turns out to be B. For action "Go", $(3, 4)$ can transition to $(4, 0)$ if the next condition is F or $(0, 5)$ if B.

Note that the intentionally simple example presented above applies to an O&M activity that requires 1 time step to complete. For a more general activity that requires n time steps to complete, we need to monitor n-step transitions to fully define the outcome of a "Go" action. There will be a total of 2^n possible sequences then (we had only 2^1 possible sequences in the example above). Among these possible sequences, the O&M activity can be successfully executed in only one case that must offer n consecutive favorable conditions. Let *"n-favorable"* represent that single successful case while *"n-bads"* represent all the other cases. For the action "Stay", the operator will always observe the weather for 1 time step. Then, the outcomes of "Stay" are the same as for the $n = 1$ case. For "Go", a state (x, i) transitions to $(x + n, 0)$ if *n-favorable* is realized but transitions to $(0, i + 1)$ or $(1, i + 1)$ or ... or $(n - 1, i + 1)$ if *n-bads* is realized. To illustrate such a general O&M activity case, we provide an example for $n = 2$.

Example. Return to the binary sequence *BFFF* considered before and its current state, $(3, 4)$. For an $n = 2$ O&M activity, we need to monitor 2-step transitions. Then, an *n-favorable* situation occurs with *BFFFFF* while all others *(BFFFBB, BFFFFB, BFFFBF)* lead to an *n-bads* situation. For action "Stay", the outcomes are the same as $n = 1$ case; $(3, 4)$ transitions to $(4, 5)$ or

to $(0, 5)$. For action "Go", $(3, 4)$ transitions to $(5, 0)$ if an *n-favorable* situation results, to $(0, 6)$ for both *BFFFBB* and *BFFFFB*; and to $(1, 6)$ for *BFFFBF*.

With the defined current state, s, and the next state, s', where $s, s' \in S$ and with action $a \in A$, a transition probability matrix $P(s'|s, a)$ and cost function $R(s', s, a)$ may be defined as shown in Fig. 4.3. An example of the transition probability matrices with lexicographically ordered states is presented in Fig. 4.5. For visualization purposes, n is assumed to be 1 and the sustained time x with favorable conditions and the downtime i are limited to 2. As explained, a "Stay" action always increases downtime by 1. When the next weather condition is *favorable* (red circle), the sustained favorable time x also increases by 1 but if the next weather is *bad* (red x), the sustained favorable time goes 0. For the action "Go", the O&M activity succeeds if conditions are *n-favorable* (green circle). Thus, *n-favorable* makes downtime 0 and increases the sustained favorable time by n. For *n-bads* (green x), downtime increases by n, and the sustained favorable time goes to one of $0, 1, \ldots, n-1$, depending on when was the last bad weather condition.

Note that the transition probability matrices need only two entries per row. These transition probabilities only depend on the sustained favorable times and are independent of downtime. Thus, the same entries repeat for states with the same current sustained favorable time but different downtimes. Figure 4.5 bottom row shows the repeating 1-step and n-step sustained favorable time transition probability matrices. Since the same entries repeat,

we only need these sustained favorable time transition probabilities to construct full transition probability matrices. Furthermore, the n-step sustained favorable time transition probability matrix is the n-th power of the 1-step transition probability matrix. Consequently, we can estimate the 1-step sustained favorable time transition probabilities by counting transitions *favorable* and *bad* from preprocessed sustained favorable time series and normalizing them to get the complete transition probability matrices.

For the cost function $R(s', s, a)$, we define c_{down} as the per unit time loss of revenue and c_{fail} as the unit failure cost. We assume that revenue loss starts being tallied right when an O&M issue arises and stops after successful O&M activity. We also assume that if the operator fails to complete the O&M activity, an incurred cost equal to $(n \cdot c_{down} + c_{fail})$ results, no matter when the failure to complete occurs since the desired action did not occur within the n time steps needed.

4.2.3 MDP Problem Solution

The complete MDP framework for the O&M optimization has been defined. We use one type of DP—namely, value iteration—to arrive at the optimal policy by recursively updating value functions. The value function of a state, s, under a policy π (defining specific ways of acting), denoted $v_\pi(s)$, is the expectation of accumulated rewards resulting from starting in state s and

Figure with four transition probability matrices:

(left) "Stay" action — color- and shape-coded symbols (top)

$s=(x,i)$	(0,0)	(1,0)	(2,0)	(0,1)	(1,1)	(2,1)	(0,2)	(1,2)	(2,2)
(0,0)				✗	●				
(1,0)				✗		●			
(2,0)				✗		●			
(0,1)							✗	●	
(1,1)							✗		●
(2,1)							✗		●
(0,2)							✗	●	
(1,2)							✗		●
(2,2)							✗		●

● favorable ✗ bad

(right) "Go" action — color- and shape-coded symbols (top)

$s=(x,i)$	(0,0)	(1,0)	(2,0)	(0,1)	(1,1)	(2,1)	(0,2)	(1,2)	(2,2)
(0,0)		●		✗					
(1,0)			●	✗					
(2,0)			●	✗					
(0,1)	●						✗		
(1,1)		●					✗		
(2,1)		●					✗		
(0,2)	●						✗		
(1,2)		●					✗		
(2,2)		●					✗		

● n-favorable ✗ n-bads

(left) "Stay" — actual transition probabilities (bottom)

$s=(x,i)$	(0,0)	(1,0)	(2,0)	(0,1)	(1,1)	(2,1)	(0,2)	(1,2)	(2,2)
(0,0)				0.72	0.28				
(1,0)				0.22		0.78			
(2,0)				0.17		0.83			
(0,1)							0.72	0.28	
(1,1)							0.22		0.78
(2,1)							0.17		0.83
(0,2)							0.72	0.28	
(1,2)							0.22		0.78
(2,2)							0.17		0.83

(right) "Go" — actual transition probabilities (bottom)

$s=(x,i)$	(0,0)	(1,0)	(2,0)	(0,1)	(1,1)	(2,1)	(0,2)	(1,2)	(2,2)
(0,0)	0.28		0.72						
(1,0)		0.78	0.22						
(2,0)		0.83	0.17						
(0,1)	0.28						0.72		
(1,1)		0.78					0.22		
(2,1)		0.83					0.17		
(0,2)	0.28						0.72		
(1,2)		0.78					0.22		
(2,2)		0.83					0.17		

Figure 4.5: An example of transition probability matrices for (left) "Stay" and (right) "Go" actions with (top) color- and shape-coded symbols (bottom) actual transition probabilities estimated from SCT.

employing policy, π,

$$
\begin{aligned}
v_\pi(s) &= E_\pi[R_{t+1} + \gamma R_{t+2} + \gamma^2 R_{t+3} + \cdots | S_t = s], \\
&= E_\pi\left[\sum_{k=0}^{\infty} \gamma^k R_{t+k+1} | S_t = s\right],
\end{aligned}
\tag{4.1}
$$

where $0 < \gamma \le 1$ is a discount rate. For the infinite-horizon MDP, as is implied by Equation 4.1, we cannot distinguish between two policies yielding the same sum of future rewards if $\gamma = 1$. Since a policy that leads to a higher reward sooner, rather than later, is generally preferred, $\gamma < 1$ is used

94

to discount future rewards gradually. For the O&M optimization problem formulated in this study, the sequential decision-making process is of finite horizon; it is initiated when an O&M issue emerges and terminates when the issue is resolved. Thus, we can use $\gamma = 1$ or when γ is close to 1. Then, we note that every policy, π, has an associated value function $v_\pi(s)$. By definition, the optimal policy π_* maximizes the expected accumulated rewards. Therefore, a policy is optimal if and only if its associated value function is maximum for all states. We can rewrite Equation 4.1 as:

$$
\begin{aligned}
v_\pi(s) &= E_\pi[R_{t+1} + \gamma R_{t+2} + \gamma^2 R_{t+3} + \cdots | S_t = s], \\
&= E_\pi[R_{t+1} | S_t = s] + \gamma E_\pi[R_{t+2} + \gamma R_{t+3} + \cdots | S_t = s], \\
&= \sum_{s' \in S} P(s'|s, a) R(s', a, s) + \gamma \sum_{s' \in S} P(s'|s, a) v_\pi(s'),
\end{aligned}
\tag{4.2}
$$

where the first term is an expected immediate reward calculated using the transition probabilities and the reward function, while the second term is the discounted future value calculated using the transition probabilities and the value function. The optimal value function associated with the optimal policy can finally be written as:

$$
v_{\pi_*}(s) = \max_{a \in A} \left[\sum_{s' \in S} P(s'|s, a) R(s, a, s') + \gamma \sum_{s' \in S} P(s'|s, a) v_{\pi^*}(s') \right].
\tag{4.3}
$$

Starting from the initial value function in which zero values are assigned to all states, Algorithm 1 shows how the value iteration recursively updates the value function until it converges to the optimal value function. As shown, we can easily establish what the optimal policy should be, once we have found the optimal value function.

95

Algorithm 1 Value Iteration

Initialize $v_0(s) = 0$

$v_1(s) \leftarrow \max\limits_{a \in A} \sum\limits_{s' \in S} P(s'|s, a)[R(s, a, s') + \gamma v_0(s')]$

$k = 1$ and $\varepsilon = $ tolerance

while $|v_k - v_{k-1}| > \varepsilon$ **do**

   $v_{k+1} \leftarrow \max\limits_{a \in A} \sum\limits_{s' \in S} P(s'|s, a)[R(s, a, s') + \gamma v_k(s')]$

   $k = k + 1$

end while

$\pi_*(s) = \operatorname*{argmax}\limits_{a \in A} \sum\limits_{s' \in S} P(s'|s, a)[R(s, a, s') + \gamma v_k(s')]$

4.2.4 Synthetic weather condition generation

To assess robustness in our MDP performance for general metocean conditions, we use a Markov chain simulation to generate synthetic weather conditions. Note that this new Markov chain is different from the one used for the MDP framework itself. This Markov chain consists of states and transition probabilities. To distinguish transition probability matrices involved in the synthetic weather condition generation from the transition probability matrices for MDP, let us denote them as TPM_{MC} and TPM_{MDP}. The state space of the Markov chain are the values of x *(sustained favorable time)*, which can transition to either 0 or $x + 1$. Therefore, stochastic simulation of the Markov chain with TPM_{MC} generates time series of sustained favorable times that match weather patterns per the target TPM_{MC}.

We define three different TPM_{MC} targets corresponding to three distinct weather patterns: (1) highly variable seas (HVS); (2) very sustained seas (VSS); and (3) calm general seas (CGS). The color-mapped 1-step sustained

96

favorable time transition probabilities are presented in Fig. 4.6. Synthetic weather time series for the distinct conditions are presented in Fig. 4.7. Consistent with its name, HVS defines greatly fluctuating seas; the likelihood of bad weather conditions is always 50%. VSS defines seas with long sustained periods of either favorable or bad weather. For VSS, when x *(sustained favorable time)* is 0, the likelihood of continuing bad weather conditions is 90%. This means that with VSS, the weather tends to stay bad when the prior period weather was bad. On the other hand, for $x \geq 1$, i.e., when favorable weather conditions have lasted at least one period, the likelihood of favorable conditions continuing is 95%. Thus, when the sea enters favorable conditions, it tends to stay in those favorable conditions. As seen in Fig. 4.7, when the weather stays calm, the sustained favorable time steadily increases. The periods through the rise to the triangular peaks in the time series are periods of favorable weather. On the other hand, the sustained favorable weather time stays at zero if the weather is bad. Figure 4.7 clearly shows the targeted highly fluctuating behavior for HVS and the long sustained periods of relatively unchanging weather for VSS. Finally, CGS describes metocean conditions stochastically similar to those recorded at the planned Scottish site (SCT) [71]. The SCT transition probability matrix was computed by counting transitions from the actual metocean time series and normalizing them. Since the data set is of limited length, not all transitions are observed. The empty white cell in Fig. 4.6 is a result of this type of lack of observations. By design, CGS has the same target transition probabilities as SCT, and the

97

empty (missing) value for SCT was interpolated, in defining CGS, from the adjacent transition probabilities. For VSS, CGS, and SCT, the sustained favorable time duration is limited to 50 time steps to avoid meaningless long dwell times of sustained favorable conditions.

Using the synthetically generated sustained favorable time series, we compute the transition matrices, TPM_{MDP}. The discussion concerning Fig. 4.5 and related explanation is what we need to count different transitions and normalize them to yield TPM_{MDP}. The procedure of analysis for given values of n, c_{down}, and c_{fail} is summarized below.

1. Choose a weather pattern and the corresponding TPM_{MC}.

2. Run stochastic simulations of sustained favorable times using Markov chain so as to yield 10^6 time steps starting from $x = 0$.

3. Count transitions *favorable* and *bad* from the generated sustained favorable time series and normalize them to obtain the 1-step sustained favorable time transition matrix.

4. Construct the complete TPM_{MDP} using the 1-step favorable time transition matrix.

5. Solve the MDP using value iteration to obtain the optimal policy.
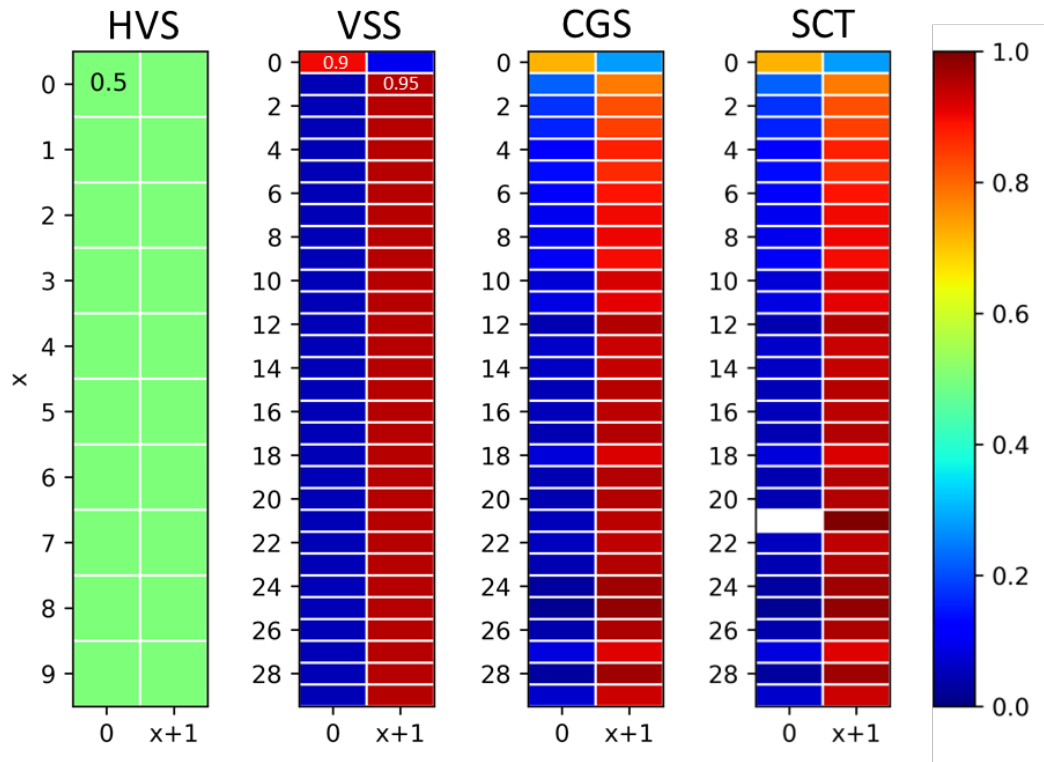
Figure 4.6: Transition probability matrices for the synthetic weather condition generation: (1) highly variable seas (HVS); (2) very sustained seas (VSS); (3) calm general seas (CGS); (4) as-recorded seas at the Scottish site (SCT).

4.3   O&M model assessment

Note that in the examples presented, a single time step is equal to 6 hours. Two cases associated with different assumptions in loss of revenue due to downtime are discussed. Additionally, a realistic example involving delousing needs at a fish farm and WEC component maintenance at the same site is introduced to assess the performance of our model for optimal O&M planning and scheduling.
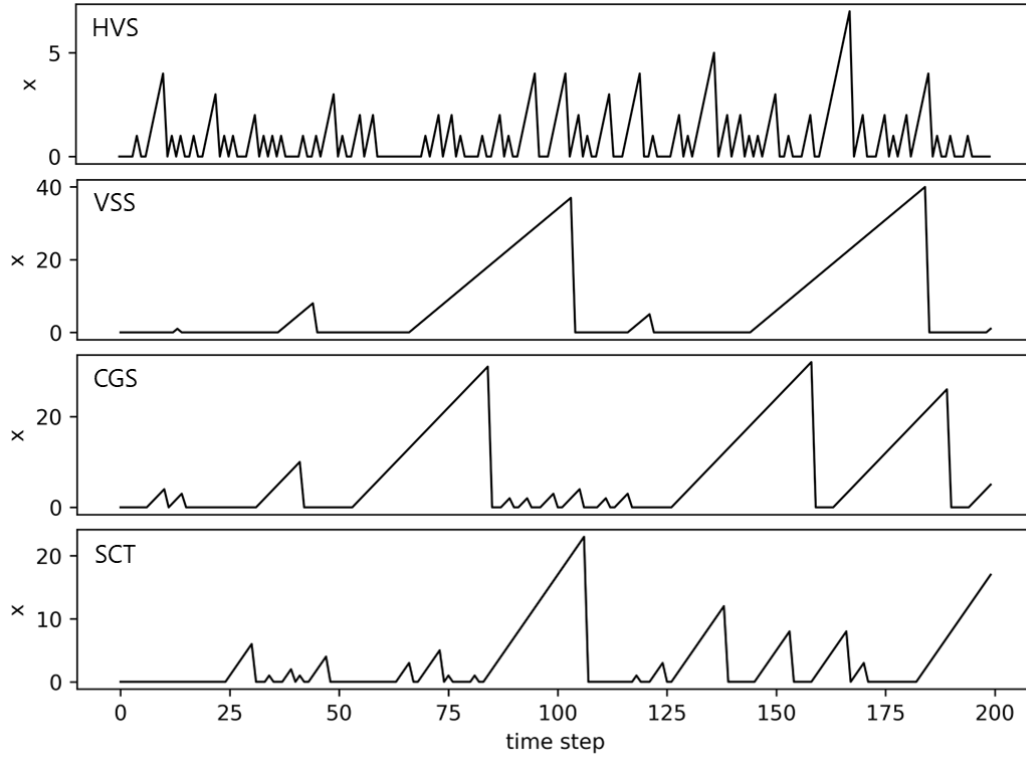
Figure 4.7: Three distinct synthetically generated weather conditions (HVS, VSS, and CGS) and observed seas at a planned Scottish site (SCT) Note that, for SCT, a time step is equivalent to 6 hours.

4.3.1 Case of constant downtime costs

The O&M issues for an energy generation sector are associated with constant (time-independent) downtime costs. From Fig. 4.3, we note that all costs are independent of downtime if c_{down} is constant. Hence, the optimal policy will also be independent of downtime. For simplicity, we select $c_{down} = -2$, and $c_{fail} = -1$ for this assessment; we are only really concerned with the ratio of c_{down} to c_{fail} when deciding on the optimal action for a given state.

100

Our MDP framework derives an optimal policy from the generated synthetic weather conditions without need for the actual transition probability matrices used to generate those data. Figure 4.8 compares computed optimal policies for $n = 1$ and $n = 3$ O&M activities. The color of each cell in the color map shown in Fig. 4.8 indicates recommended action per the optimal policy. Consider, for instance, the fourth cell for HVS which is green for some $n = 1$ activity; "Go" action is recommended. This fourth cell corresponds to states where the sustained favorable time is 3. It should be interpreted from this that an operator or crew may set out for the $n = 1$ O&M activity with HVS when favorable weather conditions have been continuing for three consecutive time steps. For the same HVS weather pattern, the suggested action for some $n = 3$ activity is indicated by a red color; this is an indication to "Stay" and not begin the needed O&M activity. In this manner, suggested actions for all the contrasting weather patterns and for two different O&M activities are represented using the color maps in Fig. 4.8.

Figure 4.8 shows that our MDP framework captures specific patterns for the different metocean conditions and produces optimal policies for O&M activities that require different planning time steps. For HVS, the policy indicates that an $n = 1$ O&M activity is feasible for all sustained favorable times, but the $n = 3$ O&M activity is risky to pursue due to the high variability of sea conditions. These results are rational and expected, given HVS's fluctuating weather pattern.

For VSS, the MDP suggests the same optimal policy for both the $n = 1$
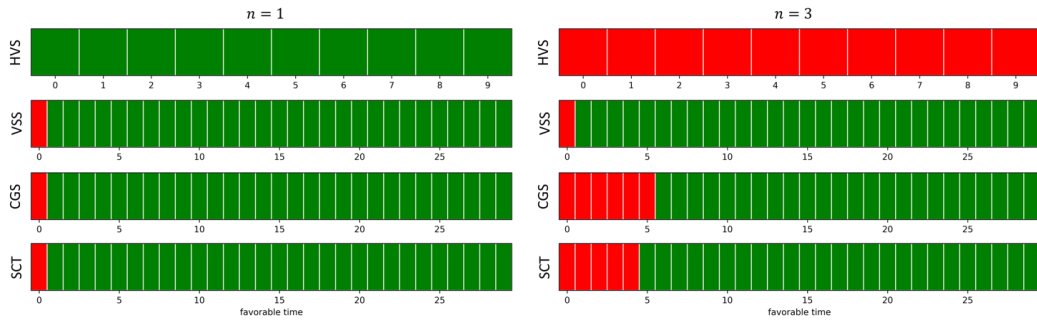
Figure 4.8: Optimal O&M policies for three synthetic metocean conditions and for the SCT case (Red: "Stay", Green: "Go") (left) $n = 1$ and (right) $n = 3$.

and $n = 3$ O&M activities. Since VSS is associated with longer period of sustained favorable and bad conditions, our MDP framework suggests that both types of activities may be undertaken as long as the weather has entered the favorable period. Therefore, the optimal policy recommends "Stay" action if the favorable time is 0 and "Go" for $x \geq 1$.

The similar optimized policies derived for the CGS and SCT cases confirms the robustness of our method (CGS transition probabilities were synthetic targets selected to match observed SCT weather). Figure 4.7 shows that CGS and SCT conditions exhibit somewhat more weather variability than VSS. They have occasional long periods of favorable weather, but we also observe a few bumpy peaks (see Fig. 4.7) indicating fluctuating conditions. The optimized policies established in Fig. 4.8 are compatible with these weather patterns of CGS and SCT. This all leads to the same policy as VSS for the $n = 1$ O&M activity, but we need to wait for longer times to start work for

the $n = 3$ activity. This is a result of the sporadic fluctuating weather conditions of CGS and SCT. Due to this unpredictable weather variability of the CGS and SCT conditions, even though not as extreme as HVS, we need to wait longer than VSS to make sure the weather will be calm throughout the planned activity.

The example case study for the constant (i.e., time-independent) downtime costs has shown how the proposed MDP framework learns different weather patterns and optimizes policies for different types of O&M activities. The optimized policies conform to the expected weather patterns, and the MDP framework rationally identifies and schedules O&M activities that are acceptable to conduct and when are appropriate times for crews/vessels to depart for the work to be carried out, while taking into consideration overall cost and safety.

4.3.2 Case of time-dependent downtime costs

For O&M issues related to some activities, such as fish farming in an aquaculture sector, the per-unit-time loss in revenue can vary with time associated with delay in addressing the needed problem or service. We consider a case where such losses in revenue are assumed to increase exponentially with downtime. If c_{down} is a function of downtime, the derived optimal policy will also depend on the downtime. We assume that $c_{down}(i) = -0.8 * e^{0.1 \cdot i}$; all other parameters are the same as in the previous case. Figure 4.9 shows the assumed $c_{down}(i)$ variation with downtime. For the constant c_{down} case considered ear-
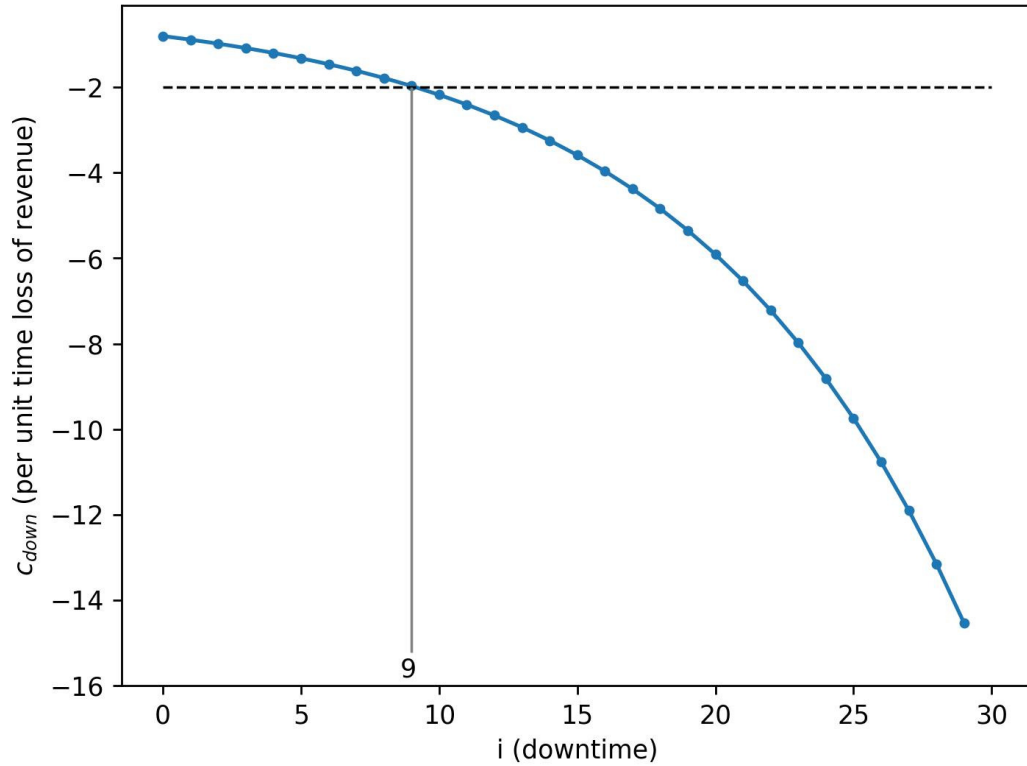
Figure 4.9: Time-dependent per unit time loss of revenue versus downtime

lier, we assumed $c_{down} = -2$. It is seen that $c_{down}(i)$ is close to -2 when downtime, $i = 9$. Although it is not possible to match the optimized policy of the previous case due to the costs with increasing downtime, we might expect a similar O&M policy around $i = 9$.

Figure 4.10 shows derived optimal policies for $n = 1$ and $n = 3$ O&M activities for all the distinct weather conditions. For this case, the optimal policy is a function of the sustained favorable time and the accumulated downtime, which makes the color map two-dimensional, as shown in Fig. 4.10. As

before, the color of each cell indicates the suggested action consistent with the optimal policy. For example, the cell for HVS and $n = 1$ activity where $(x, i) = (3, 4)$ is green, corresponding to a suggested "Go" action. It can also be interpreted then that we can set out to complete this $n = 1$ O&M activity for HVS weather conditions, whenever favorable weather conditions have been continuing for three consecutive time steps, and if the O&M issue had emerged four time steps ago. For the same $(3, 4)$ state, the suggested action for an $n = 3$ activity is red which indicates a "Stay" action. In a similar manner, suggested actions for various state and indicated policies are presented using the two-dimensional color map in Fig. 4.10.

The HVS optimized policy for $n = 1$ activity suggests that we should not start work when downtime is zero (which is obvious), and indicates that the required O&M activity is feasible for all other states. As with the constant c_{down} case, our MDP framework shows that the $n = 3$ activity is not feasible in any states due to the high probability of failure expected from the fluctuating weather patterns associated with HVS.

Up to a downtime of 14, VSS's optimized policy for the $n = 1$ activity is the same as for the previous constant c_{down} case. When the downtime exceeds 14, it is beneficial to begin the work activity, regardless of the current weather regime since $c_{down}(i)$ values and loss of revenue become too large. For the $n = 3$ activity, the optimized policy suggests that staying and waiting for favorable weather is preferred when the downtime is less than 3. This is because we might expect long-lasting calm conditions when VSS enters a favorable weather

105

regime, and its benefit is greater when compared with trading off of missed time steps and resulting loss of revenue. The optimized policy for $n = 3$ also indicates that we should not risk performing work in a bad weather regime even if $c_{down}(i)$ is so high because failure is very likely to occur.

For the $n = 1$ activity, the CGS and SCT weather patterns lead to similar results as for VSS. For the $n = 3$ activity, the recommended waiting times vary depending on the time of sustained favorable weather, x. The derived policy reflects a complex weather transition probability situation at the actual site in Scotland.

To further justify the results presented, we highlight optimized policies around $i = 9$, in Fig. 4.10, with a yellow box. As mentioned before, the derived policies do not exactly match those for the constant downtime case. Nevertheless, the results are fairly similar in the two cases. Note that Fig. 4.10 also shows analytical results for the three synthetic weather conditions (i.e., excluding SCT). These analytically derived policies resulted from using the assumed TPM_{MC} by considering it as 1-step sustained favorable time transition matrix in the TPM_{MDP} solution. Except for a few states, the simulation-based optimized policies are almost identical to these analytical answers. This establishes the the claim of sample size-based adequacy and robustness of the MDP framework.

In summary, the case study involving time-dependent downtime costs shows that the proposed MDP framework realistically captures state transition patterns from the input data and offers different but expected optimal policies

106
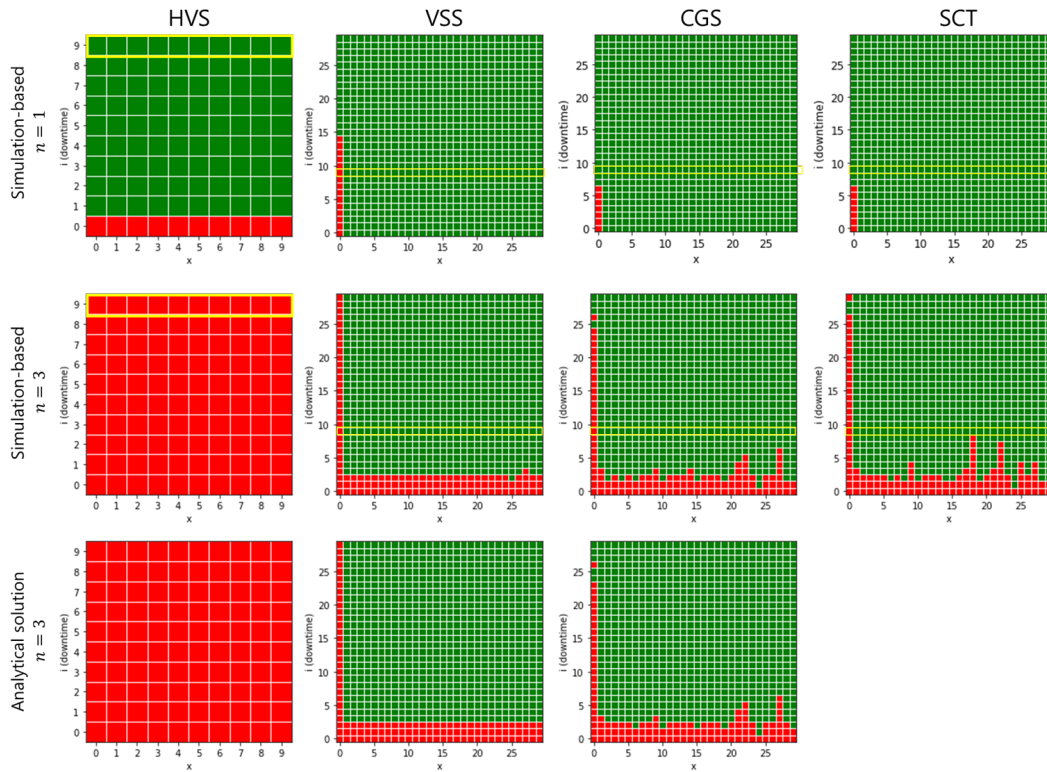
Figure 4.10: Optimal policies for three synthetic metocean conditions and for the SCT case (Red: "Stay", Green: "Go").

for the distinct metocean conditions.

4.3.3 Multiple O&M Issues: Fish farm delousing treatment and WEC component maintenance

We consider next a realistic example to illustrate the implementation of the proposed framework for multiple O&M issues at an MPP. An array of salmon net pens and WEC devices is assumed to be collocated at the MPP of interest. Among various O&M issues that arise at the MPP, a delousing

treatment at the fish farm and WEC component maintenance are selected for this case study.

Offshore salmon farming using net pens that must allow relatively unhindered flow between the farm and the external environment is of importance in such aquaculture systems [122]. Flow-through net pens have advantages in that they can limit the need for water filtration and improve fish welfare. However, they also allow the spread of pathogens and parasites to and from wild salmon [92]. Therefore, the onset of disease and its transmission are a primary threat to the continued growth of the fish in such aquaculture systems and arrays [7, 8, 72, 93, 101, 118, 123, 175]. Among various diseases associated with salmon aquaculture, sea lice have emerged as one of the main challenges in some major farmed salmon-producing regions, such as in parts of Norway and British Columbia, Canada [35, 102, 141].

Godwin et al. [61] analyzed a publicly available dataset, managed by Fisheries and Oceans Canada, of industry sea-louse counts between 2011 and 2016. Based on their analysis, we model the occurrence of delousing treatment needs as a Poisson point process with a 4-per-year mean rate. Also, $c_{down}(i) = -0.8 \times e^{0.1 \cdot i}$ is used to model the per-unit-time loss in revenue from salmon due to the sea-louse infection that causes immune system effects, stress responses, secondary infection, risk-taking behavior, reduced growth, and ultimately decreased rates of survival [35, 51, 90, 91, 120]. The Norwegian salmon aquaculture industry relies heavily on warm water thermal delousing treatments to reduce lice infestations in farms, with greater than 61% of all

treatments in 2017 registered as thermal [128]. Thermal delousing involves submerging fish in water at a temperature of 28–34°C for 20–30 seconds [127]. Accordingly, in our study, we make the assumption that each needed delousing treatment will take 18 hours to complete (this corresponds to 3 time steps, in our model that uses 6-hour increments when considering ambient environmental conditions).

Moving to the WEC devices collocated at the MPP site, some mechanical and structural components in a WEC can fail during operation [4]. We assume that a minor failure stops energy generation but can be repaired and remedied at site within 18 hours. Such a component failure is assumed to follow a Poisson point process with a once-in-a-year rate. Also, $c_{down} = -1$ is assumed to model loss of revenue from the halted energy generation. The same favorable operational conditions for both activities are assumed to apply; this corresponds to a upper limit of 2 meters on significant wave height. Lastly, we use $c_{fail} = -1$, the same for both activities and what we also used in the case study described before. Considering the relative magnitudes of c_{down} and c_{fail}, we are assuming that only non-fatal failures apply, including ecological disturbance by farmed salmon escape, damage to nets and vessels, and minor crew injuries. We have employed various simplifications and assumptions in this case study but all of the assumed values can be easily substituted with site- and project-specific values. Besides, our main goal is to demonstrate the model's applicability in realistic scenarios.

The proposed MDP framework is formulated for both the O&M activ-

109

ities with the defined/assumed parameters presented above. We use the SCT weather data for this realistic case study to develop optimal policies. Significant wave height data are obtained every 6 hours from 2008 to 2017 at the location of the planned multipurpose platform offshore Scotland. Next, the actual implementation of the policy is simulated. Using stochastic realizations for two Poisson point processes, specific instances in time need for the two O&M activities are simulated for the period from 2008 to 2017. (We note here that the simulation of a stationary Poisson process can be easily extended to allow the stochastic simulation of non-stationary components, seasonal components, or various other characteristics to represent both stochastic delousing needs and WEC repair occurrences.) The sustained intervals of time with favorable conditions and the downtime are monitored when any O&M issue arises. If the optimized policy recommends staying, the agent stays and the O&M activity is not started. If a "Go" action is suggested, the agent attempt to work and begin the activity. With every decision and interaction with the stochastic weather in sequence, incurred expenses resulting from both the per-unit-time loss in revenue and the unit failure cost are recorded in each simulation. Similar decisions are routinely made in the field by experienced operators often based on their gut feeling, prior experiences, and available weather forecasts.

Our approach uses actual archived weather data to characterize stochastic patterns at a site of interest and then arrives at optimal policies that aim at minimizing O&M costs and maximizing crew safety. In contrast to the use of such past observed weather data (to develop needed transition probabili-

ties for the model we propose), often one is expected to also rely on weather forecasts that are only a prediction of the future and, as such, derived policies and scheduling will be optimal only if such forecasts are accurate. In most situations, forecasts are associated with uncertainty and their use may lead to sub-optimal policies. To compare forecast-based decisions with our data-based optimal MDP policy-based decisions, we systematically examine the influence of different uncertainty levels in relevant forecasts on derived O&M policies at our site.

We consider a scenario at the SCT site where we use the archived records; we then have access, while planning, to the "truth" future weather conditions ahead of any point in them when we need to make a decision about any needed O&M activity. With the knowledge we have, we can take the right actions to "Go" or "Stay" that will minimize loss of revenue and avoid failure. To model forecast uncertainty, we introduce an auxiliary variable, α. Every time we need to take some O&M action, α is randomly sampled from a continuous uniform [0,1] distribution. Assuming a forecast error rate, p, if $alpha > p$, we follow the same action as we would given a "truth" future; on the other hand, when $\alpha \leq p$, we take the opposite action. This effectively means that there is a $100p\%$ probability that we will not follow the suggested policy based on our model and a $100(1-p)\%$ probability that we will. We evaluate accumulated O&M costs incurred by decisions made upon various forecast uncertainty assumptions including cases where $100p\%$ is set to 10%, 20%, 30%, 40%, and 50% .

Figure 4.11 shows stochastically simulated realizations of instances in time corresponding to the need for the two O&M activities over a 10-year period. Additionally, vertical 'stripes' in Figure 4.12 indicate selected actions to be taken (green: "Go", red: "Stay") for true future as well as for cases with 10% and 50% forecast error rates. To aid in visualization, plots at the bottom show the same scenarios but with the unimportant idle times removed and with the stripes lined up chronologically. As the error rate in forecasts increases, costs tend to increase due to more failures resulting from "Go" actions when "Stay" is indicated as well as the alternative error—i.e., "Stay" instead of "Go", which increases downtime costs. In the scenario considered, the increased failure costs due to forecast error are of greater importance. Incurred expenses during the 10 year-long simulation of operations considering different forecast error rates are computed. Each simulation of such operations is repeated 100 times in order to capture the variability in accumulated costs resulting from the uncertainty in weather forecasts. The "truth" weather scenario (i.e., assuming no weather forecast error) always leads to a single optimal O&M policy and associated actions; it also leads to a single incurred cost/expense estimate.

We compare MDP-based actions and associated costs with forecast-based actions and associated costs in Figure 4.13. Note that the former uses the MDP framework presented in Section 4.2, while the latter uses the archived weather data but the introduction of forecast error in future prediction. In the figure, "True" implies no error in the forecast. Figure 4.13 shows costs incurred
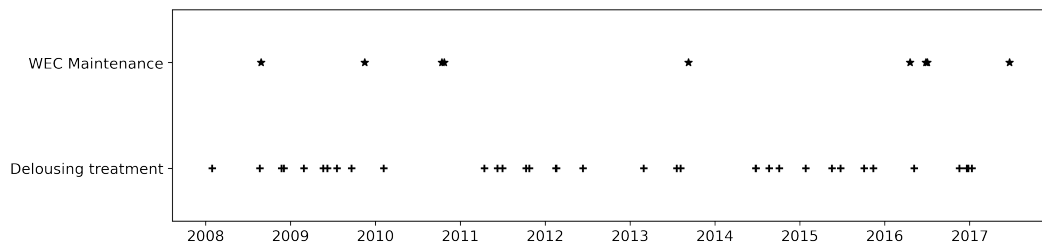
Figure 4.11: Stochastically generated realizations of instances in time corresponding to the need for the two O&M activities used in all the operation simulations.

in delousing treatment and WEC component maintenance cost accumulated over a 10 year-long simulation. The costs shown are normalized relative to the no-forecast-error case cost of the corresponding O&M activity. Note that relative cost of WEC maintenance to delousing is in the ratio 1:25 with the assumptions made in the selected example. Our MDP-based O&M policy works especially well and has lowest costs for delousing treatments, when there is no weather forecast error. In the case of WEC maintenance, the effect of weather forecast errors is reduced due to the relatively fewer times there is need for such actions. Note that with larger forecast error rates, any selected O&M policy resulting from the simulations leads to greater costs as well as wider min-max bounds on costs incurred. Our optimal policy shows a clear advantage producing a lot small amount of accumulated cost than relying only on uncertain forecasts, and also it provides consistent performances.

113
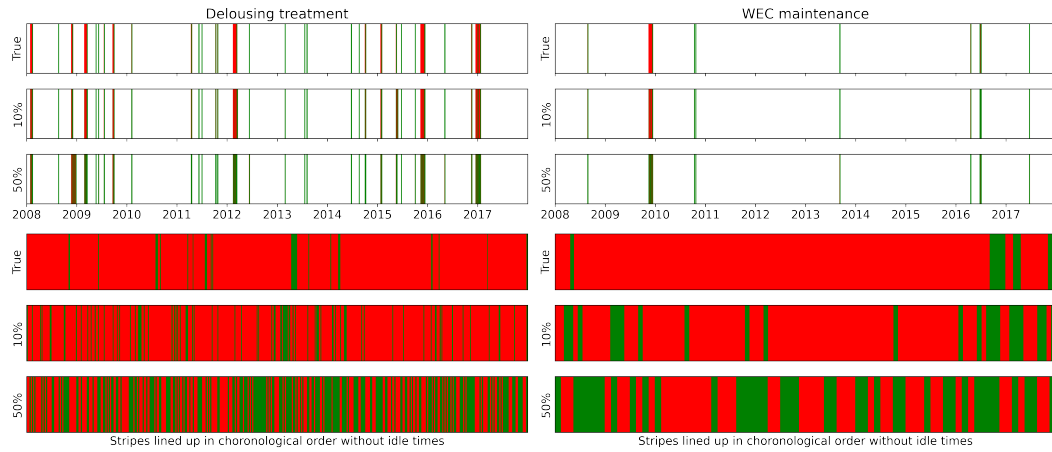
Figure 4.12: Stripes showing selected O&M actions (green: "Go", red: "Stay") for a true-future case as well as cases where there are 10% and 50% weather forecast error rates. The top row of plots displays stripes at specific dates in time. For ease in visualization, the bottom row has unimportant times removed and lines up stripes chronologically at times for needed O&M actions.

4.4 Discussions

4.4.1 Relationship with traditional weather window analysis

A key difference between the proposed methodology and traditional weather window analysis is in the final products of such analysis. Traditional weather window analysis computes statistics and probabilities associated with access and availability, based solely on metocean condition at the site of interest. Such analyses do not address the question of how such statistics and probabilities can be used to make optimal decisions pertaining to scheduling O&M activities. In other words, traditional weather window analysis generally does not consider losses in revenue and costs associated with failure that are incorporated in our proposed MDP framework. The optimal policy de-

114
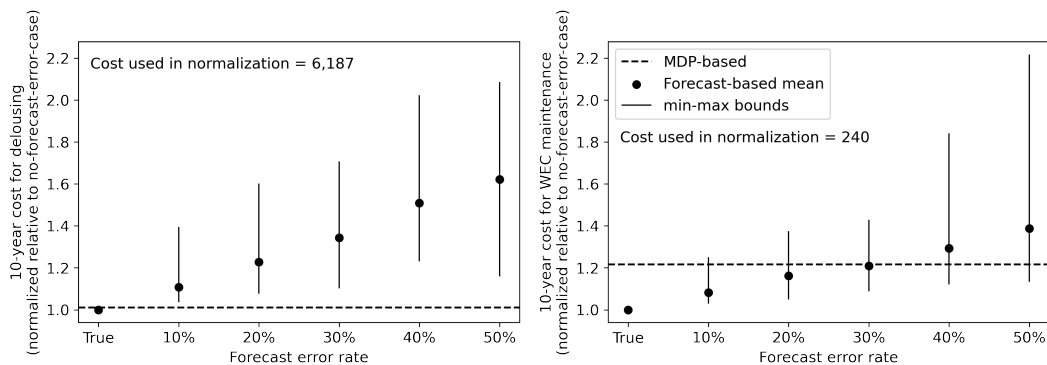
Figure 4.13: Normalized delousing treatment and WEC component maintenance costs accumulated over the 10-year period. The mean value and min-max bounds for the cases involving various weather forecast error rates are shown along with the deterministic point-estimate costs for the "true-future" case and our MDP-based optimal policy case.

rived from our proposed MDP framework can be used in daily operations and can, thus, help field operators adopt a strategy that seeks to minimize O&M costs and maximize crew safety simultaneously. Another difference between our MDP approach and traditional weather window analysis arises in how stochastic metocean conditions evident in the data are modeled. Our MDP framework uses conditional probability estimates, which quantify the likelihood that future weather conditions will be favorable and will allow O&M service, *given* how long favorable condition have been continuing. In contrast, traditional weather window analysis provides simpler statistics that allow one to infer the likelihood of accessibility and availability.

4.4.2   Implementation

While in the field, we need three sources of information to implement the proposed MDP framework that we have outlined in this work: 1) the type of O&M activity, 2) the available transportation, and 3) climate data for the site. Based on the type of O&M activity and the available transportation, the required number of time steps (each of 6-hour duration) to complete O&M activity, n; the per-unit-time loss of revenue, c_{down}; and the unit failure cost, c_{fail}, must all be defined. The weather conditions acceptable for operation are established based on the type of O&M activity and transportation. Next, we convert the collected climate data into a binary sequence of *favorable* and *bad* in order to estimate transition probabilities. With all this information, we define the MDP framework and derive the optimized policy by value iteration. Note that the optimized policy is for one O&M activity and transportation pair. For multiple O&M activities and means of transportation, we can easily derive an optimal policy for each case since the proposed framework is computationally light.

Addressing the matter of daily use of the proposed framework, operators can simply follow the action suggested by the policy. As we monitor sustained favorable time and downtime at the site, whenever an O&M issue arises, we obtain a real-time action suggestion from the policy. By following such suggestions, we minimize loss of revenue and maximize crew member safety.

4.4.3   Further Refinements of Proposed Model

The proposed framework can be extended in several ways. First, seasonality that is not addressed here can be considered by establishing independent transition probability matrices for each season using climate data. By doing so, distinct weather pattern sequences arising from seasonal differences can be taken into account in seasonal transition probability matrices. Using data at finer temporal resolution, such as with monthly or shorter segments, can be challenging due to the lack of sufficient climate data, which will lead to inaccurate transition probability estimation and suboptimal policies. As shown in other studies [71], the modeling of a few seasons (2-4, annually) is feasible with most commonly gathered climate data.

A second issue that merits consideration with the proposed framework is the possible use of multiple weather variables to define favorable and unfavorable operating conditions. As an example, if we consider both wave height and wind speed together in defining weather conditions, the problem/variable dimension for the weather must extend to 4 from 2 so as to distinguish *favorable* from *bad*, but the overall formulation stays the same otherwise. Any number of weather variables can be easily added to define favorable weather conditions. Any changes in variable dimension only affects how long and different sustained favorable time segments, given the climate data, will be relative to a single-dimension weather variable. The overall procedure and formulation remain the same as how it was introduced in Section 2. Figure 4.14 shows, for example, how sustained periods of favorable weather change when we consider

117
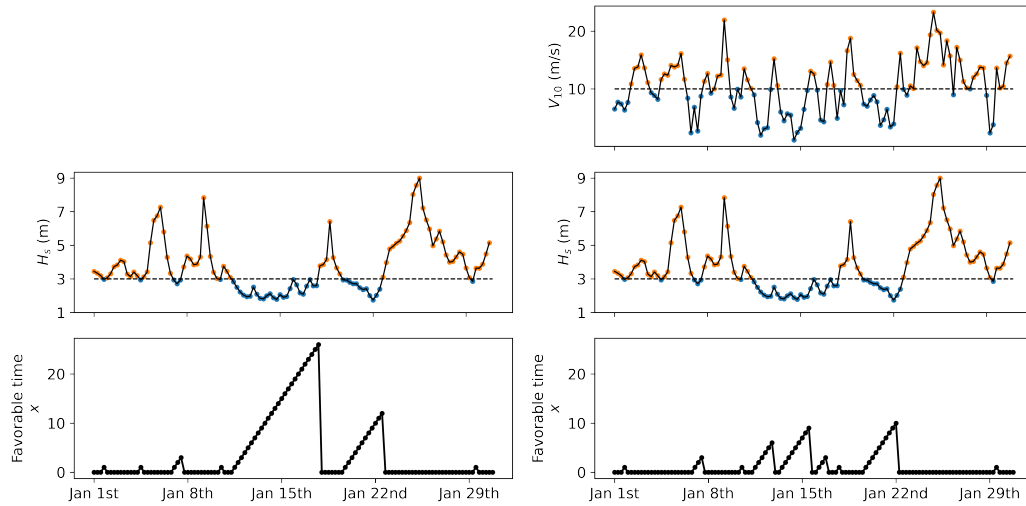
Figure 4.14: Derived sustained favorable time series by 1) a single operational condition of significant wave height (left) and 2) multiple operational conditions of significant wave height and wind speed (right).

wind speed in addition to significant wave height in policy recommendation. Here, favorable weather is first considered as when significant wave height is below 3 m, but later it is required that the wind speed must also be below 10 m/s. As can be seen, increase in the number of variables to consider leads to shorter sustained time segments where conditions are favorable for planned activities.

A third issue addresses how to consider the availability of multiple transportation types in the decision-making. Each distinct type of transportation has its own operational limits in the face of weather conditions. The possibility of multiple transportation types (vessels, helicopters, etc.) also leads to an increase in the dimension of the problem to be solved. For in-

118

stance, the action space can be expanded to "Stay", "Go with the vessel", and "Go with the helicopter" if multiple transportation types are available including a seaborne vessel as well as a helicopter. Note that such extensions can be easily introduced in our proposed MDP framework since the mathematical formulation is straightforward and scalable.

Lastly, some features in actual operation and maintenance activities at offshore facilities that have not been discussed here can be easily incorporated in our framework. For instance, some O&M activities require multiple trips to the offshore facility due to limited capacity of the available transportation. In such situations, we can consider each trip as part of some needed O&M activity, but these activities are not independent since they should be sequenced for successful resolution of the O&M need. Such an additional sequential constraint may or may not influence the optimal O&M policy. Also, the decision to "Stay"/"Go" is often, in practice, based on weather forecasts and a "gut feeling" on the part of a field expert. The proposed framework provides a more rational decision-making tool that is optimized and considers observed long-term weather patterns at the site. Of course, short-term weather forecasts are valuable information and can be incorporated in the proposed framework.

4.5   Conclusions

This study has introduced a Markov decision process (MDP) framework for planning operation and maintenance (O&M) activities around offshore multi-purpose platforms (MPPs). The framework combines considera-

119

tion of multiple offshore functions that may require a wide-ranging set of O&M activities for satisfactory performance. The robustness of the proposed MDP framework has been demonstrated and optimal policies were derived for greatly contrasting synthetic metocean conditions as well as one site with conditions matching an actual Scottish offshore site. The activities addressed included ones that needed both shorter and longer work periods. Other methods for sequential decision-making in reinforcement learning were briefly discussed. Two examples involving constant and time-dependent downtime costs and associated loss of revenue were evaluated for all the different metocean conditions. One practical example involving the managing of two separate O&M issues involving salmon net pens and wave energy converters is introduced and analyzed for a 10-year operation period. The optimal scheduling performance is compared with an uncertain forecast-based approach in this example. Derived optimized O&M plans are found to be reasonable, given the specific weather patterns and planned activities, and may be employed in future blue economy projects involving various maritime activities for planned MPPs.

Chapter 5

Summary and Future Work

Three studies have been undertaken that establish scientific frameworks that use climate and ocean data to aid in making optimized decisions for climate change adaptation and mitigation. For the first research question, *How to optimally use past data in near-future risk assessment of non-stationary extreme climate events for making better projections compared to the traditional approach that employs entire historical record with assumptions of stationarity?*, a greedy copula segmentation (GCS) algorithm is developed. It is shown that predictions based on the GCS approach are closer to the actual future than those made by a traditional model that employs all the available data. For the second research question, *How to identify an optimized plan for the sustainable reuse of decommissioned oil and gas jacket platforms for wind energy generation?*, a rational optimization strategy to maximize the benefits of sustainable reuse of an oil and gas platform for wind energy generation has been established. A realistic case study and sustainable reuse scenario for a site near Porto (Leixões), Portugal, illustrated how to arrive at an optimal plan for the sustainable reuse of a jacket platform for offshore wind energy generation. For the last research question, *How to facilitate optimal decision-making related to scheduling of a wide-ranging set of operation and maintenance ac-*

tivities of multipurpose offshore platforms?, a Markov decision process (MDP) has been formulated to provide an optimized policy that guides the scheduling of operation and maintenance (O&M) activities for offshore floating multipurpose platforms. The optimized policy derived with this formulation leads to lower accumulated costs than common practice; this is demonstrated for a wide range of general metocean conditions.

From the results of these studies, we state that the proposed algorithms and frameworks have clear advantages for use in real-world situations, allowing one to make optimized climate change adaptation and mitigation decisions. However, each study has room for further investigation and innovation, and the author intends to continue his academic journey by deeper investigation into the use of enhanced models derived from ones developed in this dissertation. For instance, GCS, as presented, has a limitation in its adoption for stochastic processes with continuous trends. Continuously changing patterns will make it harder to define families of marginal distributions and copula functions. To address this issue, a fully non-parametric variation of the model can be developed that will make it more flexible and scalable. Automated establishment of the regularization parameter is another issue that will be investigated further. The choice of the use of a sufficiently large regularization parameter, λ, that yields the same segmentation can be compared with other criteria.

A formulation based on fracture mechanics for fatigue damage accumulation can be considered for the sustainable reuse of oil and gas jacket platform study. In some cases, crack size (length) can be a more practical measurement

for monitoring the level of fatigue damage. Also, a fracture mechanics-based formulation may be easier to combine with the desire for extension of life of a structure/platform.. Other issues, such as localized fatigue damage assessment and system reliability, are possible directions for extension of the work presented in this dissertation.

The MDP model can be easily expanded to incorporate forecast information using a partially observable Markov decision process model (POMDP). By considering the uncertain forecast information as an additional state of the problem, we can arrive at a better scheduling plan that takes into account both historical patterns as well as real-time near-future predictions at the same time. In addition to the forecast information, many elements can be added to the model, such as consideration for the use of modes of crew transport, uncertainty in the definition of what constitutes a safe/favorable climate threshold, time spent to get to the service site in addition to the time to actually perform the service. Also, optimal transportation lease planning based on the proposed MDP framework will help many offshore O&M projects with limited resources and budgets.

Bibliography

[1] KA Abhinav, Maurizio Collu, Steven Benjamins, Huiwen Cai, Adam Hughes, Bo Jiang, Simon Jude, William Leithead, Cui Lin, Hongda Liu, et al. Offshore multi-purpose platforms for a blue growth: A technological, environmental and socio-economic review. *Science of the Total Environment*, 734:138256, 2020.

[2] Mahdi Abkar. Theoretical modeling of vertical-axis wind turbine wakes. *Energies*, 12(1):10, 2019.

[3] Lorenzo Alessi, José AFO Correia, and Nicholas Fantuzzi. Initial design phase and tender designs of a jacket structure converted into a retrofitted offshore wind turbine. *Energies*, 12(4):659, 2019.

[4] Simon Ambühl, Laurent Marquis, Jens Peter Kofoed, and John Dalsgaard Sørensen. Operation and maintenance strategies for wave energy converters. *Proceedings of the Institution of Mechanical Engineers, Part O: Journal of Risk and Reliability*, 229(5):417–441, 2015.

[5] Stefan Andrews, Scott Bennett, and Thomas Wernberg. Reproductive seasonality and early life temperature sensitivity reflect vulnerability of a seaweed undergoing range reduction. *Marine Ecology Progress Series*, 495:119–129, 2014.

[6] Ariane Arias-Ortiz, Oscar Serrano, Pere Masqué, Paul S Lavery, Ute Mueller, Gary A Kendrick, M Rozaimi, A Esteban, James W Fourqurean, NJNCC Marbà, et al. A marine heatwave drives massive losses from the world's largest seagrass carbon stocks. *Nature Climate Change*, 8(4):338–344, 2018.

[7] Frank Asche, Håvard Hansen, Ragnar Tveteras, and Sigbjørn Tveterås. The salmon disease crisis in chile. *Marine Resource Economics*, 24(4):405–411, 2009.

[8] Arnfinn Aunsmo, Paul Steinar Valle, Marianne Sandberg, Paul Johan Midtlyng, and Torkjel Bruheim. Stochastic modelling of direct costs of pancreas disease (pd) in norwegian farmed atlantic salmon (salmo salar l.). *Preventive veterinary medicine*, 93(2-3):233–241, 2010.

[9] Catherine Banet. Regulating the reuse and repurposing of oil and gas installations in the context of decommissioning: Creating incentives and enabling energy system integration. In *The Regulation of Decommissioning, Abandonment and Reuse Initiatives in the Oil and Gas Industry: From Obligation to Opportunities*, chapter 11. Wolters Kluwer, 2020.

[10] Viva Banzon, Thomas M Smith, Toshio Mike Chin, Chunying Liu, and William Hankins. A long-term record of blended satellite and in situ sea-surface temperature for climate monitoring, modeling and environmental studies. *Earth System Science Data*, 8(1):165–176, 2016.

[11] JC Barros, GC Fernandes, M Miguel Silva, RP Da Silva, and B Santos. Fixed platforms at ageing oil fields-feasibility study for reuse to wind farms. In *Offshore Technology Conference*. OnePetro, 2017.

[12] Austin Becker, Satoshi Inoue, Martin Fischer, and Ben Schwegler. Climate change impacts on international seaports: knowledge, perceptions, and planning efforts among port administrators. *Climatic change*, 110(1):5–29, 2012.

[13] Philipp Beiter, Walter Musial, Aaron Smith, Levi Kilcher, Rick Damiani, Michael Maness, Senu Sirnivas, Tyler Stehly, Vahan Gevorgian, Meghan Mooney, et al. A spatial-economic cost-reduction pathway analysis for us offshore wind energy development from 2015–2030. Technical report, National Renewable Energy Lab.(NREL), Golden, CO (United States), 2016.

[14] D Benasciutti and R Tovo. Cycle distribution and fatigue damage assessment in broad-band non-gaussian random processes. *Probabilistic Engineering Mechanics*, 20(2):115–127, 2005.

[15] Denis Benasciutti and Roberto Tovo. Fatigue life assessment in non-gaussian random loadings. *International journal of fatigue*, 28(7):733–746, 2006.

[16] Julius S Bendat. Probability functions for random responses: prediction of peaks, fatigue damage, and catastrophic failures. Technical report, NASA, 1964.

[17] Elzbieta M Bitner-Gregersen. Joint met-ocean description for design and operations of marine structures. *Applied Ocean Research*, 51:279–292, 2015.

[18] Elzbieta M Bitner-Gregersen, Y Garbatov, N Fonseca, A Teixeira, et al. Joint long-term models of met-ocean parameters. *CENTEC Anniversary Book, in press, AA Balkema Publishers, Taylor and Francis, The Netherlands*, 2012.

[19] Elzbieta M Bitner-Gregersen and Sverre Haver. Joint environmental model for reliability calculations. In *The First International Offshore and Polar Engineering Conference*. OnePetro, 1991.

[20] EM Bitner-Gregersen, C Guedes Soares, U Machado, and P Cavaco. Comparison of different approaches to joint environmental modelling. In *Proceedings of the 17th International Conference on Offshore Mechanics and Arctic Engineering, ASME, New York*, volume 2, 1998.

[21] HC Bloomfield, DJ Brayshaw, Alberto Troccoli, CM Goodess, Matteo De Felice, Laurent Dubus, PE Bett, and Y-M Saint-Drenan. Quantifying the sensitivity of european power systems to energy scenarios and climate change projections. *Renewable Energy*, 164:1062–1075, 2021.

[22] Günter Blöschl, Julia Hall, Juraj Parajka, Rui AP Perdigão, Bruno Merz, Berit Arheimer, Giuseppe T Aronica, Ardian Bilibashi, Ognjen Bonacci, Marco Borga, et al. Changing climate shifts timing of european floods. *Science*, 357(6351):588–590, 2017.

[23] Virginia Burkett. Global climate change implications for coastal and offshore oil and gas development. *Energy Policy*, 39(12):7719–7725, 2011.

[24] Ruth Callaway, Andrew P Shinn, Suzanne E Grenfell, James E Bron, Gavin Burnell, Elizabeth J Cook, Margaret Crumlish, Sarah Culloty, Keith Davidson, Robert P Ellis, et al. Review of climate change impacts on marine aquaculture in the uk and ireland. *Aquatic Conservation: Marine and Freshwater Ecosystems*, 22(3):389–421, 2012.

[25] S Calvo, M Canales, C Gómez, JR Valdés, and JL Núñez. Probabilistic formulation of the multiaxial fatigue damage of liu. *International journal of fatigue*, 33(3):460–465, 2011.

[26] Nick Caputi, Mervi Kangas, Ainslie Denham, Ming Feng, Alan Pearce, Yasha Hetzel, and Arani Chandrapavan. Management adaptation of invertebrate fisheries to an extreme marine heat wave event at a global warming hot spot. *Ecology and Evolution*, 6(11):3583–3593, 2016.

[27] Enrique Castillo and Alfonso Fernández-Canteli. *A unified statistical methodology for modeling fatigue damage*. Springer Science & Business Media, 2009.

[28] Letícia M Cavole, Alyssa M Demko, Rachel E Diner, Ashlyn Giddings, Irina Koester, Camille MLS Pagniello, May-Linn Paulsen, Arturo Ramirez-Valdez, Sarah M Schwenck, Nicole K Yen, et al. Biological impacts of the 2013–2015 warm-water anomaly in the northeast pacific: winners, losers, and the future. *Oceanography*, 29(2):273–285, 2016.

[29] Vince Cestone. Jackie speier, jared huffman introduce disaster relief funding bill for california crab fishermen. *KRON4*, Mar 2016.

[30] Julie Chao. Experts' predictions for future wind energy costs drop significantly, Aug 2022.

[31] William WL Cheung, Thomas L Frölicher, Vicky WY Lam, Muhammed A Oyinlola, Gabriel Reygondeau, U Rashid Sumaila, Travis C Tai, Lydia CL Teh, and Colette CC Wabnitz. Marine high temperature extremes amplify the impacts of climate change on fish and fisheries. *Science Advances*, 7(40):eabh0895, 2021.

[32] Kevern Cochrane, Cassandra De Young, Doris Soto, and Tarûb Bahri. Climate change implications for fisheries and aquaculture. *FAO Fisheries and aquaculture technical paper*, 530:212, 2009.

[33] José Correia, Nicole Apetre, Attilio Arcari, Abílio De Jesus, Miguel Muñiz-Calvente, Rui Calçada, Filippo Berto, and Alfonso Fernández-Canteli. Generalized probabilistic model allowing for various fatigue damage variables. *International Journal of Fatigue*, 100:187–194, 2017.

[34] José AFO Correia, Miguel Correia, Mads Holm, Julle Ekeborg, Grzegorz Lesiuk, José M Castro, Abílio MP de Jesus, and Rui Calçada. Evaluation of fatigue design curves for a double-side welded connection used in offshore applications. In *Pressure Vessels and Piping Conference*, volume 51678, page V06AT06A028. American Society of Mechanical Engineers, 2018.

[35] Mark J Costello. Ecology of sea lice parasitic on farmed and wild fish. *Trends in parasitology*, 22(10):475–483, 2006.

[36] X Costoya, M DeCastro, D Carvalho, Z Feng, and M Gómez-Gesteira. Climate change impacts on the future offshore wind energy resource in china. *Renewable Energy*, 175:731–747, 2021.

[37] Stephen H Crandall, William D Mark, and Ghassan R Khabbaz. The variance on Palmgren-Miner damage due to random vibration. Technical report, Massachusetts Inst of Tech, Cambridge, 1962.

[38] Ana Maria Cruz and Elisabeth Krausmann. Vulnerability of the oil and gas sector to climate change and extreme weather events. *Climatic change*, 121(1):41–53, 2013.

[39] Gordon Dalton, Tamás Bardócz, Mike Blanch, David Campbell, Kate Johnson, Gareth Lawrence, Theodore Lilas, Erik Friis-Madsen, Frank Neumann, Nikitakos Nikitas, et al. Feasibility of investment in blue growth multiple-use of space and multi-use platform projects; results of a novel assessment approach and case studies. *Renewable and Sustainable Energy Reviews*, 107:338–359, 2019.

[40] M DeCastro, S Salvador, M Gómez-Gesteira, X Costoya, D Carvalho, FJ Sanz-Larruga, and L Gimeno. Europe, china and the united states: Three different approaches to the development of offshore wind energy. *Renewable and Sustainable Energy Reviews*, 109:55–70, 2019.

[41] Det Norske Veritas. Design of offshore wind turbine structures. *DNV-OS-J101, Offshore Standard*, 2013.

[42] Det Norske Veritas. Fatigue design of offshore structures. *DNV-RP-C203, Offshore Standard*, 2016.

[43] DNV GL. Metocean characterization recommended practices for U.S. offshore wind energy. *10039663-HOU-01, Report by DNV GL, Report for Bureau of Ocean Energy Management (BOEM)*, 2018.

[44] Jinxin Dong, Zunaira Asif, Yarong Shi, Yinying Zhu, and Zhi Chen. Climate change impacts on coastal and offshore petroleum infrastructure and the associated oil spill risk: a review. *Journal of Marine Science and Engineering*, 10(7):849, 2022.

[45] Mary K Donovan, Deron E Burkepile, Chelsey Kratochwill, Tom Shlesinger, Shannon Sully, Thomas A Oliver, Gregor Hodgson, Jan Freiwald, and Robert van Woesik. Local conditions magnify coral loss after marine heatwaves. *Science*, 372(6545):977–980, 2021.

[46] C Mark Eakin, Jessica A Morgan, Scott F Heron, Tyler B Smith, Gang Liu, Lorenzo Alvarez-Filip, Bart Baca, Erich Bartels, Carolina Bastidas, Claude Bouchon, et al. Caribbean corals in crisis: record thermal stress, bleaching, and mortality in 2005. *PloS one*, 5(11):e13969, 2010.

[47] Annika Eberle, Joseph O Roberts, Alicia Key, Parangat Bhaskar, and Katherine L Dykes. NREL's balance-of-system cost model for land-

based wind. Technical report, National Renewable Energy Lab. (NREL), Golden, CO (United States), 2019.

[48] Idriss El-Thalji. Context analysis of offshore fish farming. In *IOP Conference Series: Materials Science and Engineering*, volume 700, page 012065. IOP Publishing, 2019.

[49] Fernand Ellyin. *Fatigue damage, crack growth and life prediction.* Springer Science & Business Media, 2012.

[50] European Commission. Boosting Offshore Renewable Energy for a Climate Neutral Europe. Nov 2020.

[51] Mark D Fast. Fish immune responses to parasitic copepod (namely sea lice) infection. *Developmental & Comparative Immunology*, 43(2):300–312, 2014.

[52] NRI FEMA. Heat wave.

[53] Karen Filbee-Dexter, Thomas Wernberg, SP Grace, Jonas Thormar, Stein Fredriksen, CN Narvaez, CJ Feehan, and KM Norderhaug. Marine heatwaves and the collapse of marginal north atlantic kelp forests. *Scientific Reports*, 10(1):1–11, 2020.

[54] Food and Agriculture Organization of the United Nations. The state of world fisheries and aquaculture 2020. sustainability in action. *Rome*, 2020.

[55] Martin Føre, Kevin Frank, Tomas Norton, Eirik Svendsen, Jo Arve Al-fredsen, Tim Dempster, Harkaitz Eguiraun, Win Watson, Annette Stahl, Leif Magne Sunde, et al. Precision fish farming: A new framework to improve production in aquaculture. *biosystems engineering*, 173:176–193, 2018.

[56] S Foteinis and T Tsoutsos. Strategies to improve sustainability and offset the initial high capital expenditure of wave energy converters (WECs). *Renewable and Sustainable Energy Reviews*, 70:775–785, 2017.

[57] Thomas L Frölicher, Erich M Fischer, and Nicolas Gruber. Marine heat-waves under global warming. *Nature*, 560(7718):360–364, 2018.

[58] Thomas L Frölicher and Charlotte Laufkötter. Emerging risks from marine heat waves. *Nature communications*, 9(1):1–4, 2018.

[59] Joaquim Garrabou, Daniel Gómez-Gras, Alba Medrano, Carlo Cerrano, Massimo Ponti, Robert Schlegel, Nathaniel Bensoussan, Eva Turicchia, Maria Sini, Vasilis Gerovasileiou, et al. Marine heatwaves drive recurrent mass mortalities in the mediterranean sea. *Global Change Biology*, 28(19):5708–5725, 2022.

[60] Lily GC Genevier, Tahira Jamil, Dionysios E Raitsos, George Krokos, and Ibrahim Hoteit. Marine heatwaves reveal coral reef zones susceptible to bleaching in the red sea. *Global change biology*, 25(7):2338–2351, 2019.

[61] Sean C Godwin, Martin Krkosek, John D Reynolds, and Andrew W Bateman. Sea-louse abundance on salmon farms in relation to parasite-control policy and climate change. *ICES Journal of Marine Science*, 78(1):377–387, 2021.

[62] David Hallac, Peter Nystrup, and Stephen Boyd. Greedy gaussian segmentation of multivariate time series. *Advances in Data Analysis and Classification*, 13(3):727–751, 2019.

[63] Xiaoshuang Han, Weiliang Qiao, and Bo Zhou. Frequency domain response of jacket platforms under random wave loads. *Journal of Marine Science and Engineering*, 7(10):328, 2019.

[64] Andreas F. Haselsteiner, Ryan G. Coe, Lance Manuel, Wei Chai, Bernt Leira, Guilherme Clarindo, C. Guedes Soares, Ásta Hannesdóttir, Nikolay Dimitrov, Aljoscha Sander, Jan-Hendrik Ohlendorf, Klaus-Dieter Thoben, Guillaume de Hauteclocque, Ed Mackay, Philip Jonathan, Chi Qiao, Andrew Myers, Anna Rode, Arndt Hildebrandt, Boso Schmidt, Erik Vanem, and Arne Bang Huseby. A benchmarking exercise for environmental contours. *Ocean Engineering*, 236:109504, 2021.

[65] Andreas F Haselsteiner, Ryan G Coe, Lance Manuel, Wei Chai, Bernt Leira, Guilherme Clarindo, C Guedes Soares, Ásta Hannesdóttir, Nikolay Dimitrov, Aljoscha Sander, et al. A benchmarking exercise for environmental contours. *Ocean Engineering*, 236:109504, 2021.

[66] Andreas F. Haselsteiner, Ryan G. Coe, Lance Manuel, Phong T. T. Nguyen, Nevin Martin, and Aubrey Eckert-Gallup. A Benchmarking Exercise on Estimating Extreme Environmental Conditions: Methodology and Baseline Results. In *OMAE*, volume 3: Structures, Safety, and Reliability of *International Conference on Offshore Mechanics and Arctic Engineering*, 06 2019. V003T02A049.

[67] Abraham M Hasofer and Niels C Lind. Exact and invariant second-moment code format. *Journal of the Engineering Mechanics division*, 100(1):111–121, 1974.

[68] Taemin Heo, Ding Peng Liu, and Lance Manuel. Stochastic weather window analysis in operations and maintenance planning policies for offshore floating multi-purpose platforms. In *International Conference on Offshore Mechanics and Arctic Engineering*, volume 85888, page V004T05A019. American Society of Mechanical Engineers, 2022.

[69] Taemin Heo, Ding Peng Liu, Lance Manuel, Jose AFO Correia, and Paulo Mendes. Sustainable reuse of decommissioned jacket platforms for offshore wind energy accounting for accumulated fatigue damage. In *International Conference on Offshore Mechanics and Arctic Engineering*, volume 85932, page V008T09A040. American Society of Mechanical Engineers, 2022.

[70] Taemin Heo and Lance Manuel. Greedy copula segmentation of mul-

tivariate non-stationary time series for climate change adaptation. *Progress in Disaster Science*, 14:100221, 2022.

[71] Taemin Heo, Phong TT Nguyen, Lance Manuel, Maurizio Collu, KA Abhinav, Xue Xu, and Giulio Brizzi. Operations and maintenance for multipurpose offshore platforms using statistical weather window analysis. In *Global Oceans 2020: Singapore–US Gulf Coast*, pages 1–7. IEEE, 2020.

[72] Knut A Hjelt. Norwegian regulation system and the history of the norwegian salmon farming industry. In *1. International Symposium on Cage Aquaculture in Asia, Tungkang, Pingtung (Taiwan), 2-6 Nov 1999.* AFS; WAS-SC, 2000.

[73] Alistair J Hobday, Lisa V Alexander, Sarah E Perkins, Dan A Smale, Sandra C Straub, Eric CJ Oliver, Jessica A Benthuysen, Michael T Burrows, Markus G Donat, Ming Feng, et al. A hierarchical approach to defining marine heatwaves. *Progress in Oceanography*, 141:227–238, 2016.

[74] SA Hsu, Eric A Meindl, and David B Gilhousen. Determining the power-law wind-profile exponent under near-neutral stability conditions at sea. *Journal of Applied Meteorology and Climatology*, 33(6):757–765, 1994.

[75] Boyin Huang, Chunying Liu, Eric Freeman, Garrett Graham, Tom Smith, and Huai-Min Zhang. Assessment and intercomparison of noaa daily optimum interpolation sea surface temperature (doisst) version 2.1. *Journal of Climate*, 34(18):7421–7441, 2021.

[76] American Petroleum Institute. Planning, designing, and constructing fixed offshore platforms: Working stress design. Standard, API, 2014.

[77] IPCC. Climate change 2021: The physical science basis. v. masson-delmotte et al. 2022.

[78] Dave Jackson, Alan Drumm, Sarah McEvoy, Østen Jensen, Diego Mendiola, Gorka Gabiña, Joseph A Borg, Nafsika Papageorgiou, Yannis Karakassis, and Kenneth D Black. A pan-european valuation of the extent, causes and cost of escape events from sea cage fish farming. *Aquaculture*, 436:21–26, 2015.

[79] Olivier M Joffre, Laurens Klerkx, Malcolm Dickson, and Marc Verdegem. How is innovation in aquaculture conceptualized and managed? a systematic literature review and reflection framework to inform analysis and action. *Aquaculture*, 470:129–148, 2017.

[80] Philip Jonathan and Kevin Ewans. Statistical modelling of extreme ocean environments for marine design: a review. *Ocean Engineering*, 62:91–109, 2013.

[81] Philip Jonathan, Jan Flynn, and Kevin Ewans. Joint modelling of wave spectral parameters for extreme sea states. *Ocean Engineering*, 37(11-12):1070–1080, 2010.

[82] Timothy Jones, Julia K Parrish, William T Peterson, Eric P Bjorkstedt, Nicholas A Bond, Lisa T Ballance, Victoria Bowes, J Mark Hipfner,

Hillary K Burgess, Jane E Dolliver, et al. Massive mortality of a planktivorous seabird in response to a marine heatwave. *Geophysical Research Letters*, 45(7):3193–3202, 2018.

[83] Jason Jonkman, Sandy Butterfield, Walter Musial, and George Scott. Definition of a 5-MW reference wind turbine for offshore system development. Technical report, National Renewable Energy Lab.(NREL), Golden, CO (United States), 2009.

[84] Jason Jonkman and Mike Sprague. Openfast documentation.

[85] JC Kaimal, JCJ Wyngaard, Y Izumi, and OR Coté. Spectral characteristics of surface-layer turbulence. *Quarterly Journal of the Royal Meteorological Society*, 98(417):563–589, 1972.

[86] Mark J Kaiser and Siddhartha Narra. Gulf of Mexico decommissioning: Trends and operating cost estimation. Technical report, Bureau of Ocean Energy Management, 2018.

[87] Hyeon-jin Kim, Beom-Seon Jang, and Jeong Du Kim. Fatigue-damage prediction for ship and offshore structures under wide-banded non-gaussian random loadings part i: Approximation of cycle distribution in wide-banded gaussian random processes. *Applied Ocean Research*, 101:102294, 2020.

[88] Jang K Kim, Charles Yarish, Eun Kyoung Hwang, Miseon Park, Young-dae Kim, Jang K Kim, Charles Yarish, Eun Kyoung Hwang, Miseon

Park, and Youngdae Kim. Seaweed aquaculture: cultivation technologies, challenges and its ecosystem services. *Algae*, 32(1):1–13, 2017.

[89] Kim Knowlton, Miriam Rotkin-Ellman, Galatea King, Helene G Margolis, Daniel Smith, Gina Solomon, Roger Trent, and Paul English. The 2006 california heat wave: impacts on hospitalizations and emergency department visits. *Environmental health perspectives*, 117(1):61–67, 2009.

[90] Martin Krkošek. Sea lice and salmon in pacific canada: ecology and policy. *Frontiers in Ecology and the Environment*, 8(4):201–209, 2010.

[91] Martin Krkošek, Brendan M Connors, Helen Ford, Stephanie Peacock, Paul Mages, Jennifer S Ford, Alexandra Morton, John P Volpe, Ray Hilborn, Lawrence M Dill, et al. Fish farms, parasites, and predators: implications for salmon population dynamics. *Ecological Applications*, 21(3):897–914, 2011.

[92] Martin Krkošek, Mark A Lewis, and John P Volpe. Transmission dynamics of parasitic sea lice from farm to wild salmon. *Proceedings of the Royal Society B: Biological Sciences*, 272(1564):689–696, 2005.

[93] Martin Krkošek, Crawford W Revie, Patrick G Gargan, Ove T Skilbrei, Bengt Finstad, and Christopher D Todd. Impact of parasites on salmon recruitment in the northeast atlantic ocean. *Proceedings of the Royal Society B: Biological Sciences*, 280(1750):20122359, 2013.

[94] Charlotte Laufkötter, Jakob Zscheischler, and Thomas L Frölicher. High-impact marine heatwaves attributable to human-induced global warming. *Science*, 369(6511):1621–1625, 2020.

[95] " Lazard. Lazard's levelized cost of energy analysis, December 2019.

[96] Mariella Leporini, Barbara Marchetti, Francesco Corvaro, and Fabio Polonara. Reconversion of offshore oil and gas platforms into renewable energysites production: Assessment of different scenarios. *Renewable Energy*, 135, 2018.

[97] Grzegorz Lesiuk, Nicholas Fantuzzi, Abílio MP De Jesus, and Rui AB Calcada. Fatigue damage analysis of offshore structures using hot-spot stress and notch strain approaches. *Experimental Mechanics of Solids*, 12:146, 2019.

[98] Trevor M Letcher. *Wind energy engineering: A handbook for onshore and offshore wind turbines.* Academic Press, 2017.

[99] Jia Li, Yun Peng, Ming Zhu, Kai Wang, and Jiexin Yi. Decommission in petroleum industry: Current status, future trends and policy advices. *IOP Conference Series: Earth and Environmental Science*, 237(042013), 2018.

[100] Lin Li, Zhen Gao, and Torgeir Moan. Joint distribution of environmental condition at five European offshore sites for design of combined wind

and wave energy devices. *Journal of Offshore Mechanics and Arctic Engineering*, 137(3), 2015.

[101] Yajie Liu, Ussif Rashid Sumaila, and John Paul Volpe. Potential ecological and economic impacts of sea lice from farmed salmon on wild salmon fisheries. *Ecological Economics*, 70(10):1746–1755, 2011.

[102] Yajie Liu and Hans vanhauwaer Bjelland. Estimating costs of sea lice control strategy in norway. *Preventive veterinary medicine*, 117(3-4):469–477, 2014.

[103] Heike K Lotze, Boris Worm, and Ulrich Sommer. Strong bottom-up and top-down control of early life stages of macroalgae. *Limnology and oceanography*, 46(4):749–757, 2001.

[104] Y M Low. Variance of the fatigue damage due to a gaussian narrowband process. *Structural Safety*, 34(1):381–389, 2012.

[105] YM Low. A method for accurate estimation of the fatigue damage induced by bimodal processes. *Probabilistic engineering mechanics*, 25(1):75–85, 2010.

[106] YM Low. An algorithm for accurate evaluation of the fatigue damage due to multimodal and broadband processes. *Probabilistic engineering mechanics*, 26(3):435–446, 2011.

[107] Ed Mackay, Andreas F Haselsteiner, Ryan G Coe, and Lance Manuel. A second benchmarking exercise on estimating extreme environmental

conditions: Methodology & baseline results. In *International Conference on Offshore Mechanics and Arctic Engineering*, volume 85123, page V002T02A015. American Society of Mechanical Engineers, 2021.

[108] J Maheswaran and SC Siriwardane. Fatigue life estimation of tubular joints–a comparative study. *Fatigue & Fracture of Engineering Materials & Structures*, 39(1):30–46, 2016.

[109] David J Malcolm and A Craig Hansen. Windpact turbine rotor design study: June 2000–june 2002 (revised). Technical report, National Renewable Energy Lab.(NREL), Golden, CO (United States), 2006.

[110] Jakob Mann. Wind field simulation. *Probabilistic Engineering Mechanics*, 13(4):269–282, 1998.

[111] Lance Manuel, Phong TT Nguyen, Jarred Canning, Ryan G Coe, Aubrey C Eckert-Gallup, and Nevin Martin. Alternative approaches to develop environmental contours from metocean data. *Journal of Ocean Engineering and Marine Energy*, 4(4):293–310, 2018.

[112] Lynda V. Mapes. Toxic algae creating deep trouble on west coast. *The Seattle Times*, Nov 2015.

[113] Muh Aris Marfai. Impact of sea level rise to coastal ecology: a case study on the northern part of java island, indonesia. 2014.

[114] Meredith L McPherson, Dennis JI Finger, Henry F Houskeeper, Tom W Bell, Mark H Carr, Laura Rogers-Bennett, and Raphael M Kudela.

Large-scale shift in the structure of a kelp forest ecosystem co-occurs with an epizootic and marine heatwave. *Communications biology*, 4(1):1–9, 2021.

[115] Paulo Mendes, José A.F.O. Correia, João Arrojado, Taemin Heo, Nicholas Fantuzzi, and Lance Manuel. Horizontal and vertical axis wind turbines on existing jacket platforms: Part 2 – retrofitting activities. *Structures*, 40:109–126, 2022.

[116] Paulo Mendes, José A.F.O. Correia, José Miguel Castro, Nicholas Fantuzzi, Ali Aidibi, and Lance Manuel. Horizontal and vertical axis wind turbines on existing jacket platforms: Part 1 – a comparative study. *Structures*, 32:1069–1080, 2021.

[117] Milton A Miner. Cumulative damage in fatigue. *Journal of Applied Mechanics*, 12(3):159–164, 1945.

[118] Dominic Moran and Abdulai Fofana. An economic evaluation of the control of three notifiable fish diseases in the united kingdom. *Preventive Veterinary Medicine*, 80(2-3):193–208, 2007.

[119] Walter Musial, Philipp Beiter, Jake Nunemaker, Vahan Gevorgian, Aubryn Cooperman, Rob Hammond, Matt Shields, and Paul Spitsen. 2019 offshore wind technology data update. Technical report, National Renewable Energy Lab. (NREL), Golden, CO (United States), 2020.

[120] A Mustafa, David J Speare, J Daley, Gary A Conboy, John F Burka, et al. Enhanced susceptibility of seawater cultured rainbow trout, oncorhynchus mykiss (walbaum), to the microsporidian loma salmonae during a primary infection with the sea louse, lepeophtheirus salmonis. *Journal of fish diseases*, 23(5):337–341, 2000.

[121] Erkki Niemi, Wolfgang Fricke, and Stephen J Maddox. The structural hot-spot stress approach to fatigue analysis. In *Structural Hot-Spot Stress Approach to Fatigue Analysis of Welded Components*, pages 5–12. Springer, 2018.

[122] Agriculture Organization of the United Nations. Fisheries Department. *The State of World Fisheries and Aquaculture, 2016*. Food & Agriculture Org., 2016.

[123] Jon Olaf Olaussen, Yajie Liu, and Anders Skonhoft. Wild salmon harvest with farmed salmon induced mortality. *BIOECON confer-ence, Cambridge, UK*, 2013.

[124] Eric CJ Oliver, Jessica A Benthuysen, Sofia Darmaraki, Markus G Donat, Alistair J Hobday, Neil J Holbrook, Robert W Schlegel, and Alex Sen Gupta. Marine heatwaves. *Annual Review of Marine Science*, 13:313–342, 2021.

[125] Eric CJ Oliver, Markus G Donat, Michael T Burrows, Pippa J Moore, Dan A Smale, Lisa V Alexander, Jessica A Benthuysen, Ming Feng, Alex

Sen Gupta, Alistair J Hobday, et al. Longer and more frequent marine heatwaves over the past century. *Nature communications*, 9(1):1–12, 2018.

[126] Florian Orgeret, Andréa Thiebault, Kit M Kovacs, Christian Lydersen, Mark A Hindell, Sarah Ann Thompson, William J Sydeman, and Pierre A Pistorius. Climate change impacts on seabirds and marine mammals: The importance of study duration, thermal tolerance and generation time. *Ecology Letters*, 25(1):218–239, 2022.

[127] Liv Østevik, Marit Stormoen, Øystein Evensen, Cheng Xu, Kai-Inge Lie, Ane Nødtvedt, Hamish Rodger, Andreas Skagøy, Farah Manji, and Marta Alarcón. Effects of thermal and mechanical delousing on gill health of farmed atlantic salmon (salmo salar l.). *Aquaculture*, 552:738019, 2022.

[128] Kathy Overton, Tim Dempster, Frode Oppedal, Tore S Kristiansen, Kristine Gismervik, and Lars H Stien. Salmon lice treatments and salmon mortality in norwegian aquaculture: a review. *Reviews in Aquaculture*, 11(4):1398–1417, 2019.

[129] Marco Palmieri, Salvatore Bozzella, Giuseppe Leonardo Cascella, Marco Bronzini, Marco Torresi, and Francesco Cupertino. Wind micro-turbine networks for urban areas: Optimal design and power scalability of permanent magnet generators. *Energies*, 11(10):2759, 2018.

[130] Konstantinos G Papakonstantinou and Masanobu Shinozuka. Planning structural inspection and maintenance policies via dynamic programming and markov processes. Part I: Theory. *Reliability Engineering & System Safety*, 130:202–213, 2014.

[131] Simon Michael Papalexiou, Amir AghaKouchak, Kevin E Trenberth, and Efi Foufoula-Georgiou. Global, regional, and megacity trends in the highest temperature of the year: Diagnostics and evidence for accelerating trends. *Earth's future*, 6(1):71–79, 2018.

[132] Simon Michael Papalexiou and Alberto Montanari. Global and regional increase of precipitation extremes under global warming. *Water Resources Research*, 55(6):4901–4914, 2019.

[133] Alan Pearce, Gary Jackson, Jenny Moore, Ming Feng, and Daniel J Gaughan. The "marine heat wave" off western australia during the summer of 2010/11. 2011.

[134] John F Piatt, Julia K Parrish, Heather M Renner, Sarah K Schoen, Timothy T Jones, Mayumi L Arimitsu, Kathy J Kuletz, Barbara Bodenstein, Marisol García-Reyes, Rebecca S Duerr, et al. Extreme mortality and reproductive failure of common murres resulting from the northeast pacific marine heatwave of 2014-2016. *PloS one*, 15(1):e0226087, 2020.

[135] Willard J Pierson Jr and Lionel Moskowitz. A proposed spectral form for fully developed wind seas based on the similarity theory of S A Kitaigorodskii. *Journal of Geophysical Research*, 69(24):5181–5190, 1964.

[136] Iván Pineda and Pierre Tardieu. Wind in power 2017, annual combined onshore and offshore wind energy statistics. Technical report, Wind Europe, 2018.

[137] Wojciech Popko, Fabian Vorpahl, Adam Zuga, Martin Kohlmeier, Jason Jonkman, Amy Robertson, Torben J Larsen, Anders Yde, Kristian Sætertrø, Knut M Okstad, et al. Offshore code comparison collaboration continuation (oc4), phase 1-results of coupled simulations of an offshore wind turbine with jacket support structure. In *The twenty-second international offshore and polar engineering conference*. OnePetro, 2012.

[138] Vencislau Manuel Quissanga, Elson Antonio do Nascimento, and Nelson Szilard Galgoul. Feasibility study for the reuse of a steel offshore platform as the base of a wind tower. *International Journal of Research in Engineering and Science*, 8(8):01–06, 2020.

[139] Rüdiger Rackwitz and Bernd Flessler. Structural reliability under combined random load sequences. *Computers & Structures*, 9(5):489–494, 1978.

[140] P Ragan and L Manuel. Comparing estimates of wind turbine fatigue loads using time-domain and spectral methods. *Wind Engineering*, 31, 2007.

[141] Crawford Revie, Larry Dill, Bengt Finstad, and Christopher Todd. *Sea lice working group report*. Norsk institutt for naturforskning (NINA), 2009.

[142] Richard W Reynolds, Thomas M Smith, Chunying Liu, Dudley B Chelton, Kenneth S Casey, and Michael G Schlax. Daily high-resolution-blended analyses for sea surface temperature. *Journal of climate*, 20(22):5473–5496, 2007.

[143] Giovanni Rinaldi, Anna Garcia-Teruel, Henry Jeffrey, Philipp R Thies, and Lars Johanning. Incorporating stochastic operation and maintenance models into the techno-economic analysis of floating offshore wind farms. *Applied Energy*, 301:117420, 2021.

[144] Christine Röckmann, Sander Lagerveld, and John Stavenuiter. Operation and maintenance costs of offshore wind farms and potential multi-use platforms in the dutch north sea. In *Aquaculture Perspective of Multi-Use Sites in the Open Ocean*, pages 97–113. Springer, Cham, 2017.

[145] Rui Rosa, António Marques, and Maria L Nunes. Impact of climate change in mediterranean aquaculture. *Reviews in Aquaculture*, 4(3):163–177, 2012.

[146] Max Roser and Esteban Ortiz-Ospina. Global direct primary energy consumption. *Our World in Data*, 2022. https://ourworldindata.org/grapher/global-primary-energy.

[147] Igor Rychlik. A new definition of the rainflow cycle counting method. *International journal of fatigue*, 9(2):119–121, 1987.

[148] Luís Volnei Sudati Sagrilo, Edison Castro Prates de Lima, and Arnaldo Papaleo. A joint probability model for environmental parameters. *Journal of offshore mechanics and Arctic engineering*, 133(3), 2011.

[149] Bernabé Santelices. Patterns of reproduction, dispersal and recruitment inseaweeds. *Ocearrogr A Mar Biol 471h Rez*, 28:177–276, 1990.

[150] A Schaeffer and M Roughan. Subsurface intensification of marine heatwaves off southeastern australia: the role of stratification and local winds. *Geophysical Research Letters*, 44(10):5025–5033, 2017.

[151] Thijs Nicolaas Schouten, Rommert Dekker, Mustafa Hekimoğlu, and Ayse Sena Eruguz. Maintenance optimization for a single wind turbine component under time-varying costs. *European Journal of Operational Research*, 300(3):979–991, 2022.

[152] David W Scott. *Multivariate density estimation: theory, practice, and visualization*. John Wiley & Sons, 2015.

[153] Helene Seyr and Michael Muskulus. Decision support models for operations and maintenance for offshore wind farms: A review. *Applied Sciences*, 9(2):278, 2019.

[154] Helene Seyr and Michael Muskulus. Use of markov decision processes in the evaluation of corrective maintenance scheduling policies for offshore wind farms. *Energies*, 12(15):2993, 2019.

[155] Ya-Tsune Sie, Pierre-Alexandre Château, Yang-Chi Chang, and Shiau-Yun Lu. Stakeholders opinions on multi-use deep water offshore platform in Hsiao-Liu-Chiu, Taiwan. *International Journal of Environmental Research and Public Health*, 15(2):281, 2018.

[156] L Slater, G Villarini, S Archfield, D Faulkner, R Lamb, A Khouakhi, and J Yin. Global changes in 20-year, 50-year, and 100-year river floods. *Geophysical Research Letters*, 48(6):e2020GL091824, 2021.

[157] Louise J Slater, Bailey Anderson, Marcus Buechel, Simon Dadson, Shasha Han, Shaun Harrigan, Timo Kelder, Katie Kowal, Thomas Lees, Tom Matthews, et al. Nonstationary weather and water extremes: a review of methods for their detection, attribution, and management. *Hydrology and Earth System Sciences*, 25(7):3897–3935, 2021.

[158] Dan A Smale, Thomas Wernberg, Eric CJ Oliver, Mads Thomsen, Ben P Harvey, Sandra C Straub, Michael T Burrows, Lisa V Alexander, Jessica A Benthuysen, Markus G Donat, et al. Marine heatwaves threaten global biodiversity and the provision of ecosystem services. *Nature Climate Change*, 9(4):306–312, 2019.

[159] Vaclav Smil. *Energy transitions: global and national perspectives*. ABC-CLIO, 2016.

[160] Pedro MM Soares, Daniela CA Lima, Alvaro Semedo, William Cabos, and Dmitry V Sein. Climate change impact on northwestern

african offshore wind energy resources. *Environmental Research Letters*, 14(12):124065, 2019.

[161] Giovanni Solari. Turbulence modeling for gust loading. *Journal of Structural Engineering*, 113(7):1550–1569, 1987.

[162] John Dalsgaard Sørensen. Framework for risk-based planning of operation and maintenance for offshore wind turbines. *Wind Energy: An International Journal for Progress and Applications in Wind Power Conversion Technology*, 12(5):493–506, 2009.

[163] Tyler Stehly, Philipp Beiter, and Patrick Duffy. 2019 cost of wind energy review. Technical report, National Renewable Energy Lab.(NREL), Golden, CO (United States), 2020.

[164] Simone Strydom, Kathy Murray, Shaun Wilson, Bart Huntley, Michael Rule, Michael Heithaus, Cindy Bessey, Gary A Kendrick, Derek Burkholder, Matthew W Fraser, et al. Too hot to handle: Unprecedented seagrass death driven by marine heatwave in a world heritage area. *Global change biology*, 26(6):3525–3538, 2020.

[165] Richard S Sutton and Andrew G Barto. *Reinforcement Learning: An Introduction*. MIT press, 2018.

[166] The White House. FACT SHEET: Biden Administration Jumpstarts Offshore Wind Energy Projects to Create Jobs. Mar 2021.

[167] Isabelle Tobin, W Greuell, Sonia Jerez, F Ludwig, R Vautard, MTH Van Vliet, and François-Marie Bréon. Vulnerabilities and resilience of european power generation to 1.5 c, 2 c and 3 c warming. *Environmental Research Letters*, 13(4):044024, 2018.

[168] Isabelle Tobin, Sonia Jerez, Robert Vautard, Françoise Thais, Erik Van Meijgaard, Andreas Prein, Michel Déqué, Sven Kotlarski, Cathrine Fox Maule, Grigory Nikulin, et al. Climate change impacts on the power generation potential of a european mid-century wind farms scenario. *Environmental Research Letters*, 11(3):034013, 2016.

[169] Verónica Torralba, Francisco J Doblas-Reyes, and Nube Gonzalez-Reviriego. Uncertainty in recent near-surface wind speed trends: a global reanalysis intercomparison. *Environmental Research Letters*, 12(11):114019, 2017.

[170] Stephen P Truchon, Louis P Brzuzy, Deborah Fawcett, and Mark Fonseca. Innovative assessments for selecting offshore-platform-decommissioning alternatives. *Oil and Gas Facilities*, 4(05):47–55, 2015.

[171] Jan van der Tempel. *Design of support structures for offshore wind turbines*. PhD thesis, TU Delft, 2006.

[172] Erik Vanem. Joint statistical models for significant wave height and wave period in a changing climate. *Marine Structures*, 49:180–205, 2016.

[173] Paul S Veers. Three-dimensional wind simulation. Technical report, Sandia National Labs., Albuquerque, NM (USA), 1988.

[174] Paul S Veers, Steven R Winterstein, Clifford H Lange, and Tracy A Wilson. Users manual for FAROW: Fatigue and Reliability of Wind Turbine Components: Version 1.1. Technical report, Sandia National Labs., Albuquerque, NM (United States), 1994.

[175] Knut Wiik Vollset, Randi Ingebjørg Krontveit, Peder A Jansen, Bengt Finstad, Bjørn Torgeir Barlaup, Ove Tommy Skilbrei, Martin Krkošek, Pål Romunstad, Arnfinn Aunsmo, Arne J Jensen, et al. Impacts of parasites on marine survival of atlantic salmon: A meta-analysis. *Fish and Fisheries*, 17(3):714–730, 2016.

[176] Vanessa R von Biela, Mayumi L Arimitsu, John F Piatt, Brielle Heflin, Sarah K Schoen, Jannelle L Trowbridge, and Chelsea M Clawson. Extreme reduction in nutritional value of a key forage fish during the pacific marine heatwave of 2014-2016. *Marine Ecology Progress Series*, 613:171–182, 2019.

[177] John C Wekell, Erich J Gauglitz Jr, Harold J Bamett, Christine L Hatfield, Doug Simons, and Daniel Ayres. Occurrence of domoic acid in washington state razor clams (siliqua patula) during 1991-1993. *Natural Toxins*, 2(4):197–205, 1994.

[178] Yoga Arob Wicaksono, Dominicus Danardono Dwi Prija Tjahjana, and

Syamsul Hadi. Influence of omni-directional guide vane on the performance of cross-flow rotor for urban wind energy. In *AIP Conference Proceedings*, volume 1931, page 030040. AIP Publishing LLC, 2018.

[179] Sonja Wild, Michael Krützen, Robert W Rankin, William JE Hoppitt, Livia Gerber, and Simon J Allen. Long-term decline in survival and reproduction of dolphins following a marine heatwave. *Current Biology*, 29(7):R239–R240, 2019.

[180] David Wilkie and Carmine Galasso. Impact of climate-change scenarios on offshore wind turbine structural performance. *Renewable and Sustainable Energy Reviews*, 134:110323, 2020.

[181] Ryan Wiser, Joseph Rand, Joachim Seel, Philipp Beiter, Erin Baker, Eric Lantz, and Patrick Gilman. Expert elicitation survey predicts 37% to 49% declines in wind energy costs by 2050. *Nature Energy*, 6(5):555–565, 2021.

[182] B Yeter, Y Garbatov, and C Guedes Soares. Spectral fatigue assessment of an offshore wind turbine structure under wave and wind loading. *Developments in Maritime Transportation and Exploitation of Sea Resources. London, UK: Taylor & Francis Group*, pages 425–433, 2014.

[183] B Yeter, Y Garbatov, and C Guedes Soares. Fatigue damage assessment of fixed offshore wind turbine tripod support structures. *Engineering Structures*, 101:518–528, 2015.

[184] B Yeter, Y Garbatov, and C Guedes Soares. System reliability of a jacket offshore wind turbine subjected to fatigue. In *Progress in the Analysis and Design of Marine Structures*, pages 939–950. CRC Press, 2017.

[185] Barbara Zanuttigh, Elisa Angelelli, Giorgio Bellotti, Alessandro Romano, Yukiko Krontira, Dimitris Troianos, Roberto Suffredini, Giulia Franceschi, Matteo Cantù, Laura Airoldi, et al. Boosting blue growth in a mild sea: analysis of the synergies produced by a multi-purpose offshore installation in the Northern Adriatic, Italy. *Sustainability*, 7(6):6804–6853, 2015.

Vita

Taemin Heo was born in Seoul, Republic of Korea on 26 Dec 1992, the son of Jaeho Heo and Seunghee Song. He received Bachelor's and Master of Science degrees in Civil and Environmental Engineering from Seoul National University in 2016 and 2018, respectively. He entered the doctoral program in the Department of Civil, Architectural, and Environmental Engineering at the University of Texas at Austin in 2018. Because of overlapping needs for his research, he completed a series of courses and wrote a report that allowed him to receive another Master of Science degree in Computational Science, Engineering, and Mathematics from the University of Texas at Austin in 2021.

Permanent address: 287, Gwanak-ro, Gwanak-gu
Seoul, Republic of Korea, 08726

This dissertation was typeset with LaTeX[†] by the author.

[†]LaTeX is a document preparation system developed by Leslie Lamport as a special version of Donald Knuth's TeX Program.